Development of an Expansion Plug Wedge Test to Evaluate the Mechanical Properties of Clad Tubing Structure

Jy-An John Wang
Hao Jiang

April 6, 2016

OAK RIDGE NATIONAL LABORATORY
MANAGED BY UT-BATTELLE FOR THE US DEPARTMENT OF ENERGY

Materials Science and Technology Division
Oak Ridge National Laboratory

DEVELOPMENT OF AN EXPANSION PLUG WEDGE TEST TO EVALUATE THE MECHANICAL PROPERTIES OF CLAD TUBING STRUCTURE

Jy-An John Wang and Hao Jiang

Date Published: January 2016

CONTENTS

LIST OF FIGURES

LIST OF TABLES

ACRONYMS

ANL	Argonne National Laboratory
DOF	degrees of freedom
EDM	electrical discharge machining
FEA	finite element analysis
FEM	finite element method
FMDP	Fissile Materials Disposition Program
IAEA	International Atomic Energy Agency
ID	internal diameter
MOX	mixed oxide
NNSA	National Nuclear Security Administration
OD	outer diameter
ORNL	Oak Ridge National Laboratory
PIE	post irradiation examination
PNNL	Pacific Northwest National Laboratory

ACKNOWLEDGMENTS

EXECUTIVE SUMMARY

To determine the tensile properties of irradiated fuel cladding in a hot cell, a simple test was developed at the Oak Ridge National Laboratory (ORNL) and is described fully in US Patent Application 20060070455, "Expanded plug method for developing circumferential mechanical properties of tubular materials." This method is designed for testing fuel rod cladding ductility in a hot cell using an expandable plug to stretch a small ring of irradiated cladding material. The specimen strain is determined using the measured diametrical expansion of the ring. This method removes many complexities associated with specimen preparation and testing. The advantages are the simplicity of measuring the test component assembly in the hot cell and the direct measurement of the specimen's strain. It was also found that cladding strength could be determined from the test results.

In this test method, an axial compressive load is applied to a cylindrical plug of polyurethane (or other material) that has been fitted inside a short ring of the test material, resulting in radial expansion of the specimen. The amount of the specimen's increase in diameter is used to calculate the circumferential strain accrued during the test. The other two basic measurements are (1) the total applied load and (2) the amount of plug compression (extension). A simple procedure is used to convert the load-circumferential strain data from the ring tests into material pseudo stress-strain curves.

Early in the test program, it was recognized that a number of issues could impact the accuracy of the results and introduce potential shear failure of the specimen due to inherited plug barrel effect and large axial compressive stress from the expansion plug test. Two of the more significant issues are:
1. A highly nonuniform stress and strain distribution may occur in the gage section of the clad due to early test set-up. To ensure reliable testing and test repeatability, the potential for highly nonuniform stress distribution or displacement/strain deformation must be eliminated at the gage section of the specimen.
2. Significant compressive stresses may be induced by clad bending deformation due to a clad bulging or barreling effect. This would cause very significant localized shear stress in the clad and result in a high risk of shear failure.

The combined effects of these deficiencies would lead to highly unconservative predictions in the strength and ductility of the tested clad and the associated mechanical properties.

Systematic studies have been conducted to overcome/mitigate these deficiencies. Through detailed parameter investigation on specific geometry designs, careful filtering of material for the expansion plug, and inclusion of newly designed parts to the testing system, a new method has been established to improve the non-conservatism of the ORNL previously used method of the expansion plug test system. A modified expansion plug testing protocol has been developed based on the new method.

To closely resemble thin-wall theory, a revised procedure has been developed to determine the hoop stress σ_θ with χ factor in finite element analysis (FEA). The generated stress-strain curve agrees well with tensile test data in both the elastic and plastic regions. The modified expansion plug testing protocol has been developed and validated in finite element method (FEM) simulation.

Based on FEA design, ring specimen sizing was developed and a number of specimens fabricated for test validation. The newly developed wedge inserts design was initially designed for eight wedge inserts, but to facilitate easy sample preparation and implementation during the test, the decision was made to proceed with four wedge inserts for experimental validation of the testing method. Five generations of ring-wedge-plug pilot specimens have been designed, fabricated, and tested. More than 50 pilot tests have been conducted on 24 ring specimens and plugs. The fifth generation pilot test successfully achieved

uniform ring radial dilatation. The fifth generation ring specimen sets were considered to be most optimized design and fabrication to produce repeatable results.

The test data processing procedure was developed based on the energy approach to convert test load displacement measurements into hoop stress-strain curves for pilot testing results. Friction energy due to shear stress was estimated by FEA simulation and deducted from the total work. β factor was applied to the strain hardening region to correct the calculated works, and α factor was applied to deduct friction energy. Power function was generated to smooth the transition area between elastic and material hardening regions. The resulting ring test's converted material hoop stress-strain curve agreed well with tensile test data.

Based on the proposed test method and the optimized test specimen design that has been demonstrated in the pilot tests, the proposed expanded plug wedge testing protocol validates that the measured piston compressive load, plug extension, and ring radial expansion can be effectively and accurately converted into the hoop stress-strain curve for clad tubing material characterization.

1. INTRODUCTION AND BACKGROUND

Fuel and clad operating and potential failure mechanisms must be examined extensively to verify fuel rod performance and to produce data that can be used for fuel qualification. One of the essential examinations is the cladding mechanical properties test. In a hot-cell environment, conventional tensile testing might not reflect the cladding true characteristics due to complexities associated with specimen preparation and testing, in addition to the orientation dependent material properties. Under the auspices of the National Nuclear Security Administration's (NNSA's) Fissile Materials Disposition Program (FMDP), Hendrich, et al. [1] invented an expanded plug method and applied it to conduct post irradiation examination (PIE) to ascertain the performance of the fuel rods contained in the mixed oxide (MOX) lead test assemblies. The advantages of the method described in the patent application are (1) simplicity of use of the test component assembly in the hot cell, and (2) direct measurement of specimen strain. It was also found that cladding strength could be determined from the test results.

It is important to understand the thin-walled pressurized cylinder model on which the expanded plug method was based. If the cylinder walls are thin and the ratio of the thickness to the internal diameter is less than about $\frac{1}{20}$, then it can be assumed to be a thin-walled vessel [1,2,3]. The three principal stresses in the shell are circumferential or hoop stress, longitudinal stress, and radial stress. For the thin-walled cylinder, it may be assumed that the hoop and longitudinal stresses are constant across the thickness. The radial stress is small and can be neglected. As shown in Fig. 1, the hoop stress can be described as

$$\sigma_\theta = \frac{F}{tl},$$

(1)

where F is the force exerted circumferentially on an area of the cylinder wall that has a radial thickness t and an axial length l.
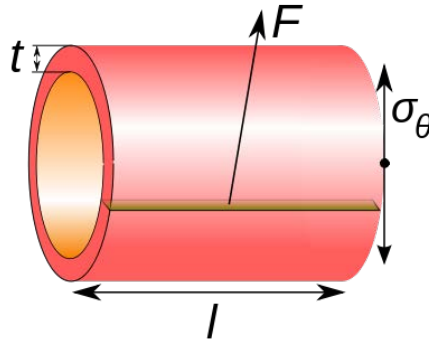
Fig. 1. Circumferential stress of cylinder.

Using the Young-Laplace equation, the hoop stress created by an internal pressure on a thin-walled cylindrical pressure vessel can be estimated as

$$\sigma_\theta = \frac{Pr}{t},$$

(2)

where P is the internal pressure, t is the wall thickness, and r is the inside radius of the cylinder.

When the cylinder has an *r/t* ratio of less than 10, the thin-walled cylinder equations are no longer valid. Between inside and outside surfaces, stresses can vary significantly, and shear stress through the cross section can no longer be neglected. Estimation of stress and strain becomes much more complicated.

A simple test was developed at Oak Ridge National Laboratory ORNL and is fully described in US Patent Application 20060070455, "Expanded plug method for developing circumferential mechanical properties of tubular materials" [4]. The schematic is shown in Fig. 2. This method is designed for testing fuel rod cladding ductility in a hot cell using an expandable plug to stretch a small ring of the irradiated cladding material. The basic approach of this test method is to apply an axial compressive load to a cylindrical plug of polyurethane (or other materials) fitted inside a short ring of the test material to achieve radial expansion of the specimen. Three major measurements are made: total applied load, extension of plug compression, and radial expansion of the specimen. The radial expansion of the specimen is used to calculate the circumferential strain accrued during the test.
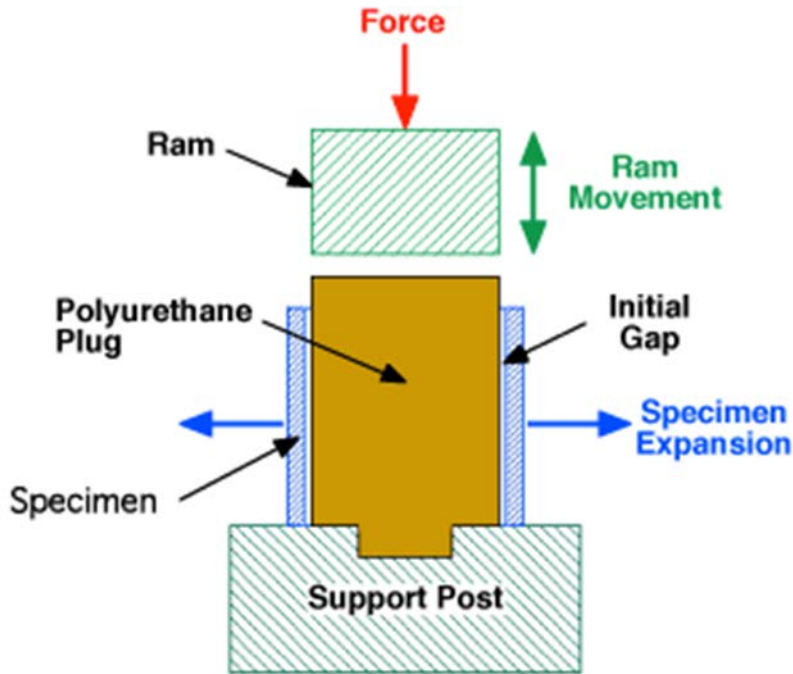
Fig. 2. Expanded plug test.

A general procedure has been developed to determine the circumferential stress (σ_{CIR}) in the expanded ring specimen [5]. The circumferential stress is calculated using a scaling parameter called a Γ-factor (Γ), the load (*P*), and the specimen dimensions as shown below.

$$\sigma_{CIR} = \frac{\Gamma P}{tl}, \tag{3}$$

where
$$\Gamma = \frac{\sigma_{Yield}}{P_{Yield}} tl,$$

σ_{Yield} = yield stress of a quality assured material determined using a standard tensile test,

P_{Yield} = load at 0.2% plastic strain offset measured using a ring specimen of the above QA'd material,

18

t = ring specimen thickness, and

l = ring specimen axial length.

Therefore, the load and radial expansion data from the ring tests can be converted into material pseudo stress-strain curves to examine mechanical properties, such as Young's modulus, yield strength, and strain-hardening characteristics.
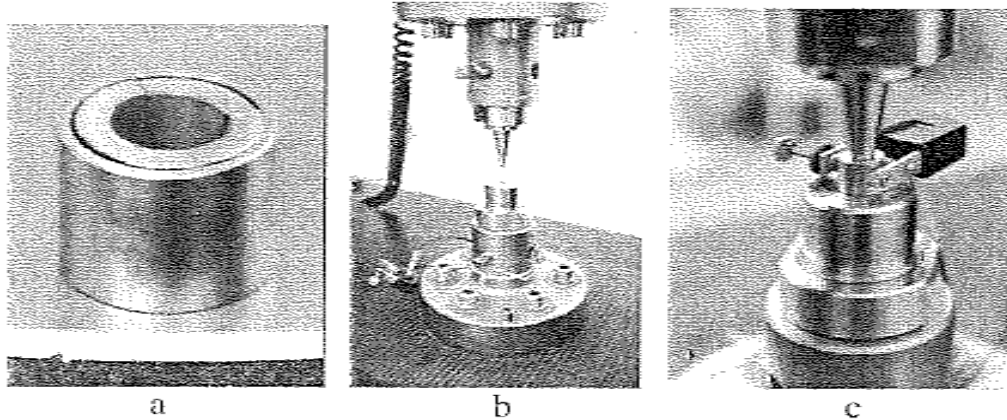
Fig. 3. The mandrel test device: (a) cladding tube with segment, (b) loading device, and (c) loaded specimen with extensometer for strain measurement.

In nuclear engineering and design, intensive research is focused on material characterization of fuel cladding. Among the vast literature, Nilsson et al. [6] and Kim et al. [7] performed similar investigations on fuel cladding using ring specimens. Nilsson et al. assessed the segmented expanding mandrel (SEM) test for material properties and a structural integrity assessment of nuclear fuel claddings (Fig. 3). The loading is induced by expanding segments which are placed radially inside a cladding tube to simulate cracked fuel that expands thermally. The test is appropriate to assess how defects and microstructure affect ductility. Kim et al. evaluated the hoop-directional mechanical properties comprising strength such as yield strength and ultimate tensile strength, as well as mechanical ductility such as uniform elongation and total elongation. The ring tensile tests were performed to study the mechanical properties of high-burnup fuel cladding under a hoop loading condition in a hot cell. The schematic test procedure and a photograph of the ring specimen are illustrated in Fig. 4.

19
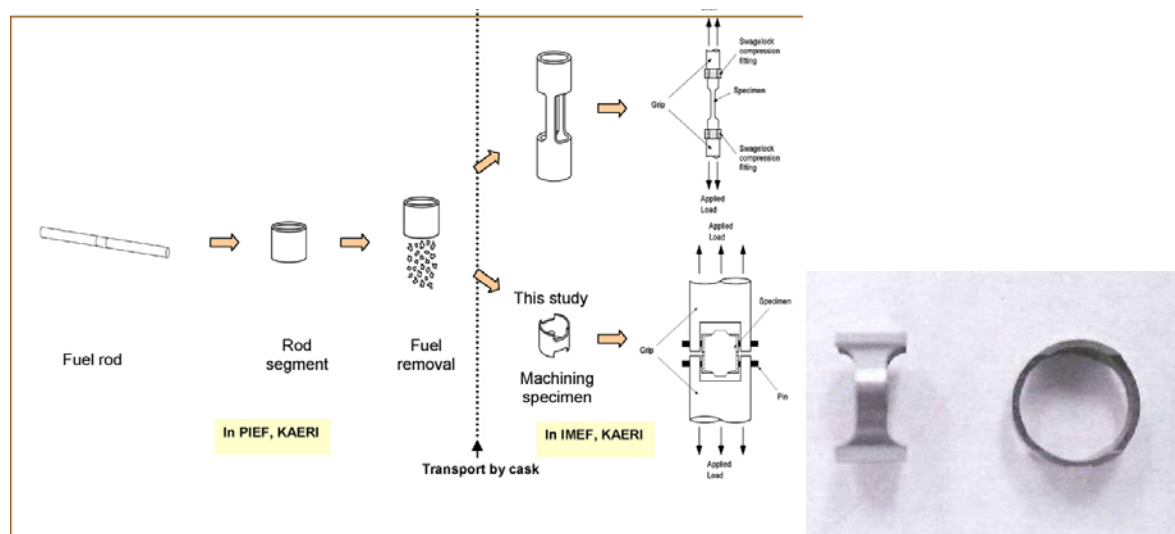
Fig. 4. Ring tensile test procedure and ring specimen.

2. SCOPE OF CURRENT RESEARCH

The objective of this research project is (1) to use finite element analysis (FEA) to evaluate the patent method of the expanded plug for developing mechanical properties in fuel cladding, and (2) to use the results of the study to seek improvement in the expansion plug method for better performance of mechanical property testing in a hot cell. The project was divided into three stages:

1. evaluation of the existing expanded plug method for mechanical property testing using FEA,
2. development of a modified expansion plug testing protocol, and
3. experimental validation of expansion plug wedge test on ring specimen.

In the first stage, a series of finite element models was established to study the expanded plug testing system with various plug and cladding materials at room temperature and at an elevated temperature. Unconstrained and fully constrained compressive tests were performed on polyurethane material. The hyperelastic material properties of the polyurethane plug were calibrated from both tests, and this provided input for the finite element model (FEM). Detailed stress and strain distribution was examined in FEA. The resultant FEM circumferential stress and radial strain of fuel cladding were validated with tensile test data and compared to mechanical properties generated from ring expansion clad testing data, as well. The results showed several deficiencies in the expanded plug method and provided important guidance for the second stage of the study.

To mitigate the deficiencies associated with the current expansion plug test, a significant effort was dedicated to improving the test design. Systematic studies were conducted, such as a detailed parameter investigation of geometry designs, selection of expansion plug material, and design of new parts for the testing system. A modified expansion plug testing protocol has been developed to improve the conservatism in the current expanded plug test in FEA.

Based on the FEA design, five generations of ring-wedge-plug pilot specimens have been fabricated, and tested, in several iterations. More than 50 pilot tests have been performed and carried out on 24 ring specimens and plugs. Test data processing procedure based on energy approach was developed to convert test system load- displacement measurements into hoop stress-strain curves of the targeted ring materials.

3.   EVALUATION OF CURRENT EXPANDED PLUG METHOD USING FEA

Even though the current expanded plug method was patented back in 2006 and the method was used in testing even before that time, system simulation and evaluation using FEA has never been fully conducted due to unresolved issues with respect to numerical deficiency. In this project, a significant effort was dedicated to solve the numerical problem and establish feasible finite element models using ABAQUS codes.

3.1   FEA OF ROOM TEMPERATURE RING EXPANSION CLAD TESTING

As discussed in Sect. 1, the test method was originally developed to perform room-temperature circumferential tensile testing of nuclear fuel cladding in a hot cell by radially expanding a ring specimen of the test material. This was accomplished by axially compressing a cylindrical plug of polyurethane fitted inside the specimen.

3.1.1   Bilinear Material Model for Expansion Plug

A 3D FEM model of the ring expansion clad testing system was developed based on the test setup, as shown in Fig. 5. This first version of the model failed because it had too many contact surfaces, causing a numerical convergence problem. Learning from this preliminary FEA study, the modified 3D FEM model was established as illustrated in Fig. 6.
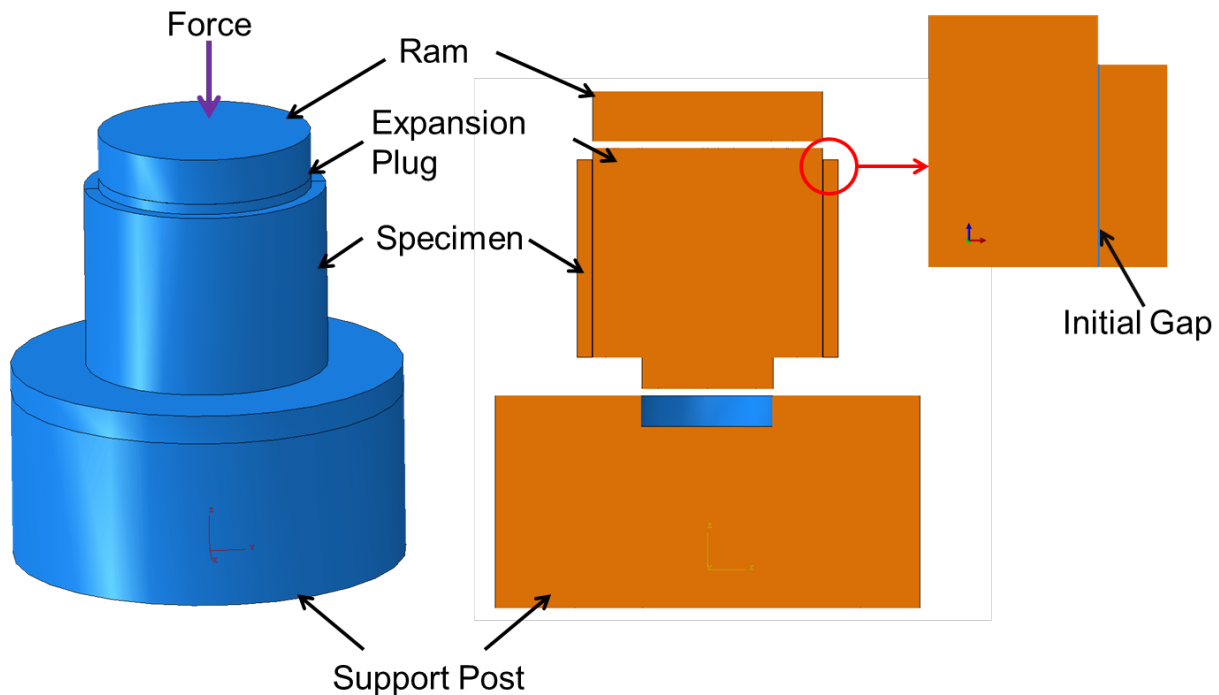
Fig. 5. Preliminary 3D FEM model of the ring expansion clad testing system.
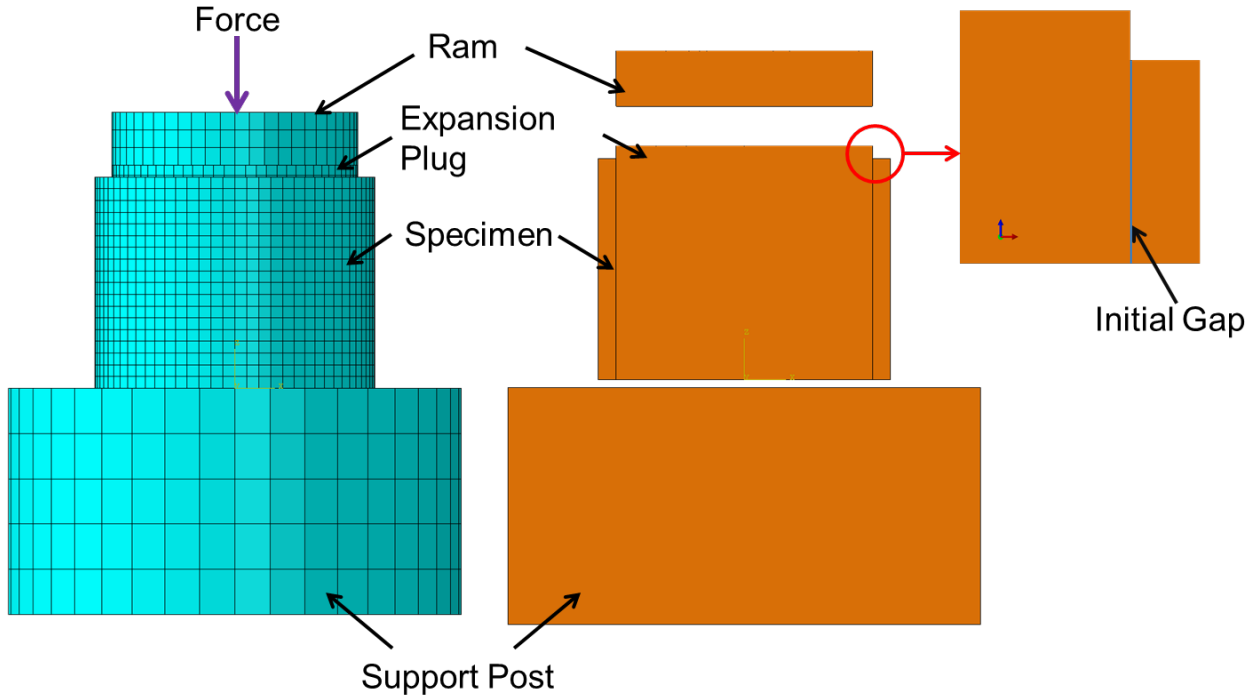
Fig. 6. Modified 3D FEM model of the ring expansion clad testing system.

In the modified model (Fig. 6), the expansion plug geometry was simplified, and contact surfaces to the support were eliminated without oversimplification. The slightly modified version has resolved the numerical difficulty and effectively represents the expanded plug method using FEA. In this model, the expansion plug was made of polyurethane at room temperature. The ring specimen was made of ferritic steel. The ram and support post used high strength steel as a rigid support. The material properties are listed in Table 1. The geometry of the components of the expanded plug testing system in Fig. 2 was modeled with respect to the current test setup. The ring length was simulated as 0.28 in., the outer diameter (OD) of the ring was 0.37 in., and the inner diameter (ID) was 0.326 in. The plug length was set to 0.296 in., and the plug OD was 0.325 in. Hence the initial gap in Fig. 6 between the ring specimen and the expansion plug was 0.0005 in. Pressure load was applied to the top of the ram, while the bottom surface of the support post was constrained in six degrees of freedom (DOF). A general contact was defined as being between the outer surface of the cylindrical expansion plug and the inner surface of the ring specimen.

Table 1. Material properties of components with bi-linear material model of expansion plug

	Young's modulus (psi)	Tensile yield stress (psi)	Poisson's ratio
Polyurethane [a]	69,618	20,015	0.476
Ferritic steel [b]	2.9×10^7	45,000	0.3
High strength steel [c]	3.0×10^7	280,000	0.28

[a] Zhenyuan, "Behaviors of polyurethane filled double skin steel tubular members," *Applied Mechanics and Materials* 94; Efunda, "Material Properties."
[b] AK Steel, "430 Stainless Steel Product Data Sheet"
[c] Thrash, *Southwire Company Overhead Conductor Manual*.

In Table 1, it can be seen that the hyperelastic material polyurethane was simplified as perfectly elastic plastic material (bilinear model) per literature. Due to the lack of hyperelastic data for polyurethane at this

first stage of the study, the FEA simulation was carried on the bilinear material model for the expansion plug to obtain preliminary results and to guide further investigation.

Fig. 7 shows the von Mises stress distribution in the ring expansion clad testing system for the bilinear expansion plug material model. Maximum stress occurred in the cladding for the whole system. The stress distributed nonuniformly in the clad. In this case the pressure load was 7,000 psi. Contact pressure inside the inner surface of the ring specimen also shows nonuniform distribution in Fig. 8.
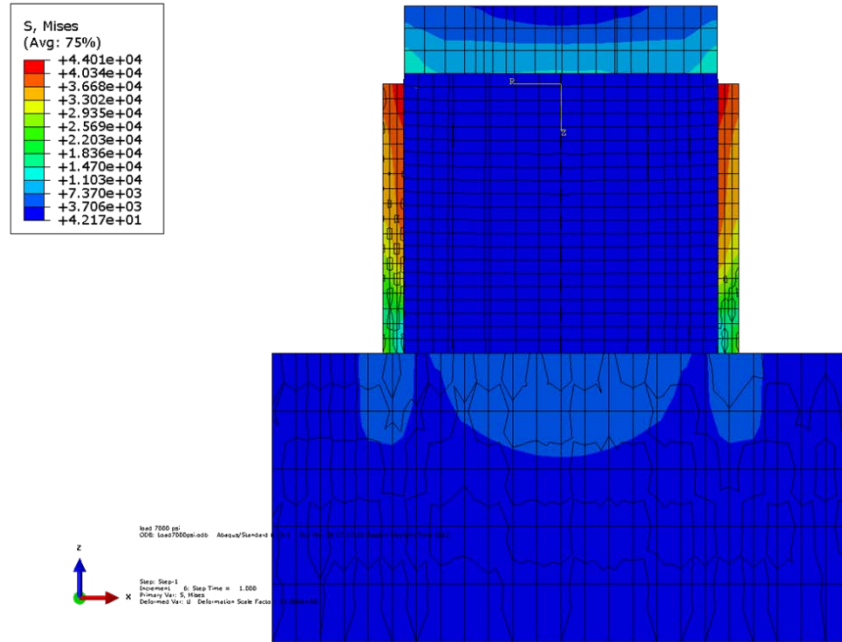
Fig. 7. Nonuniform stress distribution in the clad for FEM with the bi-linear material model of polyurethane.
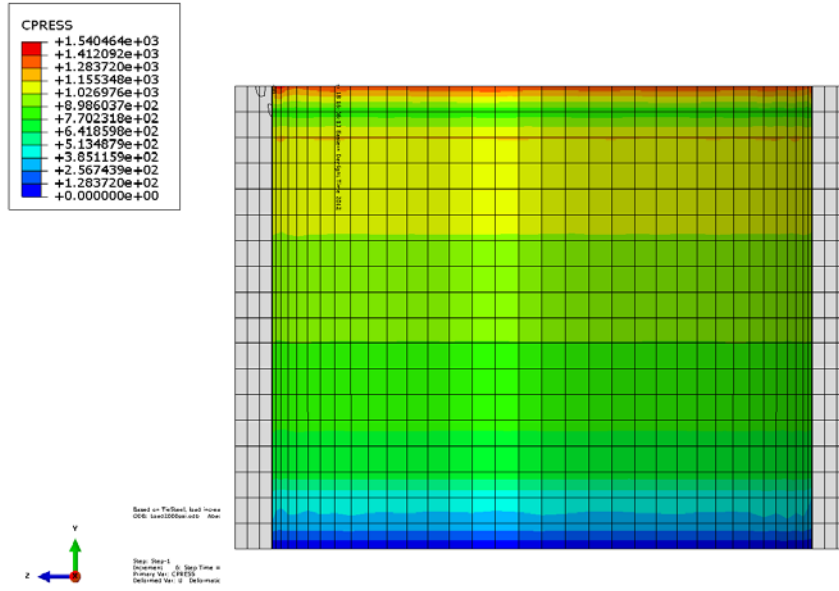
Fig. 8. Nonuniform contact stress in the clad for FEM with the bi-linear material model of polyurethane.

Fig. 9 and Fig. 10 show complex stress fields in the cladding during a plug extension test and can no longer resemble simple pressure capsule stress distributions based on thin-walled cylinder theory. Shear

stress σ_{RZ}, radial stress σ_{RR}, circumferential stress (hoop stress) σ_{TT}, axial stress σ_{ZZ}, and von Mises stress all show gradient distributions through a cross section of the ring specimen. All these preliminary results indicate that the circumferential tensile properties test of the ring specimen using the current ORNL patented expanded plug method is much more complicated than the thin-walled cylinder and needs thorough investigation, especially for the hyperelastic material model of the polyurethane plug.
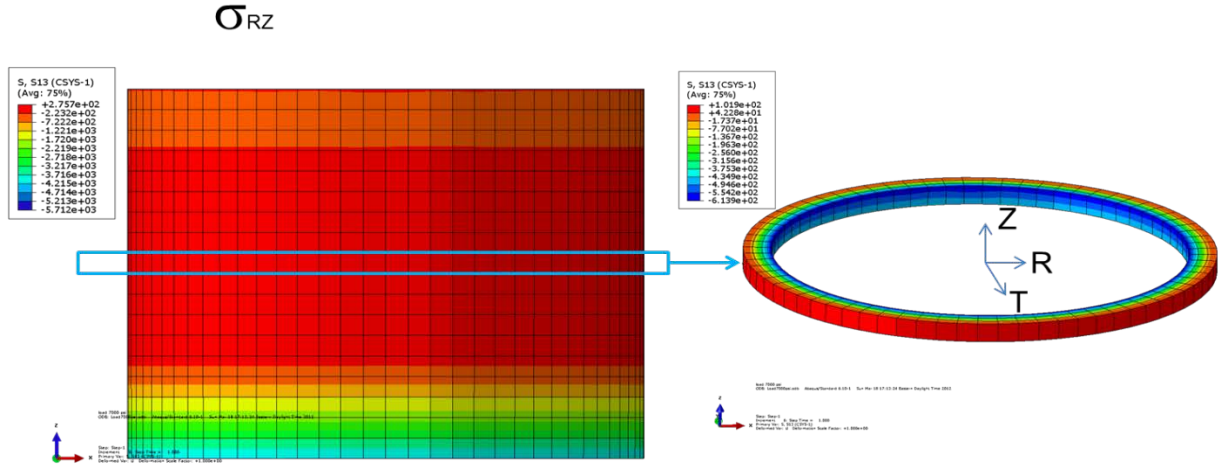
Fig. 9. Shear stress distribution in the clad for FEM with bi-linear material model of polyurethane.
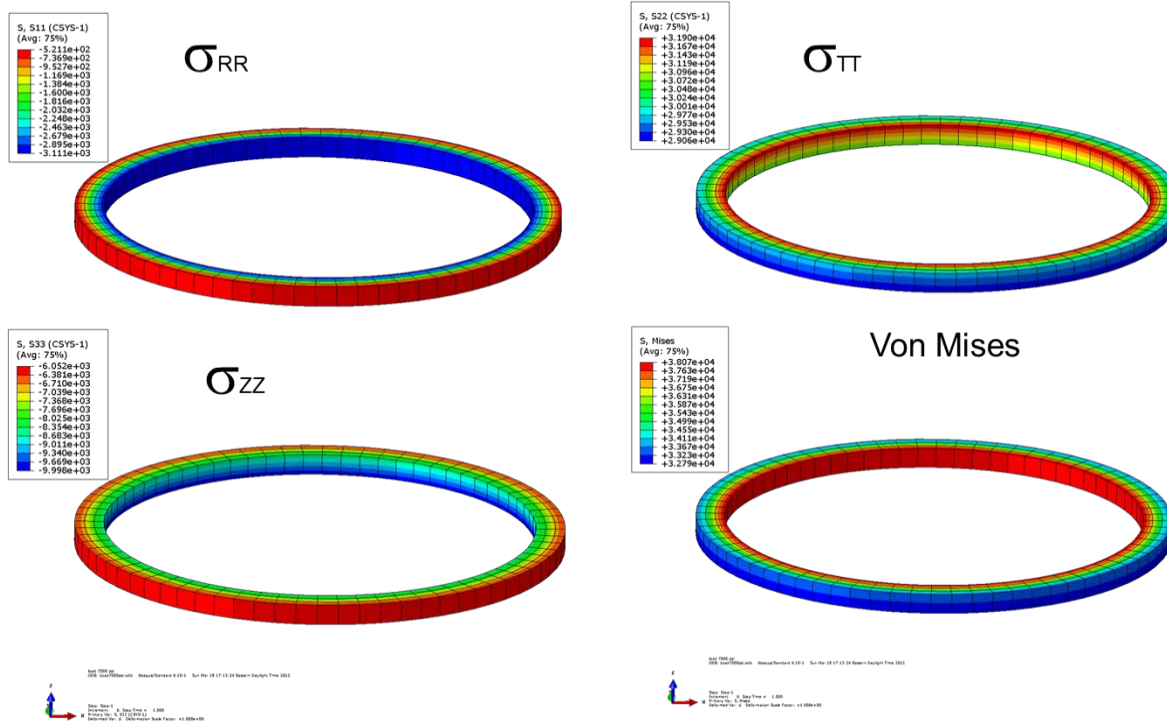
Fig. 10. Stress distribution at the midsection of the clad for FEM with bilinear material model of polyurethane.

3.1.2   Hyperelastic Material Model for Expansion Plug

The modified 3D FEM model of the ring expansion clad testing system (Fig. 6) was analyzed further in this study of the hyperelastic material model for a polyurethane plug, as shown in Fig. 11. To allow for direct comparison to existing test data and to validate simulation results, the material of the ring specimen

was a zirconium alloy known as M5. Polyurethane material was used for the expansion plug. High strength steel was still used for the ram and the support post. The geometry of the components was exactly as shown in Fig. 6. The boundary condition remained fixed at 6 DOF at the bottom surface of the support post. The load was 1040 lbf for testing an unirradiated M5 ring specimen at room temperature.
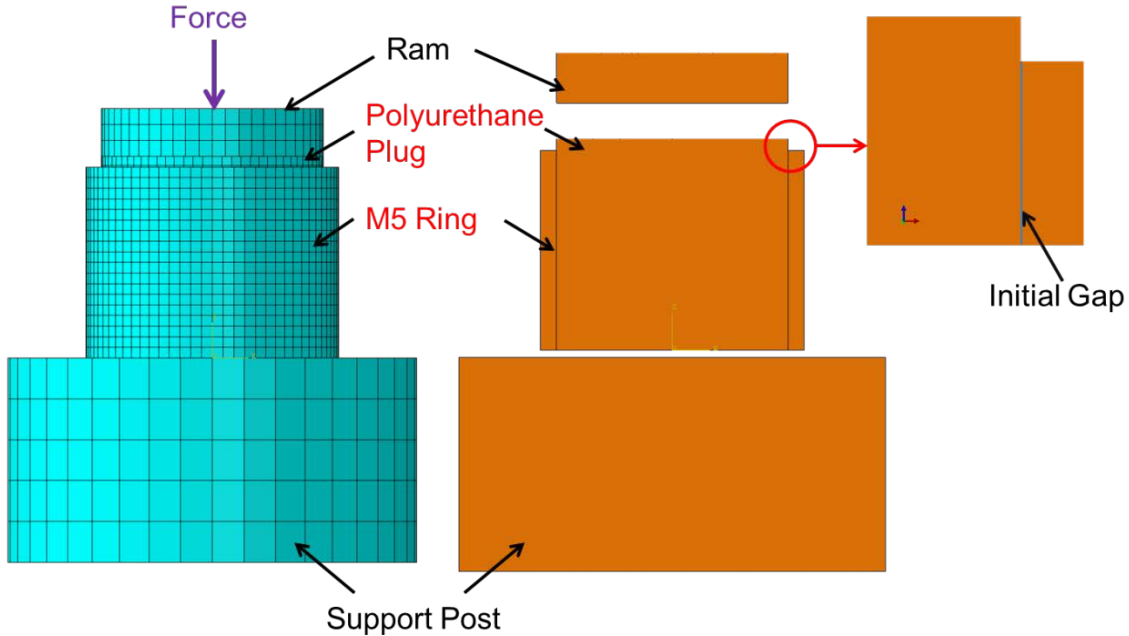
Fig. 11. 3D FEM model of ring expansion clad test system with hyperelastic material model for expansion plug.

For hyperelastic characterization of the polyurethane material, the hyperelastic material model in ABAQUS was used to simulate the material behavior of polyurethane during the ring expansion clad testing at room temperature. Fig. 12 shows an example of a typical final test data set for input into a curve fitter [12]. The objective of the testing was to define and satisfy the input requirements of the mathematical material models that exist in the structural nonlinear FEA model.
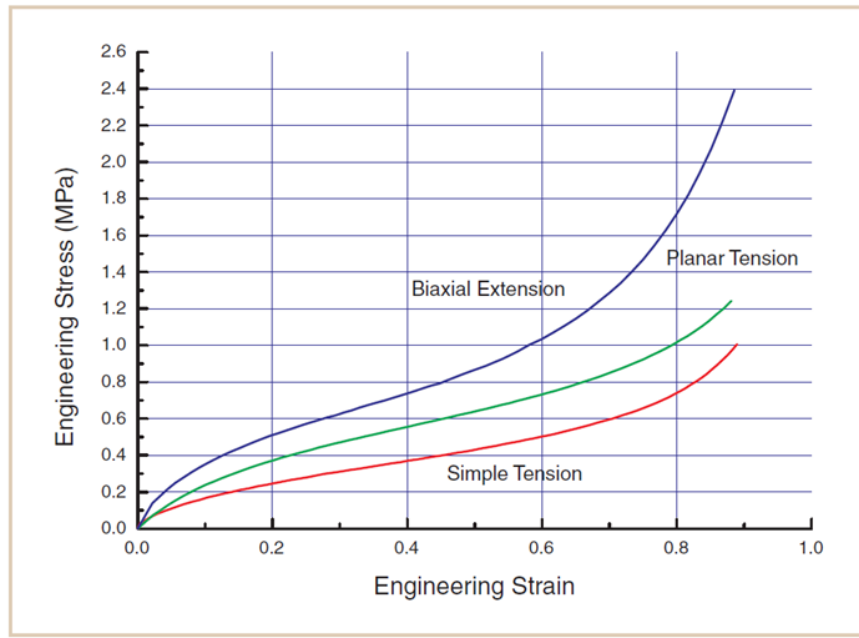
Fig. 12. Typical final data set for input into a curve fitter.

Two tests were identified for the test data set to generate hyperelastic material model parameters for the polyurethane plug: an unconstrained compressive test (or uniaxial compressive test, Fig. 13a) and a fully constrained compressive test (or volumetric test, Fig. 13b).

- The **uniaxial compression experiment** is popular for testing hyperelastic material. When testing for analysis, pure states of strain are desired, which is especially difficult to achieve experimentally in compression due to friction. Therefore, lubrication between the specimen and the platen is needed to reduce shear strain induced by friction.

- The **volumetric compression experiment** examines the compressibility of the material. A cylindrical specimen is constrained in a fixture and compressed (Fig. 13b).

In these tests, six polyurethane specimens with 0.358 in. diameters and 0.295 in. lengths were prepared: three for each type of test.

(a) Uniaxial compressive test   (b) Volumetric test

Fig. 13. Hyperelastic material properties testing for polyurethane plug.

Data from these tests are indicated by the blue line in Fig. 14. The test data were evaluated in ABAQUS/CAE using the hyperelastic model to determine the optional strain energy potential and to calibrate coefficients as an input parameter in the FEA model. Fig. 14 reveals that the strain energy potential form of Yeoh [13] as a hyperelastic material model is a good match with both unconstrained compressive test data and fully constrained test data. The three coefficients C_{10}, C_{20}, and C_{30} of deviatoric behavior for the Yeoh form, calibrated from unconstrained uniaxial test data (Fig. 14a), are 1319, -708, and 699, respectively. The compressibility of polyurethane needs to be specified. If the material is considered incompressible, the three coefficients of compressibility—D_1, D_2, and D_3—can be defined as zeros. However, polyurethane exhibits nearly incompressible material behavior, so the coefficients D_1, D_2, and D_3 are computed from volumetric test data (Fig. 14 b) as 1.296×10^{-5}, 5.648×10^{-7}, and -4.362×10^{-8}, respectively. The other strain energy potential of the Marlow form uses unconstrained and constrained test data directly. Therefore, in the following study, both the Yeoh and the Marlow forms were used in the FEA model as hyperelastic material behavior for the polyurethane plug.

(a)　　　　　　　　　　　　　　　　　　　　(b)
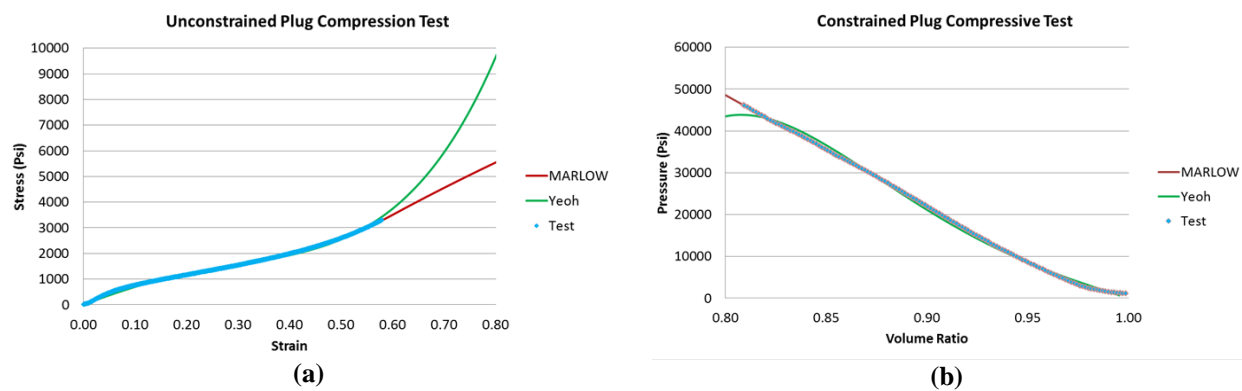
Fig. 14. Hyperelastic material property test data for polyurethane.

The material properties of components simulated in the system model in Fig. 11 are listed in Table 2. Unirriadiated M5 material properties are cited from Morris et al. 2012 [5], Chapter 8 "Cladding mechanical testing." Fig. 15 illustrates the stress-strain curve for unirradiated M5 cladding obtained from a tensile test also cited in Fig. 193 of Morris et al. 2012 [5]. Table 3 is also taken from Table 57 in Morris et al. [5], summarizing tensile properties for unirradiated M5 cladding tube tests. The ultimate strength of unirradiated M5 cladding is up to 74.3 ksi. Strain hardening data were generated on the basis of tensile test data, and they were entered into the FEA model as plastic material behavior of M5 during the ring expansion test simulation.

Table 2. Material properties of components with hyperelastic material model of expansion plug

	Young's modulus (psi)	Tensile yield stress (psi)	Poisson's ratio
Unirradiated M5 [a]	1.312×10^7	55,800	0.326
High strength steel [b]	3.0×10^7	280,000	0.28
Polyurethane	Hyperelastic Yeoh form:		

	C10,	C20,	C30,	D1,	D2,	D3
	1319,	-708,	699,	1.296e-5,	5.648e-7,	-4.362e-8

Hyperelastic Marlow form: use test data

[a] Morris, *MOX PIE Fuel and Clad Examination Final Report*.
[b] Thrash, *Southwire Company Overhead Conductor Manual*.
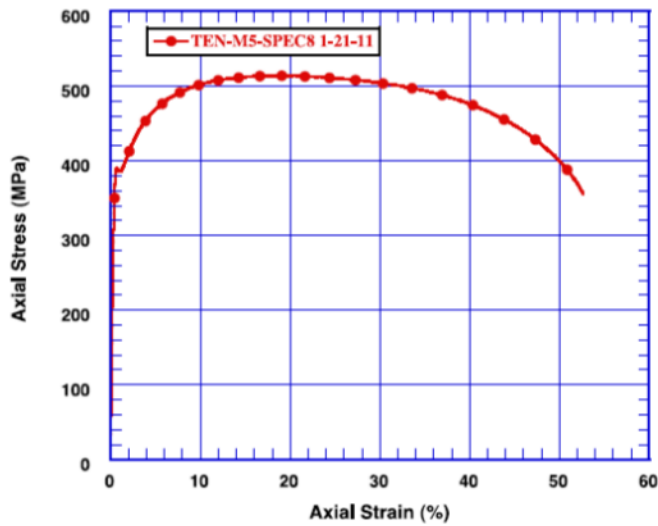
Fig. 15. Stress-strain curve for unirradiated M5 cladding from tensile test cited [5, Fig. 193].

Table 3. Tensile properties summary for unirradiated M5 cladding tube tests cited [5, Table 57]

Specimen	Elastic Strain Rate (s⁻¹)	Yield Strength (MPa)	(ksi)	Ultimate Strength (MPa)	(ksi)	Elastic Modulus (GPa)	(ksi)	Uniform Elongation (%)	Total Elongation (%)
TEN-M5-SPEC5	0.000551	391.4	56.8	517.6	75.1	91.77	13309.8	16.5	48.4
TEN-M5-SPEC6	0.000530	392.8	57.0	516.9	75.0	95.59	13864.2	16.3	49.0
TEN-M5-SPEC7	0.000360	386.3	56.0	514.4	74.6	88.25	12799.2	17.7	51.1
TEN-M5-SPEC8	0.000348	386.2	56.0	513.9	74.5	89.59	12992.9	18.9	52.6
TEN-M5-SPEC9	0.000104	376.1	54.5	506.8	73.5	85.54	12406.3	18.9	54.3
TEN-M5-SPEC10	0.000099	377.6	57.4	505.9	73.4	92.02	13346.6	18.3	53.4
Average		385.1	55.8	512.6	74.3	90.46	13119.8	17.8	51.5
Std Dev		6.92	1.00	5.03	0.73	3.47	503.90	1.15	2.40

FEA results are shown in the following figures. Fig. 16 reveals that, at the end of the loading process, a polyurethane plug was pushed into the ring specimen. The ring bulged out at the middle section. The von Mises stress distribution in the clad is not uniform. Maximum stress occurred in the clad within the whole system, which is similar to the result in Fig. 7. The simulation results for FEM with the hyperelastic material model of polyurethane plug using the Yeoh form and the Marlow form are very close to each other, which indicates that the hyperelastic material model is reliable.
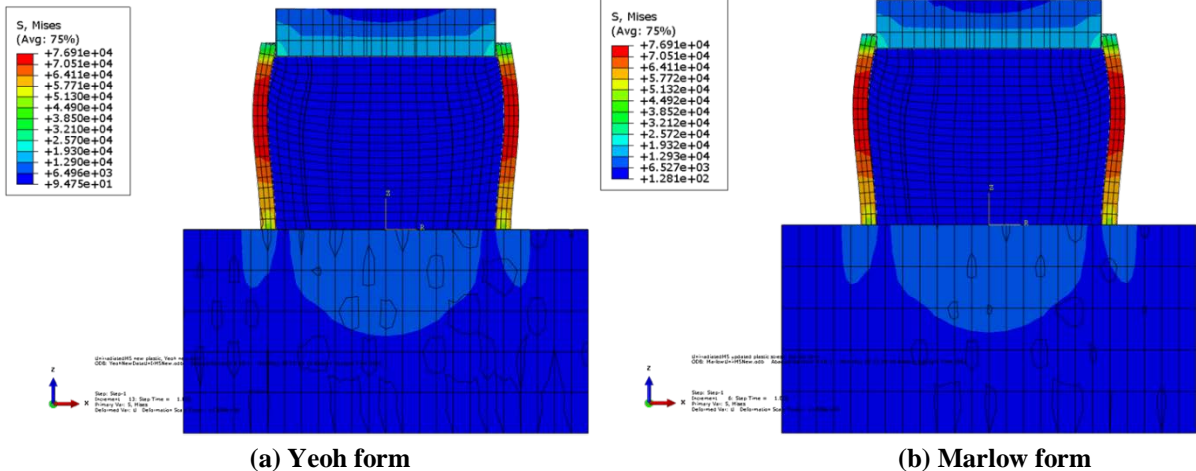
(a) Yeoh form **(b) Marlow form**

Fig. 16. Nonuniform stress distribution in the clad for FEM with hyperelastic material model of polyurethane plug.

Fig. 17 shows nonuniform contact stress distribution in the clad for FEM with the hyperelastic material model of the polyurethane plug. Fig. 18 shows the radial dilatation distribution in the clad along the gage section. The hyperelastic material model using the Yeoh form or the Marlow form does not exhibit much difference in the resultant strain, either. Radial strain results in highly nonuniform distribution. Maximum strain occurs at the ring bulge-out section. Compared to the test of the unirradiated M5 ring specimen at room temperature (Fig. 19), the simulation results show a very close deformation shape.
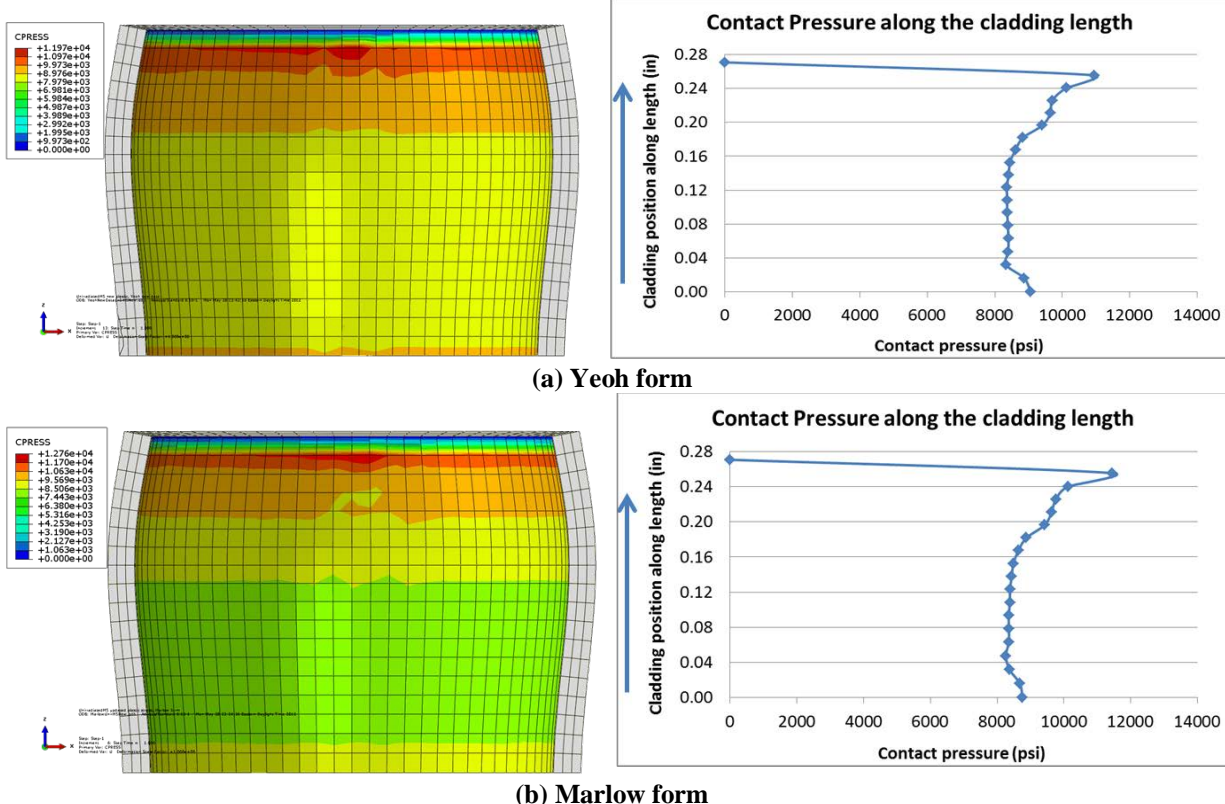
(a) Yeoh form

(b) Marlow form

Fig. 17. Nonuniform contact stress distribution in the clad for FEM with a hyperelastic material model of the polyurethane plug.

30

(a) Yeoh form

(b) Marlow form
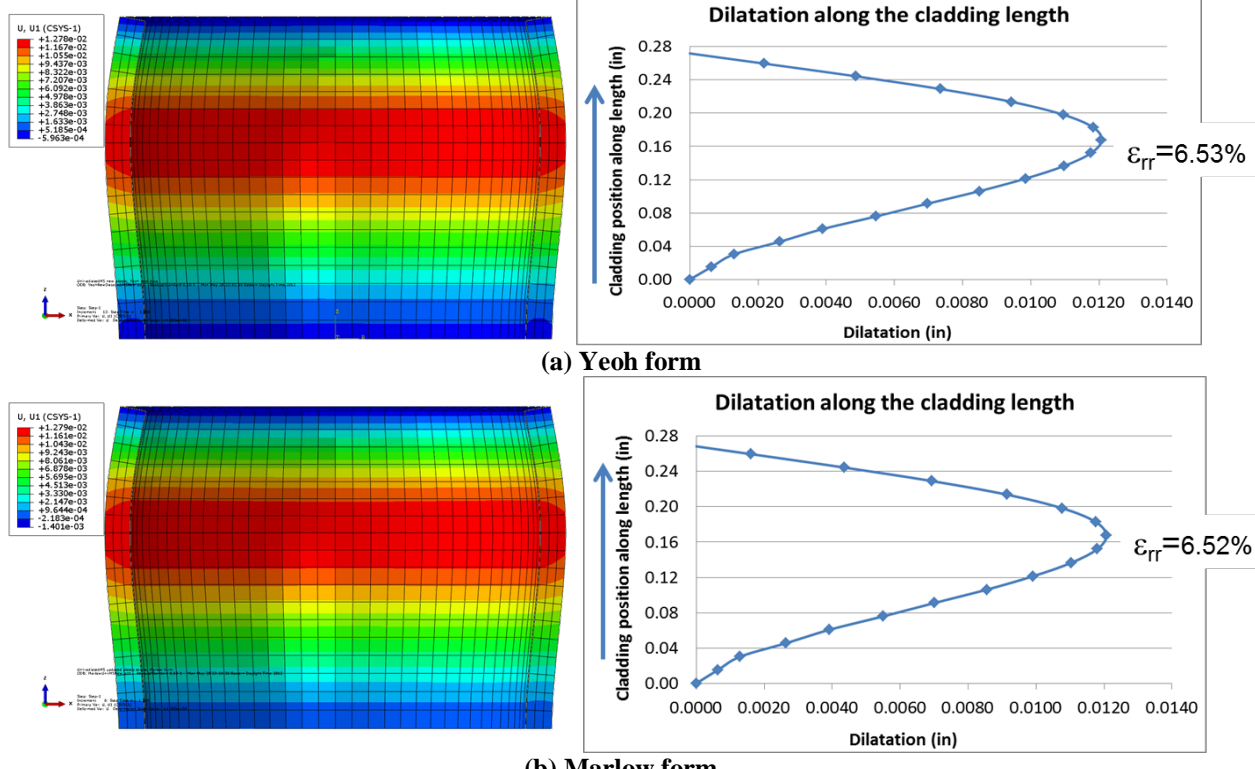
**Fig. 18. Nonuniform radial dilatation in the clad for FEM with
a hyperelastic material model of the polyurethane plug.**
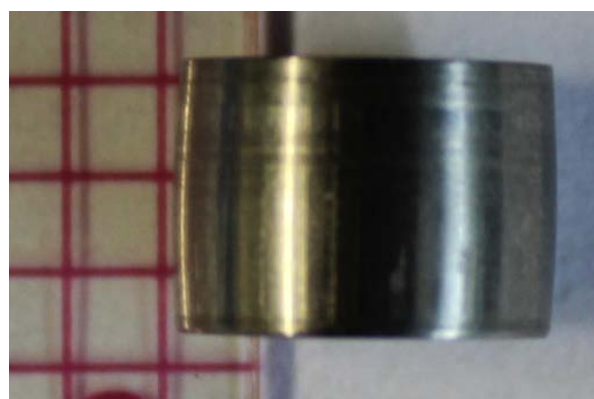
**Fig. 19. Tested unirradiated M5 ring
specimen at room temperature.**

In ring expansion plug clad testing, the increase in diameter of the specimen was continuously monitored and recorded using noncontacting proximity transducers (Fig. 20). The test apparatus used four proximity transducers to provide greater precision in the measurement of ring expansion and, therefore providing greater accuracy in the strain measurement. The specimen's increase in diameter was used to calculate the circumferential strain accrued during the test. Tested radial dilatation of the unirradiated M5 specimen was compared with the FEA results (Fig. 18) in Table 4. The FEA results match the test data very well, within 3% deviation. This validates that the 3D FEM model in Fig. 11 with the hyperelastic material model of the polyurethane plug can be used to represent the ring expansion clad testing system and to evaluate the existing expanded plug method for mechanical property testing using FEA.

31
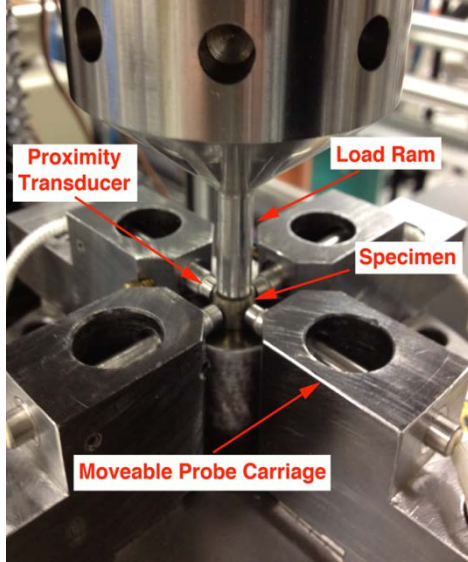
Fig. 20. Test setup for ring tensile testing using proximity transducers.

Table 4. Radial dilatation of unirradiated M5 specimen comparison between test and FEA

	Max radial dilatation (%)
Unirradiated M5 ring test raw data[a]	6.34
Unirradiated M5, hyperelastic material model of Yeoh form (Fig. 18)	6.53
Unirradiated M5, hyperelastic material model of Marlow form (Fig. 18)	6.52

[a] Morris, *MOX PIE Fuel and Clad Examination Final Report*.

Fig. 21 illustrates a true hoop stress-strain curve of unirradiated M5 cladding from FEA results. Hoop stress and strain data were selected from three locations through the cross section: the out node, middle node, and in node (Fig. 21). Hoop stress in the middle circle of the ring specimen matches the tensile test data very well, while hoop stresses in the inner circle and the outer circle are close to tensile test data in the elastic region. In the plastic behavior region, the inner circle of the ring specimen experiences much lower hoop stress than the tensile test indicates. On the other hand, the outer circle of the ring specimen exhibits higher hoop stress than the test. Mixed modes in the cladding caused the complexity of the stress distribution. Fig. 22 illustrates the FEA axial stress-strain curve of unirradiated M5 cladding. Significant compressive stress is observed in the inner circle of the cladding.
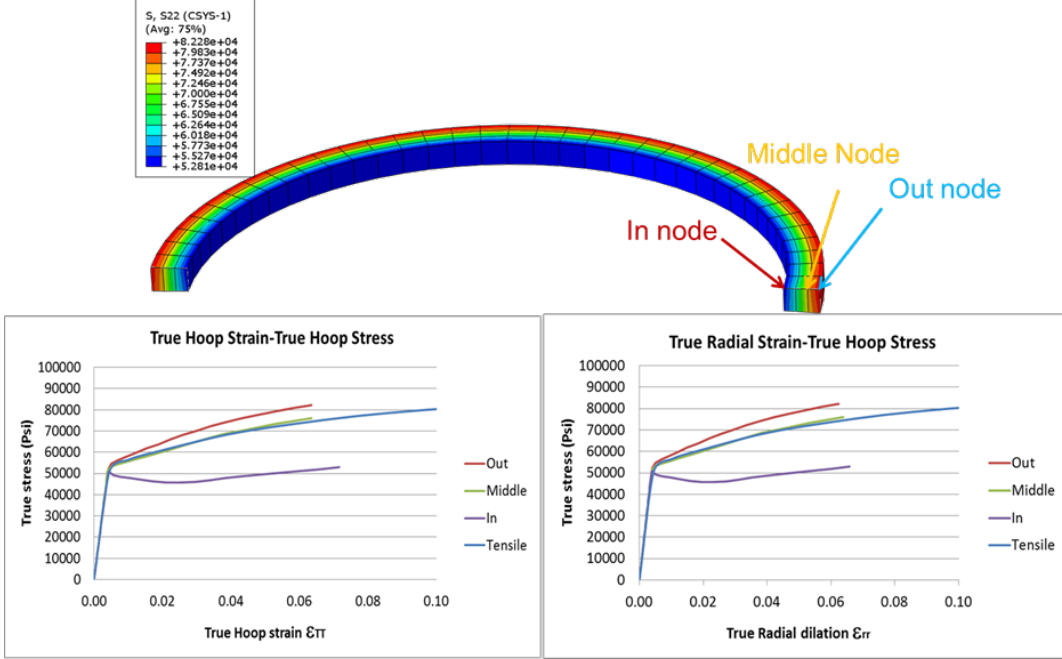
Fig. 21. FEA true hoop stress-strain curve of unirradiated M5 cladding vs. tensile test data.
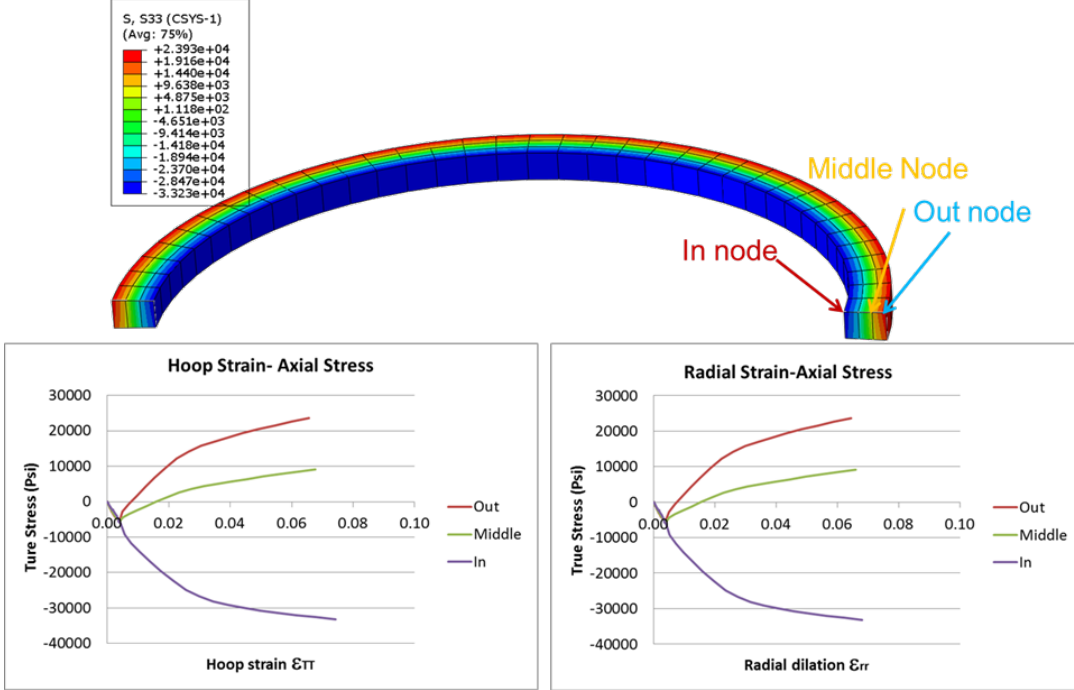
Fig. 22. FEA axial stress-strain curve of unirradiated M5 cladding.

Table 5 shows the stress range in unirradiated M5 cladding from the FEA results. Due to nonuniform distribution, the stress exhibits a wide range, especially the hoop stress σ_{TT} and the axial stress σ_{ZZ}. Significant compressive stress for σ_{ZZ}, -32 ksi, was induced by clad bending deformation due to the clad bulging or barreling effect. The barreling effect caused very large localized shear stress in the clad wall; max shear stress = $(\sigma_{TT} - \sigma_{ZZ})/2 = (53.3 + 32.7)/2 = 43$ ksi. This will result in the testing material having a high risk of shear failure.

Table 5. True stress range in unirradiated M5 cladding from FEA results

	σ$_{RR}$ (ksi)	σ$_{TT}$ (ksi)	σ$_{ZZ}$ (ksi)	σ$_{RZ}$ (ksi)	von Mises (ksi)
Hyperelastic material model, Yeoh form	-7.46 ~ -1.32	53.3~82.5	-32.7~23.8	0.80~1.95	76.9~74.4
Hyperelastic material model, Marlow form	-7.51 ~ -1.32	53.8~82.4	-32.2~23.4	0.81~1.98	76.9~74.5

As shown in Fig. 23a, inside the pressurized cylinder, the axial stress is in tension on the basis of thin-walled cylinder theory. However, significant compressive stress profiles were observed in the expansion plug's tested clad. Compressive stress in cladding can further induce lateral expansion of the clad wall, in addition to that induced by the internal pressure from the plug's lateral expansion. Therefore, the sources of lateral expansion in a plug expansion test include two parts: (1) internal pressure induced by plug lateral expansion and (2) lateral bulging deflection induced by compressive/tension bending stress in the clad and minor lateral shear stress at inner clad wall (Fig. 23b).

(a) Pressurized cylinder
(axial stress is in tension)
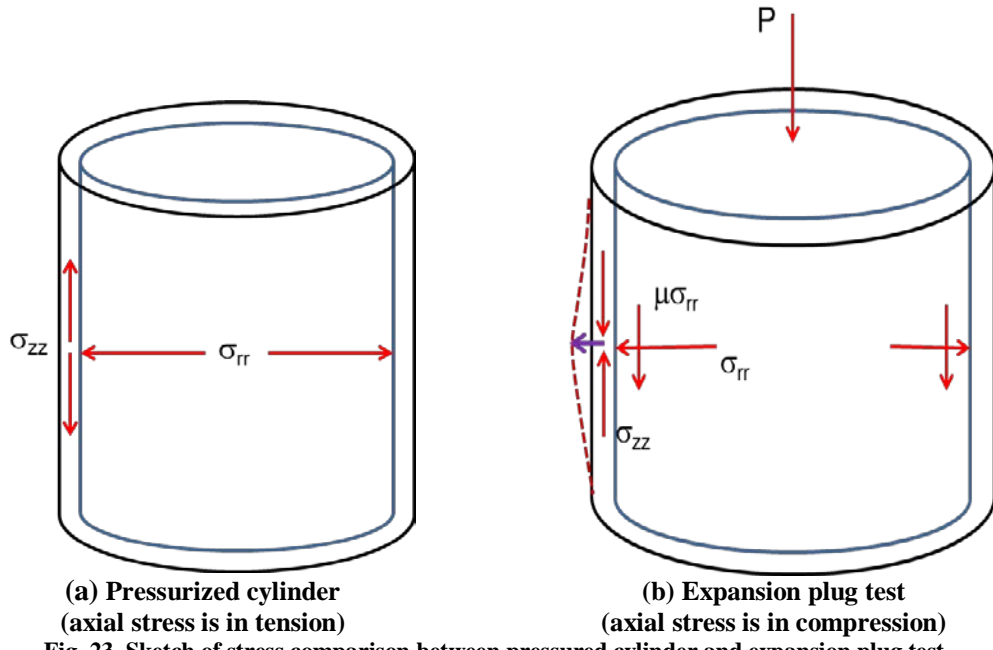
(b) Expansion plug test
(axial stress is in compression)
Fig. 23. Sketch of stress comparison between pressured cylinder and expansion plug test.

Fig. 24 shows Mohr's circles for determining localized failure contour. Mohr's circles demonstrate that shear failure could be the dominant failure mode of the expansion plug test. In a typical pressurized cylinder stress profile, as shown in Fig. 24a, hoop stress is about two times that of axial stress for a thin shell. However, in a typical expansion test clad stress profile, hoop stress is about three times that of axial stress, and axial stress becomes compressive stress (Fig. 24b). Based on the above finding, the maximum shear stress for an expansion plug test would be much greater than that of a typical pressurized vessel, so the expansion plug's tested clad can result in a shear failure with the fracture plane at 45° to that of axial orientation, as indicated in Fig. 25 for failure samples from Jaramillo et al. 2006 [14]. This is in contrast to the conventional pressure vessel rupture test, in which the axial split fracture is normally observed (Fig. 26), reproduced from the International Atomic Energy Agency (IAEA) Nuclear Energy Series No. NF-T-2.1 [15]. Therefore, the shear failure mode could be the dominant failure mode in the expansion plug test.
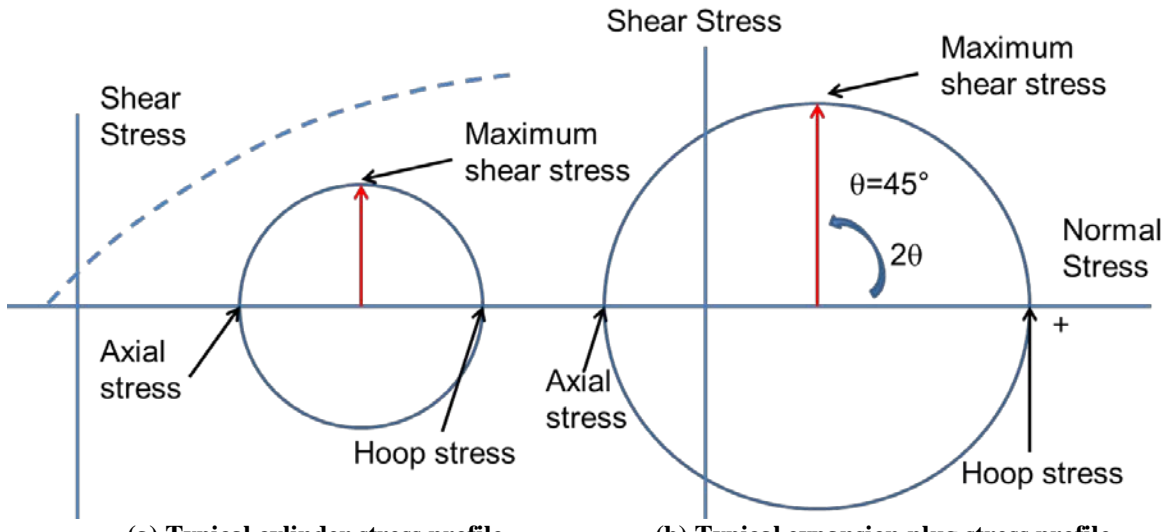
(a) Typical cylinder stress profile   **(b) Typical expansion plug stress profile**
Fig. 24. Mohr's circles demonstrate the potential shear failure.
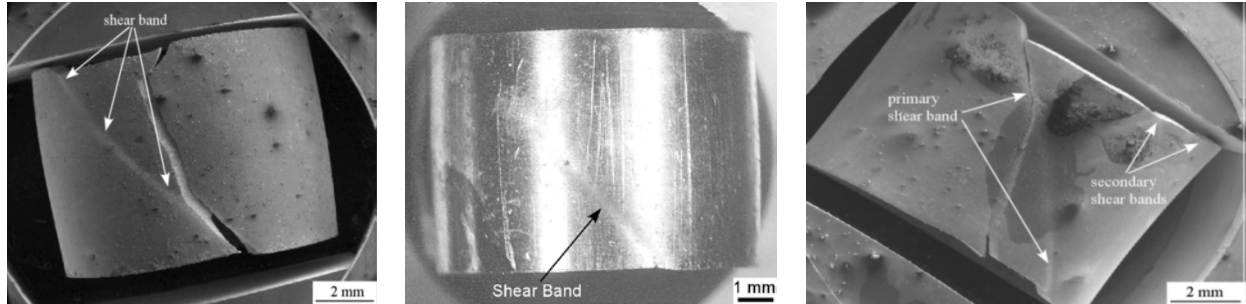
Fig. 25. Fuel cladding failed samples [14].
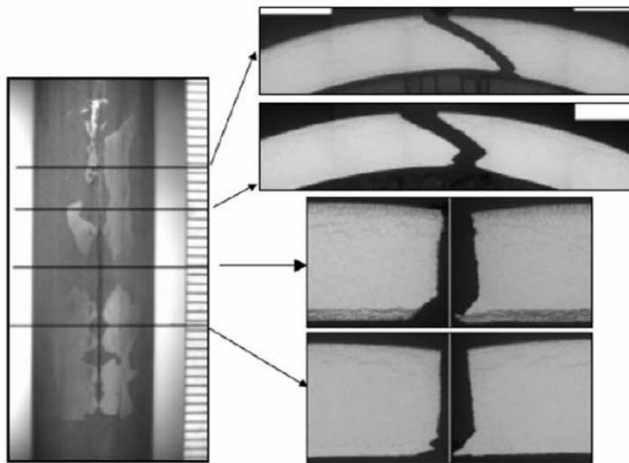
FIG 5.50. Visual appearance and cross-sectional metallography of a failed segment rod (irradiated five cycles, RTP: 446 W/cm, failed after 22 min hold).

Fig. 26. Typical axial splitting in high-burnup clad [15].

Unirradiated M5 ring test raw data (James G. Hemrick, ORNL) is shown in Fig. 27. Following the general procedure discussed in Sect. 1.2, the raw test data were processed (Fig. 28). Ring specimen thickness was 0.0215 in., and ring specimen axial length (gage length) was 0.2815 in. Yield stress used

unirradiated M5 tensile tube test data, 55.8 ksi. The load at 0.2% plastic strain offset in the test was identified as 950 lbf. Based on equation (3) shown in Sect. 1 [3], the calculated Γ-factor was 0.36, which is very different from the supposed constant Γ-factor of 0.53 [3]. This resultant Γ-factor contradicts the general procedure defined in "Custom Pressure Vessels" [3]. This scaling parameter is intended to be used to convert load to stress in the expanded-plug loading test. It is not related specifically to the material being tested, so the value of Γ-factor can be taken as a constant applied to test data from other material, as cited from "Custom Pressure Vessels" [3]. However, when this procedure was implemented, it was discovered that Γ-factor is dependent on the material and geometry, so it is not necessarily constant for different materials.

Fig. 27. Unirradiated M5 ring test raw data.

$$\Gamma = \frac{\sigma_{Yield}}{P_{Yield}} t l = 0.36$$

$t = 0.0215$ in
$l = 0.2815$ in
$\sigma_{Yield} = 55.8$ ksi (tensile data)
$P_{yield} = 950$ lbf
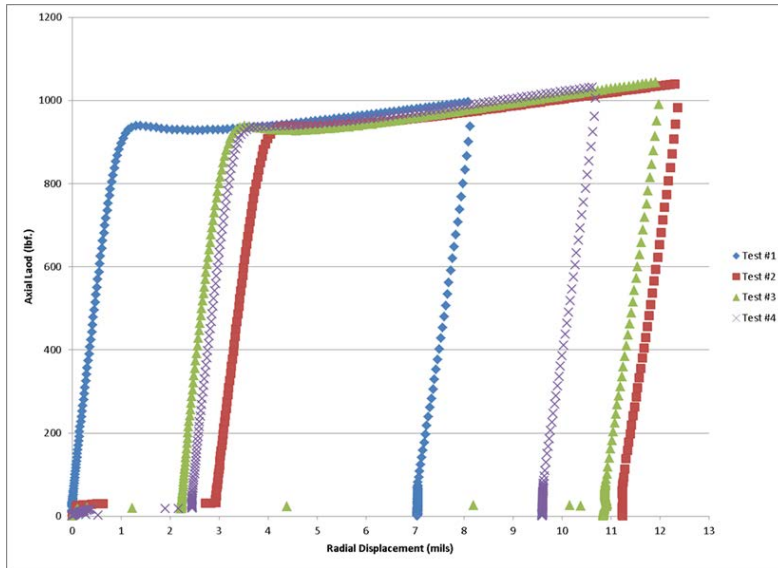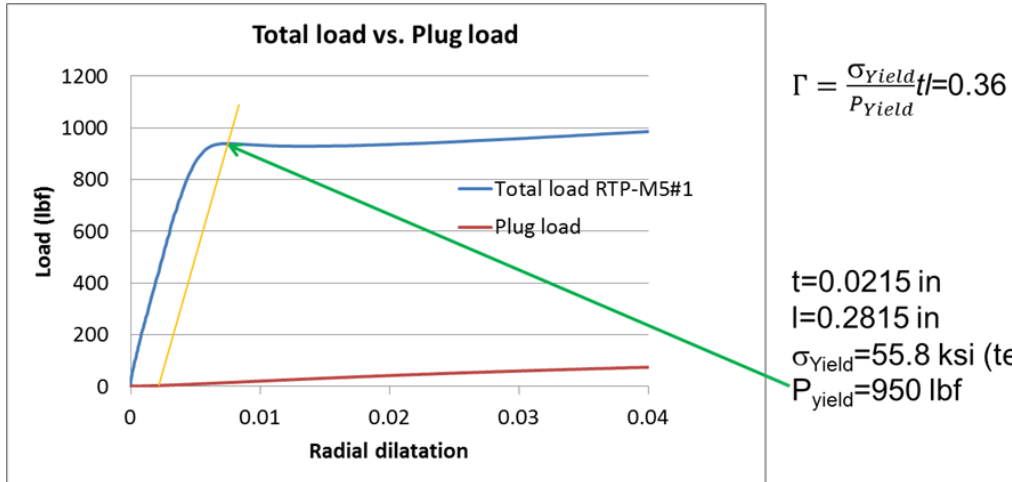
Fig. 28. Test data processing using general procedure.

Using the calculated Γ-factor, the load-circumferential strain data from the ring test was converted into material pseudo-stress-strain curves (Fig. 29). Based on this FEM study, the stress profiles in an expansion plug tested cladding (Fig. 21) are significantly more complicated than the simplified equation shown in Fig. 29 would indicate. The stress-strain curve from ring test data of the unirradiated M5 specimen appears much lower than the tensile test data. The other significant issue regarding the ring test

data is that the stress-strain curve does not show strain hardening characteristics. A ring test cannot run to ultimate yield strength.
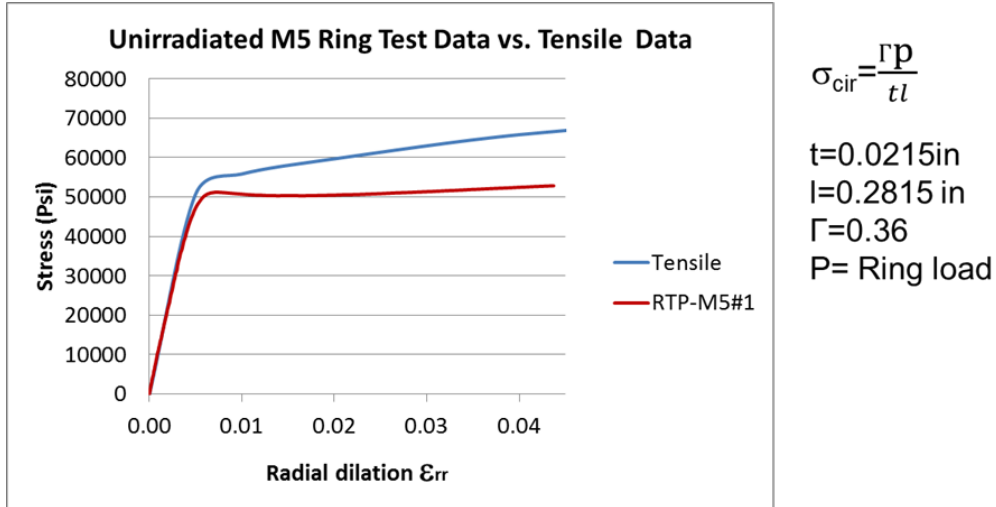
Fig. 29. Circumferential stress calculated from ring test data vs. tensile test data.

The circumference strain estimated from the expansion plug test overestimates the strain deformation according to the defined hoop stress. This is because the additional lateral expansion was contributed by the lateral (buckle) deformation induced by the compressive stress within the clad wall instead of by the compressive pressure induced by the deformed plug alone. This has been proven by previous round robin test results, as shown in Table 6 [16]. At room temperature, uniform elongation of ORNL data is significantly greater than those from other organizations.

Table 6. Summary of round robin test results

T (^{o}C)	Organization	Yield Strength (MPa)	Ultimate Strength (MPa)	Uniform Elongation (%)	Total Elongation (%)	Meas. Total Elongation (%)
20±2	ANL	698±7	767±8	2.1±0.5	8±1	----
32	CEA	667±15	767±3	3.0±0.3	23±0	----
RT	EdF	707±15	782±0	1.6±0.1	17±0	----
RT	JAERI	708±15	807±1	3.8±0.2	41±0	37±3
33	RRC-KI/RIAR	TBD[a]	TBD[a]	TBD[a]	TBD[a]	----
RT	ORNL	703±8[b]	>793[b]	>8[b]	a	a

(a) Was not measured in ORNL tests
(b) Was estimated in ORNL tests

The defined hoop stress obtained from the simplified scale factor approach significantly underestimates the true combined stress fields experienced by an expansion plug tested clad system, as indicated by this FEM analysis. The above combined effects of the overestimated circumference strain plus the associated underestimated stress will result in nonconservative predictions in the strength and ductility of the tested clad, as well as the associated mechanical properties.

Furthermore, based on Jaramillo et al. 2006 [14], as shown in Fig. 30, the hoop stress ratio at or above the yield evaluated from scaling and thin/thick wall ID is about 1.2, which is roughly equal to the hoop stress/von Mises stress ratio obtained from FEM analysis. This indicates that the simplified equation used in the expansion plug underestimates the real stress field experienced by the expansion plug tested clad.
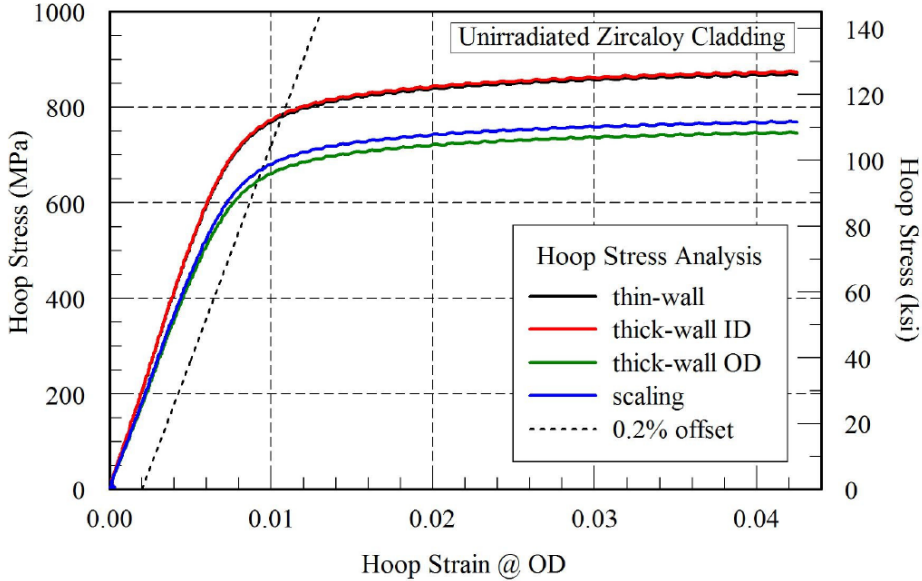
Fig. 30. Hoop stress-strain curves calculated using thin-walled pressurized cylinder, thick-walled pressurized cylinder, and uniaxial tensile test scaling method [14, Fig. 36].

When the existing expanded plug method for mechanical property testing is evaluated using FEA, the test failure mode involved with positive hoop stress, the negative axial stress, and the shear stress can result in a 45° shear failure for ductile materials. This is not normally seen in a pipe rupture scenario. The FEA proves that stress fields in a clad material induced by the expansion plug test can be quite complicated and do not resemble pressurized cylinder clad stress-strain behaviors. The compressive axial stress and shear stress in a plug-clad system cannot be ignored in the expansion plug test.

3.2   FEA OF ELEVATED TEMPERATURE (350°C) RING EXPANSION CLAD TESTING

Copper was selected as the expansion plug material for the expanded plug test to be conducted at the elevated temperature of 350°C. As shown in Fig. 31, the FEM model of the ring expansion clad test system with the copper plug at 350°C followed the room temperature model discussed in Fig. 11. The ring specimen in this FEA study was Zircaloy-4. The ram and support were still made of high strength steel. The geometry of the Zircaloy-4 ring specimen remained the same as that used with the unirradiated M5 specimen, while the geometry of the copper plug changed according to the test setup. The copper plug had a length of 0.29 in. and an OD of 0.324 in., which enlarged the initial gap to 0.001 in. Loading, boundary, and contact conditions remained the same as in the room-temperature model.
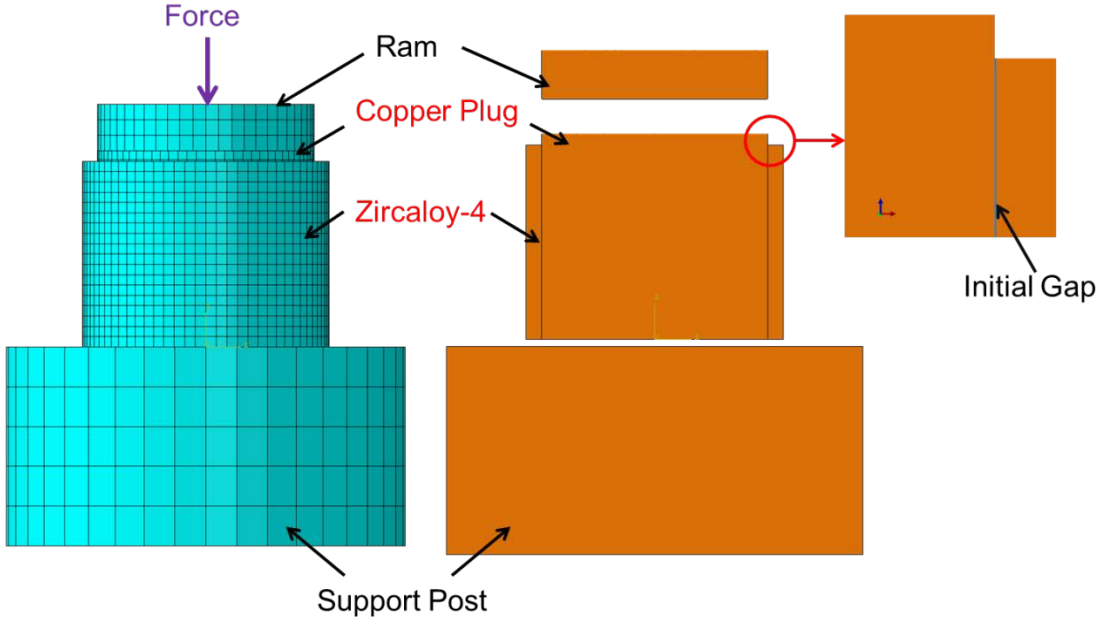
Fig. 31. 3D FEM model of ring expansion clad test system with copper plug at elevated temperature.

Fig. 32 shows the copper plug material property test data at 350°C (Hemrick). Data indicated highly plastic material behavior for copper at the elevated temperature. Therefore, the deformation plasticity material model in ABAQUS/CAE was chosen to simulate the copper plug's behavior during the expansion plug test at 350°C. Input parameters of the deformation plastic model were calibrated from test data. The component material properties are summarized in Table 7. Both unirradiated and irradiated Zircaloy-4 claddings were simulated, and results were compared side by side.
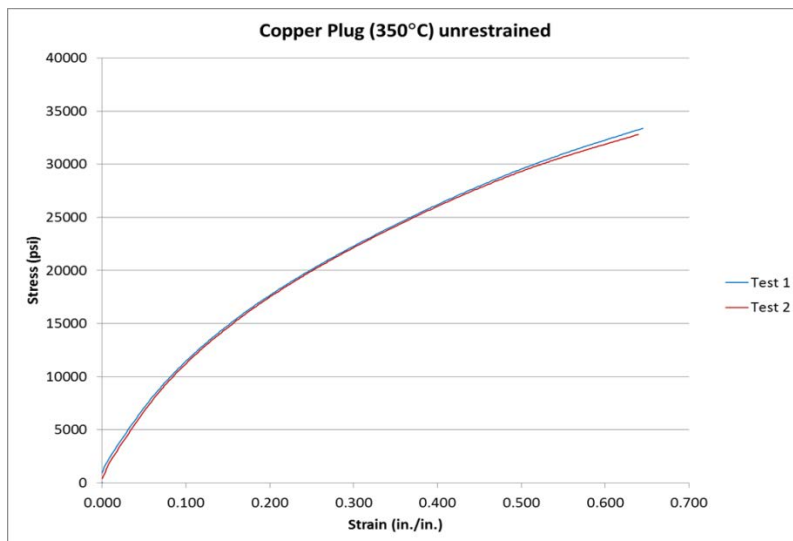
Fig. 32. Copper plug material property test data at 350°C.

Table 7. Summary of component material properties for FEA at elevated temperature

	Young's modulus (psi)	Poisson's ratio	Yield stress (psi)	Hardening exponent	Yield offset
Copper: deformation plastic model	153,000	0.306	5,000	1.18	0.2%
Unirradiated Zircaloy-4 at 350°C [a]	9.18×10^6	0.353	54,195		
Irradiated (1.20E+26 n/m²) Zircaloy-4 at 350°C [a]	10.4×10^6	0.353	88,993		
High strength steel	3.0×10^7	0.28	280,000		

[a] Wang, Progress Letter Report on U-Frame Test Setup and Bending Fatigue Test for Vibration Integrity Study (Out-of-Cell Fatigue Testing Development – Task 2.2)
[b] Thrash *Southwire Company Overhead Conductor Manual.*

Stress distribution in the ring expansion clad testing system at 350°C from FEA results is shown in Fig. 33. Typical load stresses for testing at 350°C were on the order of 45 ksi (ring hoop stress) for unirradiated AREVA material and 85 ksi for irradiated material tests. This corresponds to axial loads on the copper plug on the order of 2,300 lbf for unirradiated materials and 3,325 lbf on the irradiated materials . As in the room-temperature FEA results, the stress distribution is nonuniform, and Zr-4 rings bulge at the middle of the gage section. The stress distributions in both unirradiated and irradiated Zr-4 cladding appear to be similar. Table 8 summarizes the stress ranges resulting in Zr-4 cladding at 350°C. Irradiated Zr-4 cladding under higher loading experiences a higher stress level than unirradiated Zr-4 cladding. As in the room-temperature results, significant compressive stress was observed in σ_{ZZ}, which was induced by the clad bulging effect. Maximum shear = $(\sigma_{TT} - \sigma_{ZZ})/2 = (48,435+32,462)/2 = 40,448$ psi for unirradiated Zr-4 cladding.
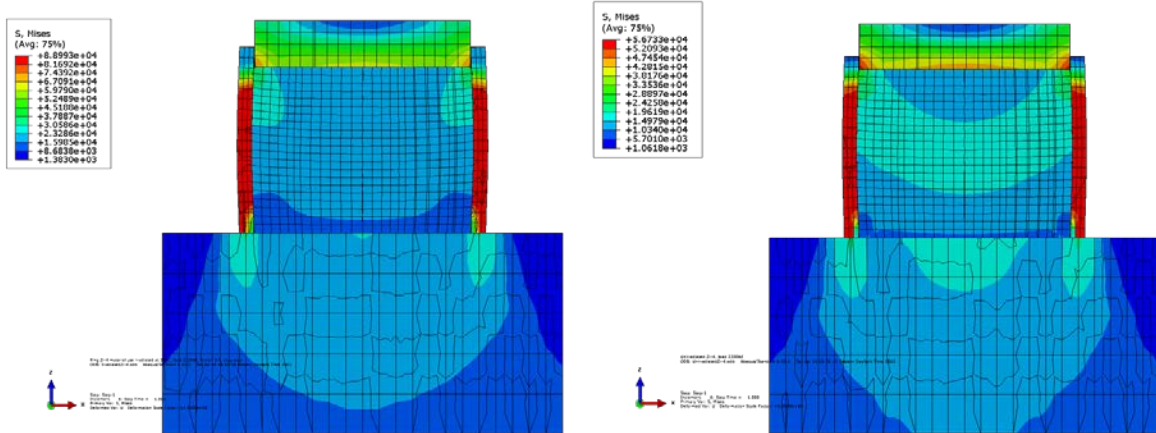
(a) Irradiated Zr-4 ring, load 3325 lbf   **(b) Unirradiated Zr-4 ring, load 2300 lbf**

Fig. 33. Nonuniform stress distribution in Zr-4 clad for FEM with deformation plastic material model of copper plug at 350°C.

Table 8. Stress range in Zircaloy-4 cladding from FEA results at 350°C

	σ_{RR} (psi)	σ_{TT} (psi)	σ_{ZZ} (psi)	σ_{RZ} (psi)	von Mises (psi)
Irradiated Zr-4	-7798~ -1273	48713~83191	-53180~ -9229	874~6011	88993
Unirradiated Zr-4	-4246~ -767	29649~48435	-32462~ -9374	674~3502	54195

Fig. 34 shows nonuniform contact stress distribution in Zr-4 clad for FEM with the deformation plastic material model of copper plug at 350°C. Fig. 35 shows nonuniform radial dilatation distribution along the gage length. FEA results are similar to those of unirradiated M5 cladding at room temperature. Maximum radial strain occurs at the cladding bulge-out section: 2.01% for irradiated Zr-4 cladding and 1.7% for unirradiated Zr-4 cladding. Fig. 36 shows the deformed test specimen. The ring specimen bulges at the middle of the gage section, similar to FEA. However, it was learned from the irradiated test that uniform elongation of the irradiated ring specimen is ~3.4%, which is much higher than the maximum FEM radial strain.

(a) Irradiated Zr-4 ring, load 3,325 lbf
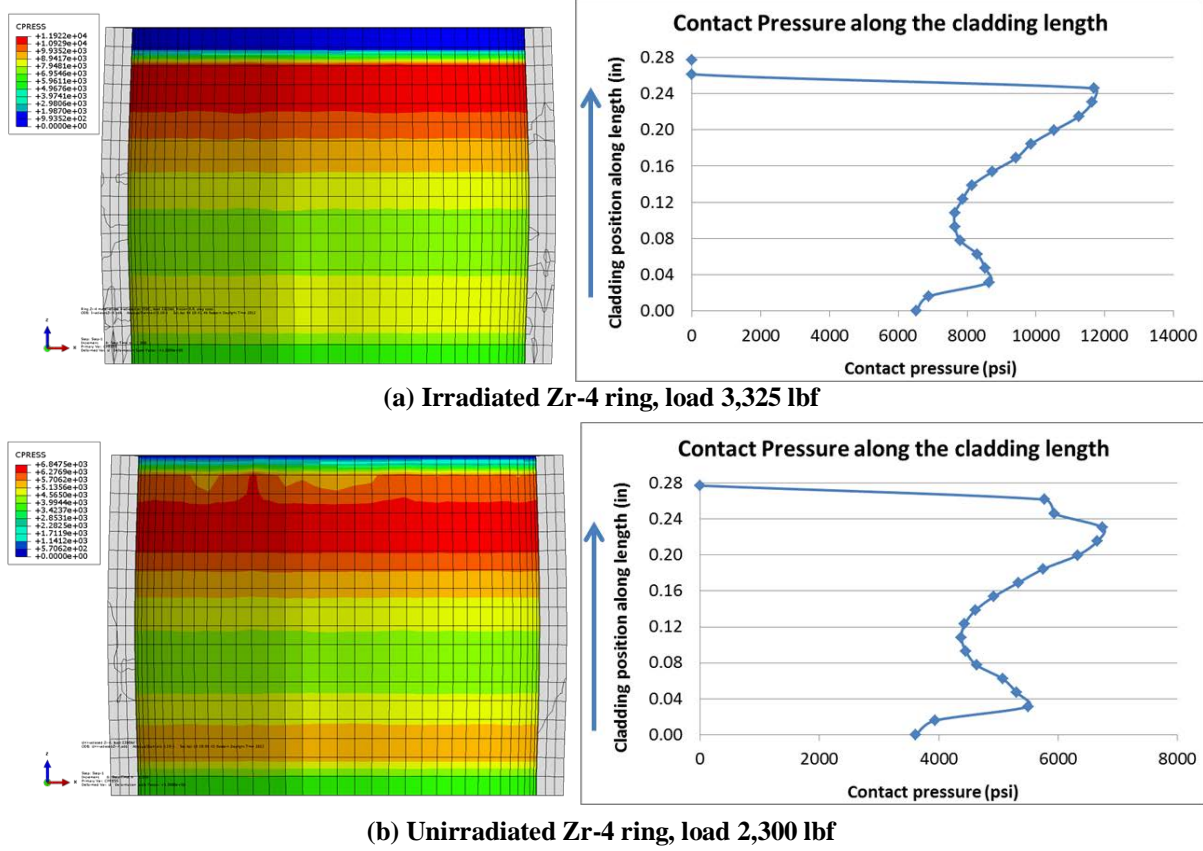
(b) Unirradiated Zr-4 ring, load 2,300 lbf
Fig. 34. Nonuniform contact stress distribution in Zr-4 clad for FEM
with deformation plastic material model of copper plug at 350°C.

41
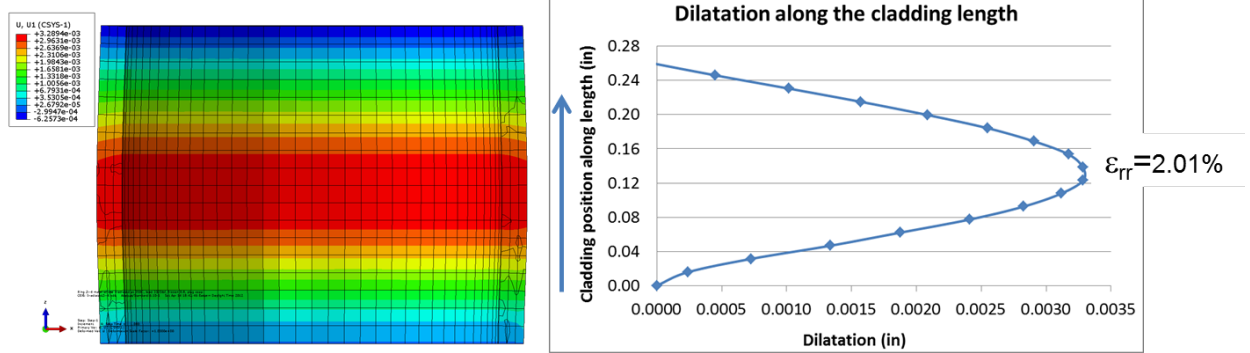
(a) Irradiated Zr-4 ring, load 3,325 lbf
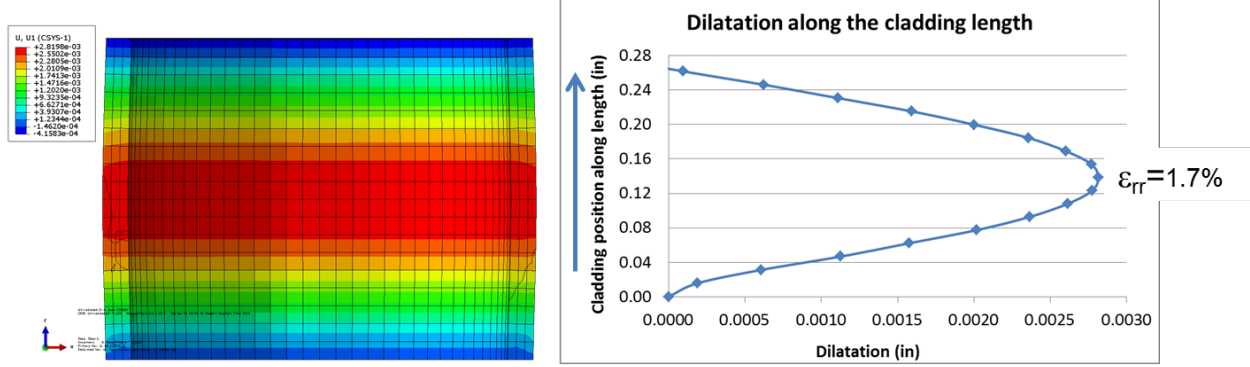
(b) Unirradiated Zr-4 ring, load 2,300 lbf
Fig. 35. Nonuniform radial dilatation in Zr-4 clad for FEM with deformation plastic material model of copper plug at 350°C.
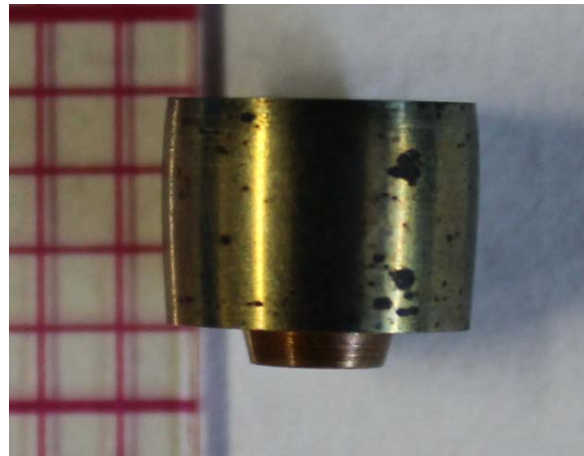
Fig. 36. Tested unirradiated ring specimen with copper plug.

4. DEVELOPMENT OF MODIFIED EXPANSION PLUG TESTING PROTOCOL WITH WEDGE INSERTS

Finite element simulations on the previously developed ORNL expanded plug test show significant nonuniform stress distribution and highly nonuniform radial dilatation in the expansion plug tested clad. The barreling effect produces significant bending stress into the clad wall—both tensile and compressive stress in the same cross section. This results in a very large localized shear stress field in the clad wall portion with compressive stress. To mitigate the mentioned deficiencies associated with the current expansion plug test, systematic studies have been conducted. A method has been established to improve the non-conservatism in the expansion plug test system. The modified expansion plug testing protocol was developed based on the new method.

4.1 DESIGN MODIFICATIONS OF THE EXPANDED PLUG TEST

There are three main differences between the proposed modified expanded plug test design and the previous design. The first proposed modification of the expanded plug test is to use aluminum as the material for the expansion plug instead of polyurethane (Fig. 37). The test design is as simple as the previous design. An axial compressive load is applied to a cylindrical plug of aluminum. As the plug is pressed down, it expands in the radial direction. In the process, radial extension of the outside ring of the test material can be obtained. As in the previous test, the load-circumferential strain data from the ring tests will be converted into material stress-strain curves in a separate procedure.
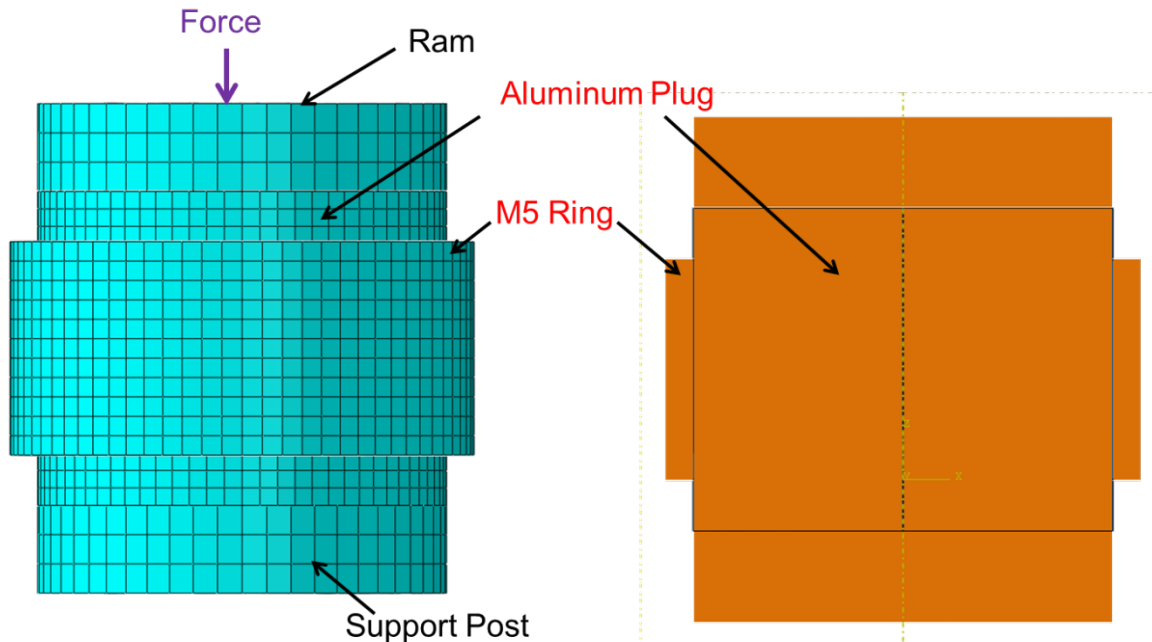
Fig. 37. FEM model of first proposed design modification.

The second proposed modification is to use a test specimen with a shorter axial length than that used in the previous design. A series of size effect studies was performed for the axial length of the clad and expansion plug. From these recent systematic investigations, an optimized length was determined that will produce a more uniform stress and strain distribution within the gage section. The third difference lies in the friction in the interface between clad and plug. Lubrication is considered in the interface in order to reduce the interfacial shear stress and the consequence of axial compressive stress.

In Fig. 37, the geometry of this first design modification model has been optimized in FEA. The length of the ring is shorter (0.17 in.), and the OD and ID of the ring are the same as in the current ORNL design (0.37 and 0.326 in. respectively). The OD of the plug is 0.326 in. The plug length is 0.25 in. The bottom surface was constrained to 6 DOF in the FEM model. Pressure load was applied on the top of the ram. The general contact was defined as between the outer surface of the expanded plug and the inner surface of the ring specimen. The friction in the interface between the clad and the plug were set to 0.04 [20] to simulate the lubrication effect. As in the previous studies, the ring material was unirradiated M5, the plug material was aluminum 6061-T6, and the ram and support were still high strength steel. The component material properties are listed in Table 9.

Table 9. Component material properties of the first design modification

	Young's modulus (psi)	Tensile yield stress (psi)	Poisson's ratio
Unirradiated M5 [a]	1.312×10^7	55,800	0.326
High strength steel [b]	3.0×10^7	280,000	0.28
Aluminum 6061-T6[c]	1.0×10^7	40,000	0.33

[a] Morris, *MOX PIE Fuel and Clad Examination Final Report.*
[b] *Thrash Southwire Company Overhead Conductor Manual.*
[c] Kaufman, *Properties of Aluminum Alloys: Tensile, Creep, and Fatigue Data at High and Low Temperatures.*

FEM simulation results exhibit apparent improvement in the stress and strain distribution at the gage section, as shown in Fig. 38 and Fig. 39. However, at the middle of the gage section, the ring specimen appears to shrink in instead of bulging out due to the impact of plug deformation. Therefore, the stress and strain distributions are not perfectly uniform to meet the design requirement.
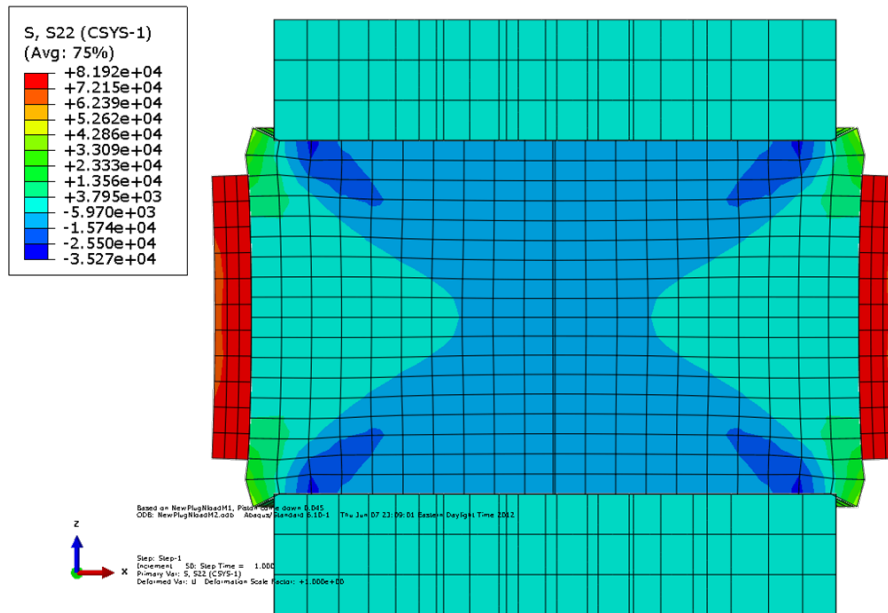
Fig. 38. Improved stress distribution in the clad for the first design modification.
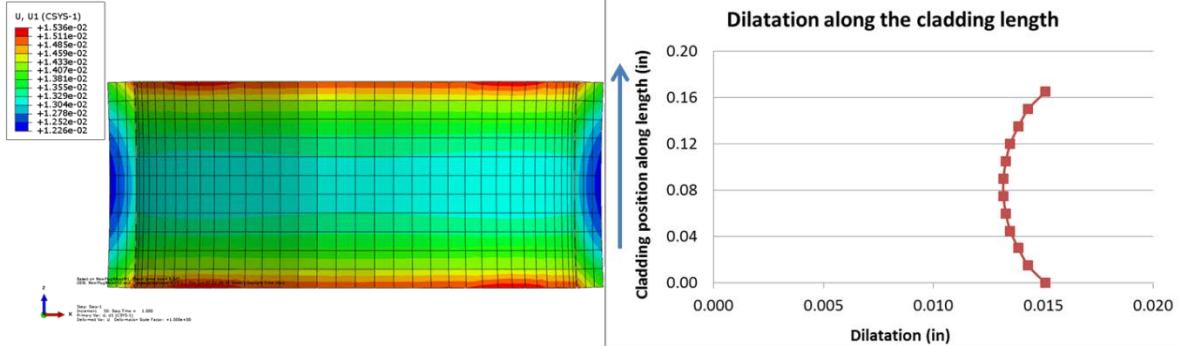
Fig. 39. Improved radial dilatation distribution at the gage section for the first design modification.

Fig. 40 shows true hoop stress-strain curves from FEA results. Hoop stress and strain data were selected from three locations through the cross section. Stress-strain curves of the three locations collapse together. Curves match the tensile test data well in the elastic region, while the values are slightly lower than the tensile test data in the plastic region. Compared to the FEA results from the current ORNL expanded plug test design in Fig. 21, the resultant stress-strain curves are more consistent through the cross section and are a better match with tensile test data.
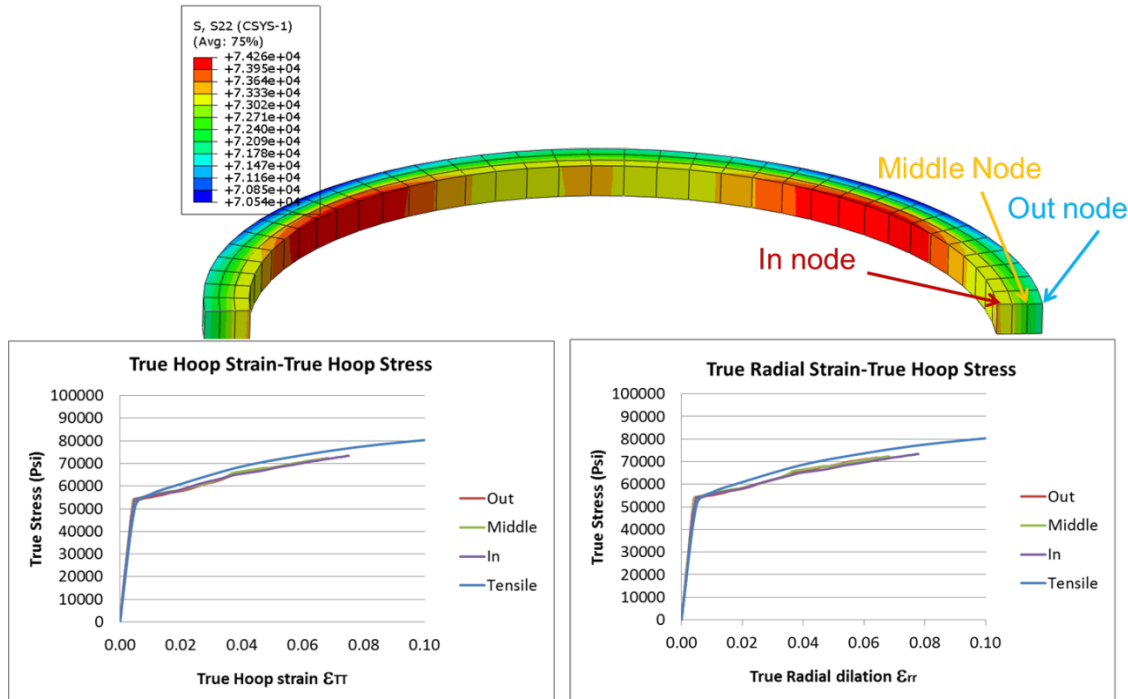
Fig. 40. FEM true hoop stress-true strain curves vs. tensile test data for the first design modification.

Fig. 41 shows axial stress-strain curves from FEA results for the first design modification. Results reveal the significant reduction in axial stress induced by the barreling effect. Compressive axial stress is one order of magnitude lower than the results shown in Fig. 22.

45
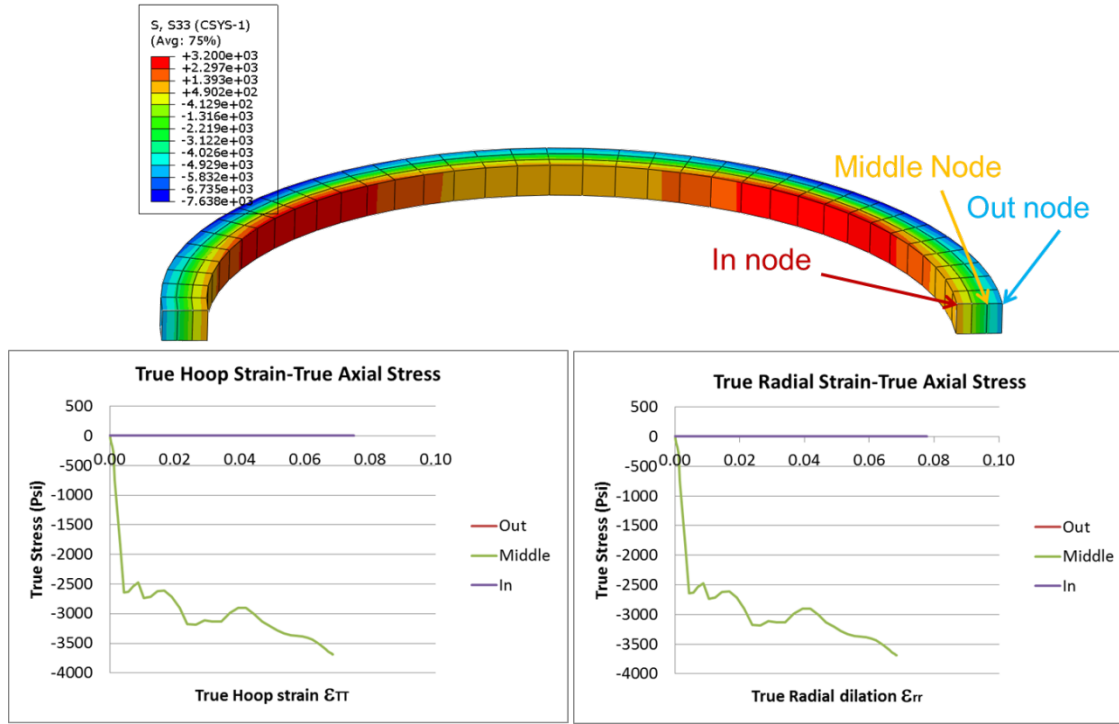
Fig. 41. FEM true axial stress-true strain curves for the first design modification.

4.2 MODIFIED EXPANSION PLUG TEST DESIGN WITH WEDGE INSERTS

In addition to the first proposed modification, an expanded plug test has been developed with rigid wedges inserted between the clad and the plug. The FEM model of this version of design modification is shown in Fig. 42. The working mechanism is similar to the other expanded plug test designs. However, as the eight rigid wedges are introduced in between the tested ring and plug, the expanded plug is not directly pressing on the test specimen, reducing the impact of the plug's bulging effect to ring deformation. The compressive plug pushes against the rigid wedges, moving in the outward radial direction, transferring the stress and deformation onto the tested ring.
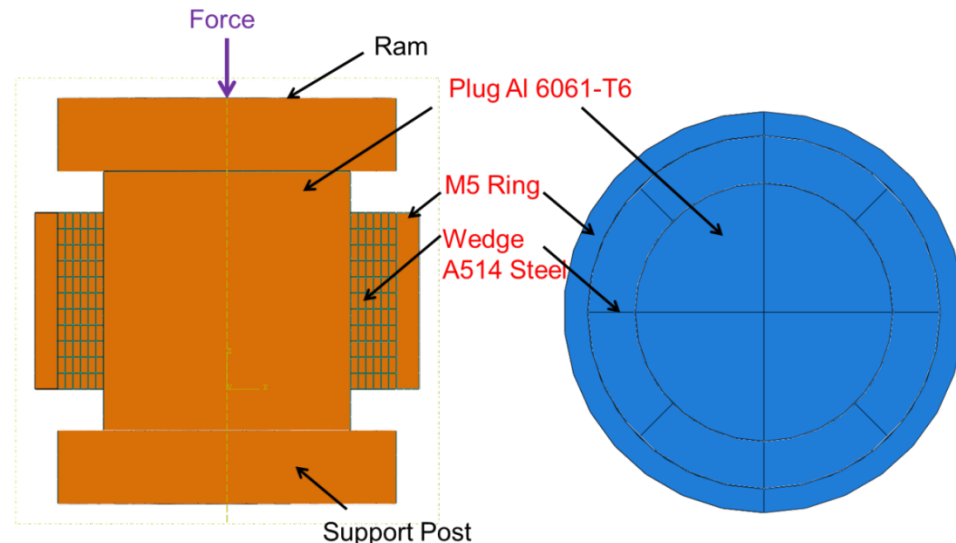
Fig. 42. FEM model of modified expanded plug test design with eight wedge inserts.

Through detailed parameter investigation of specific geometry designs, the modified expanded plug test design with wedge inserts has an optimized geometry, as modeled in Fig. 42. Especially for the wedge inserts, several iterations of the FEA study had to be performed to reach the final design. Once the essential thickness of the wedge was determined, the OD and ID of the wedge were decided accordingly. The plug diameter has been modified accordingly with respect to the inserted wedges. To achieve even expansion in the radial direction of the ring specimen, the wedge inserts were cut into eight pieces. The geometry of the specimen ring is the same as that of the first modification, as well as the axial length of the plug. The ring length is 0.17 in., the OD is 0.37 in., and the ID is 0.326 in. The wedges are rigid with eight pieces. The length of the wedges is 0.17 in., the ID is 0.238 in., and the OD is 0.326, corresponding to the ring's ID. Hence, the thickness of the wedges is 0.044 in. The plug length is 0.25 in., and the OD of the plug is 0.238 in., corresponding to the wedge's ID.

Material selection for the testing system is crucial. After careful filtering, A514 steel was chosen for the wedge inserts, and aluminum 6061-T6 was used for the expansion plug. Ring material is unirradiated M5. The ram and support port are still made of high strength steel. The component material properties of testing system are listed in Table 10.

Table 10. Component material properties of modified expanded plug test design with wedge inserts

	Young's modulus (psi)	Tensile yield stress (psi)	Poisson's ratio
Unirradiated M5 [a]	1.312×10^7	55,800	0.326
High strength steel [b]	3.0×10^7	280,000	0.28
Aluminum 6061-T6[c]	1.0×10^7	40,000	0.33
A514 steel [d]	2.97×10^7	100,000	0.285

[a] Morris, MOX PIE Fuel and Clad Examination Final Report. [b] Thrash Southwire Company Overhead Conductor Manual.
[c] Kaufman, Properties of Aluminum Alloys: Tensile, Creep, and Fatigue Data at High and Low Temperatures
[d] USS Steel Design Manual.

In the FEM model in Fig. 42, the loading and boundary conditions were the same as in the FEM model in Fig. 38 for the first modification design. The difference was the contact. Due to the wedge insert between the clad and the expansion plug, general contact was defined as both in the interface between the wedges and plug and the interface between clad and wedges. Low friction was also applied in those interfaces to reduce shear stress. During simulation, the plug was compressed down 0.08 in. and pushed all the way into the wedge-ring specimen.

Fig. 43 shows hoop stress distribution in the clad for the modified expanded plug test design with wedge inserts. Fig. 44 shows uniform radial dilatation distribution along the gage length. FEM simulation has proved that by using this approach, more improvement has been gained regarding the uniform stress and strain distribution at the gage section than in the first modified design that optimized the geometry alone. It also results in a more uniform stress distribution at contact interfaces between the wedge and the ring. It is noted that a deformed ring is not perfectly round in the radial direction. At the wedge opening section, the ring is concave, and at the wedge and ring contact section, the ring is convex. The wedge and ring contact section (convex section) is much larger than the wedge opening section (concave section). FEA results show that the resultant stress-strain curves in the convex section are a better match with tensile data than that in the concave section. Therefore, circumferential measurement is suggested at the convex section in the testing.
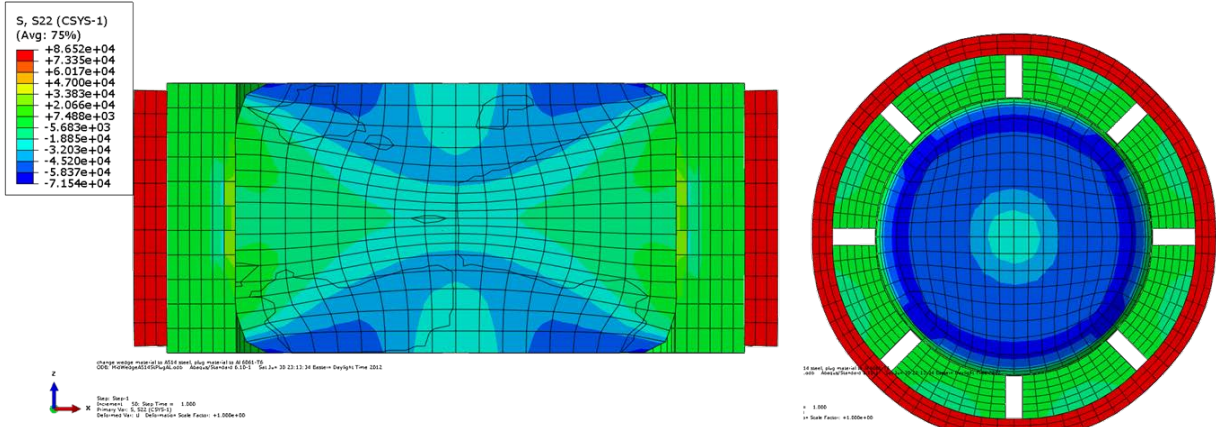
Fig. 43. Uniform stress distribution in the clad for modified expanded plug test design with eight wedge inserts.
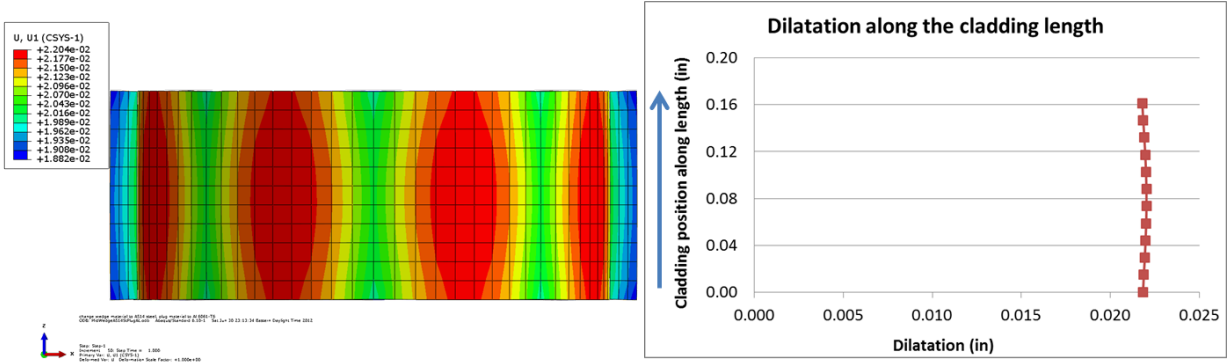
Fig. 44. Uniform radial dilatation distribution at the gage section for modified expanded plug test design with eight wedge inserts.

The resultant hoop stress-strain curves in the clad convex section from FEA results are compared with tensile test data in Fig. 45. Stress and strain data were still selected from three locations through the cross section. In the elastic region, all curves match very well. In the plastic region, stress-strain curves from the middle and outer circles have very good agreement with tensile test data up to an ultimate strength of 74.3 ksi, which is slightly low for data from the inner circle. Fig. 46 illustrates axial stress-strain curves for the modified expanded plug test design with wedge inserts. FEA results also show significantly lower axial compressive stresses than those of the previous ORNL expansion plug method.
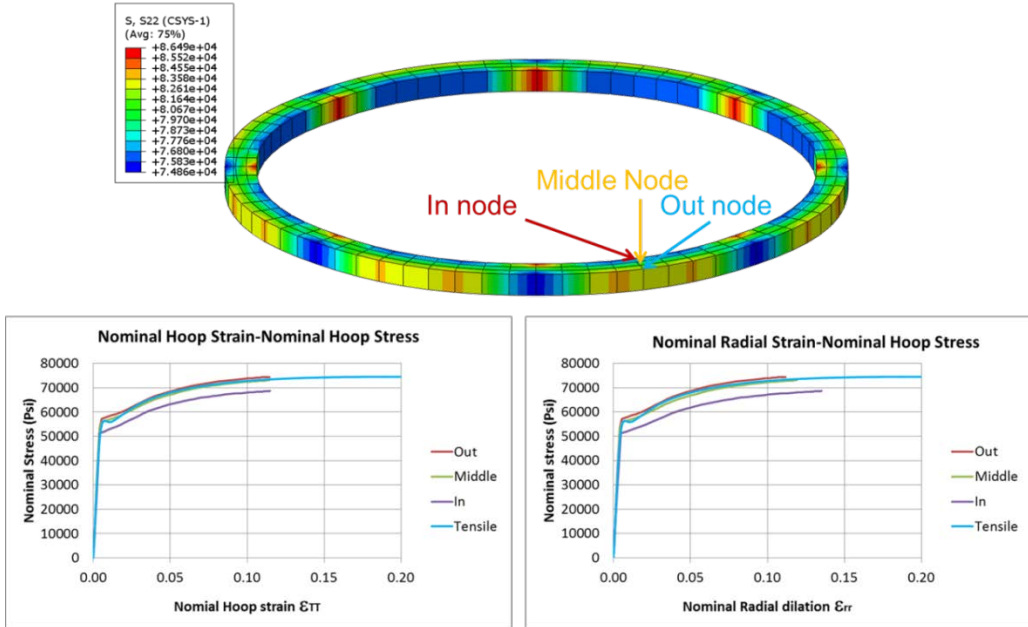
Fig. 45. FEM nominal hoop stress–nominal strain curves vs. tensile test data for modified expanded plug test design with eight wedge inserts.
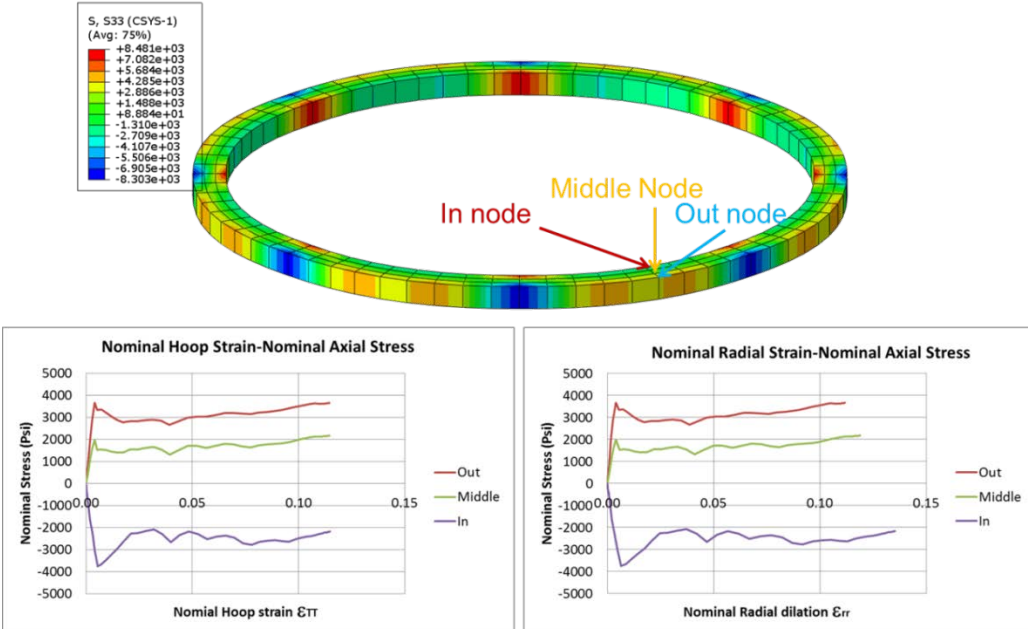
Fig. 46. FEM nominal axial stress–strain curves for modified expanded plug test design with eight wedge inserts.

A general procedure has been developed to determine the hoop stress σ_θ in the tested ring specimen. A scaling factor called χ-factor is used to correlate the ring load P into hoop stress σ_θ, as shown below.

$$\sigma_\theta = \chi \frac{Pr}{t} \tag{4}$$

where

$$\chi = \frac{\sigma_{Yield}}{P_{Yield}} \frac{t}{r}$$

49

and
χ = scale factor,
σ_{Yield} = yield stress of material determined by a standard tensile test,
P_{Yield} = load of 0.2% plastic strain offset measured in expanded plug test,
t = ring specimen thickness, and
r = ring specimen inner diameter.

The yield load P for the ring test data from the FEA results was determined as shown in Fig. 47. The total load is not transmitted to the ring specimen via expansion of the plug, as the plug itself has stiffness that must be accounted for. By measuring the load-extension response of a free plug (a plug without a ring specimen surrounding it), the ring load was separated from the total load and the plug load, shown in Fig. 46a. Then, using 0.2% plastic strain offset, the yield load was identified as 395 lbf from the resultant ring load in the FEA result for the modified expanded plug test design with wedge inserts.
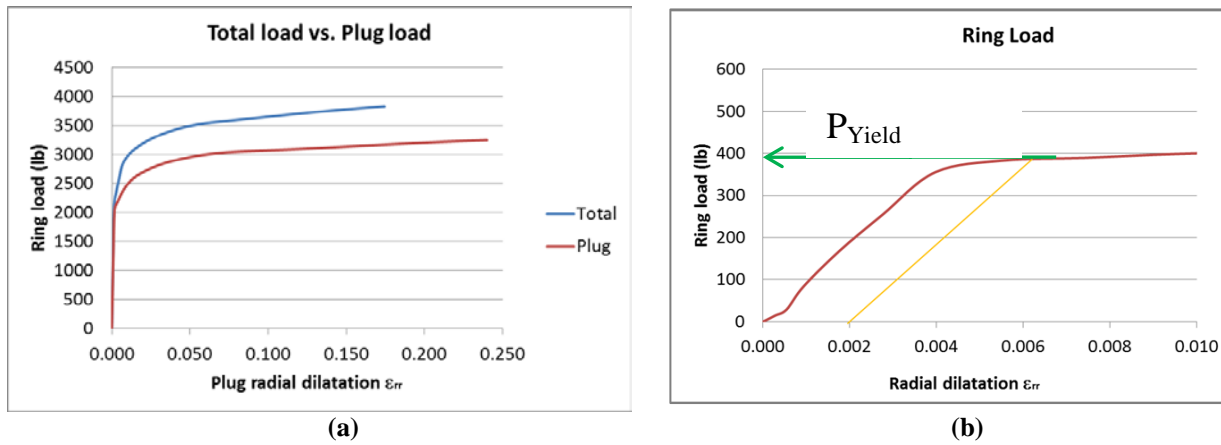
(a)   **(b)**
**Fig. 47. Ring yield load for modified expanded plug test design with
eight wedge inserts determined by the 0.2% strain offset method.**

By applying equation (4), the scaling χ-factor was calculated as 9.53. The ring specimen has a thickness of 0.022 in., with an inner radius of 0.326 in. The yield stress used unirradiated M5 tensile tube test data, 55.8 ksi. The yield load was determined as above. The ring load from FEA was converted into hoop stress using equation (4), as shown in Fig. 48. The generated stress-strain curve agrees with rgw tensile test data perfectly in both the elastic and plastic regions. The modified expansion plug testing protocol has been developed and validated in FEM simulation.

$$\sigma_\theta = \chi \frac{\mathrm{pr}}{t}$$
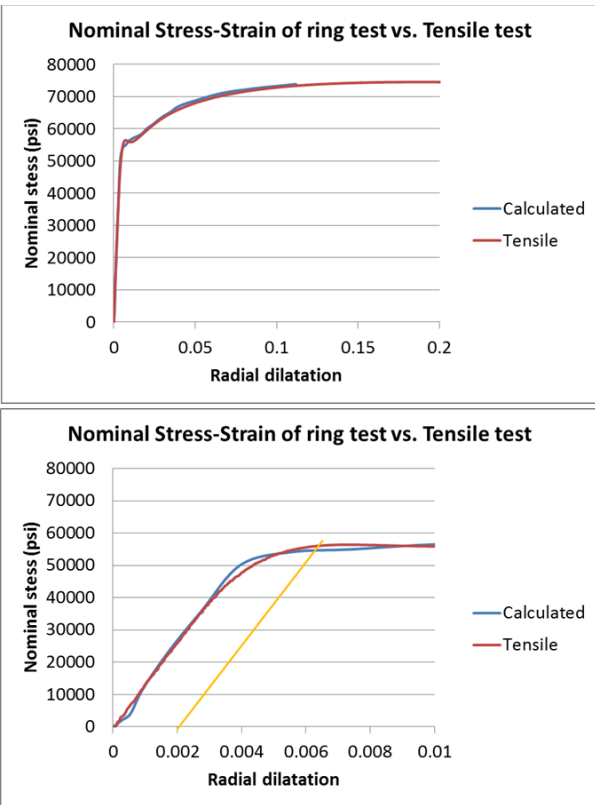
$$\chi = \frac{\sigma_{Yield}}{P_{Yield}}\frac{t}{r} = 9.53$$

t=0.022 in
r=0.326 in
σ_{Yield}=55.8 ksi (tensile data)
P_{yield}=395 lbf

Yield stress matches with tensile test data;
Ultimate tensile strength matches with tensile test data;
Young's modulus matches with tensile test data.

Fig. 48. Ring load–radial strain data from the ring test converted into material stress-strain curve for modified expanded plug test design with eight wedge inserts.

5. DESIGN MODIFICATION AND TEST VERIFICATION OF EXPANSION PLUG WEDGE TEST METHOD

At the beginning of the experimental verification for the proposed testing protocol, the modified expanded plug test design with eight wedge inserts, as shown in Fig. 42, was the starting point. It was soon realized that eight wedge inserts were difficult to machine and assemble due to their small specimen dimension. Therefore, the wedge inserts design was revised to include four wedges for feasible specimen fabrication and sample installation (Fig. 49). Except for the change to four wedge inserts, the geometry and materials for the test design components are exactly the same as shown in Fig. 42.
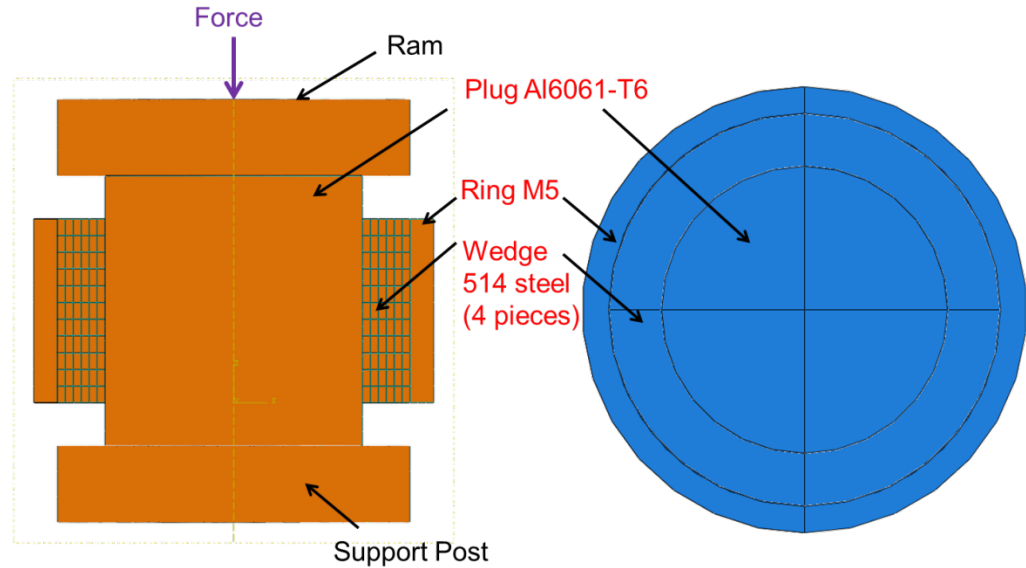
Fig. 49. Modified expanded plug test design with four wedge inserts.

As in the eight-wedge design (Fig. 43 and Fig. 44), the modified expanded plug test design for the four-wedge design results in uniform stress distribution and uniform radial dilatation on the clad (Fig. 50 and Fig. 51. Stress level and radial dilatation are in the same range for both eight- and four-wedge designs. Thus, the resultant difference between the two designs is negligible. In the experimental test verification, test specimens are fabricated based on the four-wedge design.
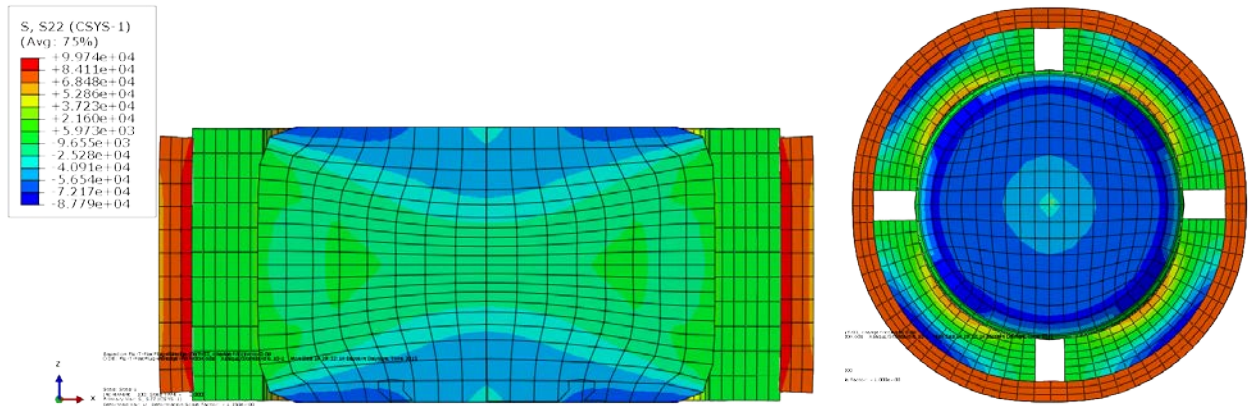

**Fig. 50. Uniform stress distribution in the clad for modified expanded plug test design with four-wedge design.**
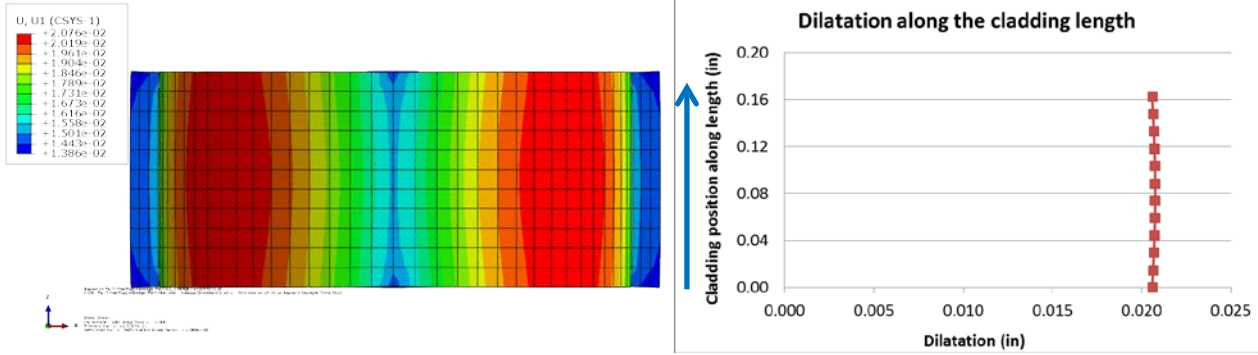
Fig. 51. Uniform radial dilatation distribution at the gage section for modified expanded plug test design with four-wedge design.

5.1 SPECIMEN FABRICATIONS AND PILOT TESTING

Multipurpose 6061 aluminum pieces with diameters of 0.236 in. and 0.315 in. were purchased for the machining plug, and hardened easy-to-machine P20 tool steel with a 0.5 in. diameter was purchased for making wedge inserts. The wedges were machined as four pieces. M5 cladding tube with and OD of 0.374 in. and thickness of 0.022 in. was provided by a vendor.

5.1.1 Testing system for verifying expanded plug test design with four wedge inserts

The testing equipment is a legacy machine used in a previous expansion plug test. Fig. 52a shows the MTS electromagnetic load frame used to apply an axial compressive load to a cylindrical aluminum plug.
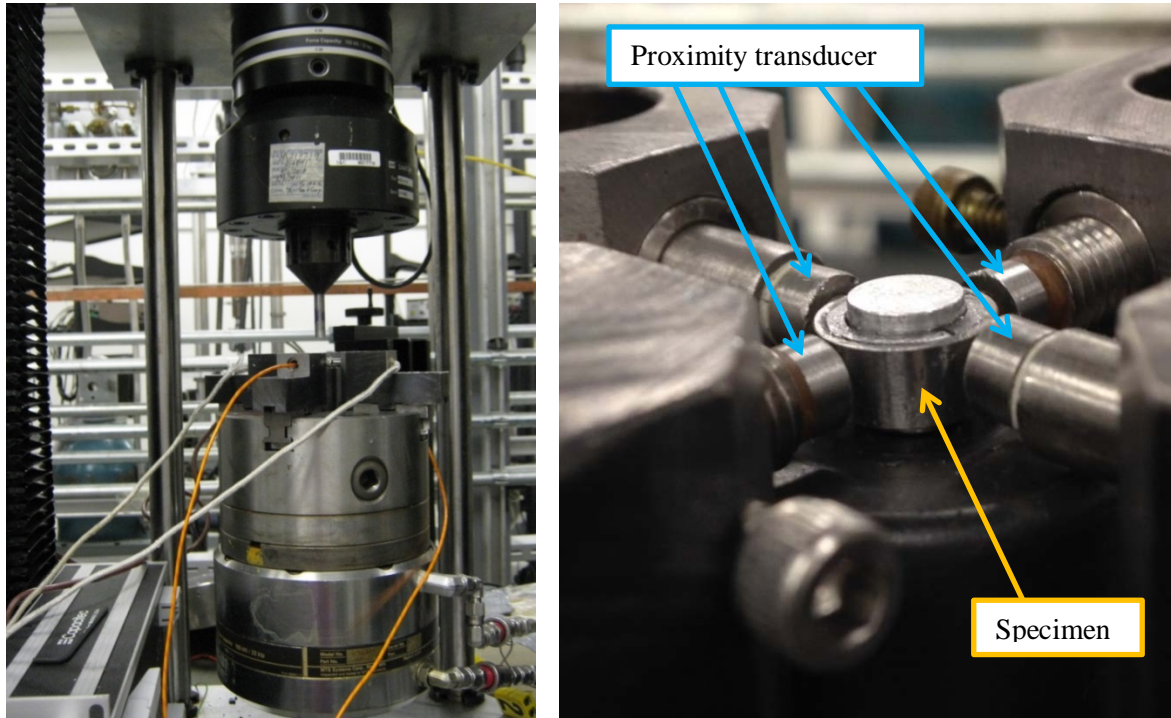
(a) MTS electromagnetic load frame　　　　　　　**(b) Four proximity transducers**

Fig. 52. Testing equipment for verifying expanded plug test design with four wedge inserts.

The aluminum plug was deformed and fitted into a short testing ring specimen. The deformed plug pushed against the four wedge inserts and caused them to move outward radially to achieve radial expansion of the tested ring specimen. Measurements were made of the total applied load, the extension of plug compression, and the radial expansion during the test. The radial expansion of the specimen was measured with four proximity transducers, as shown in Fig. 52b and used to calculate the circumferential strain. The load and radial expansion data can be converted into material stress-strain curves to examine the mechanical properties of the tested ring specimen, such as Young's modulus, yield strength, and strain-hardening characteristics.

(a) Control penal   (b) Test data review
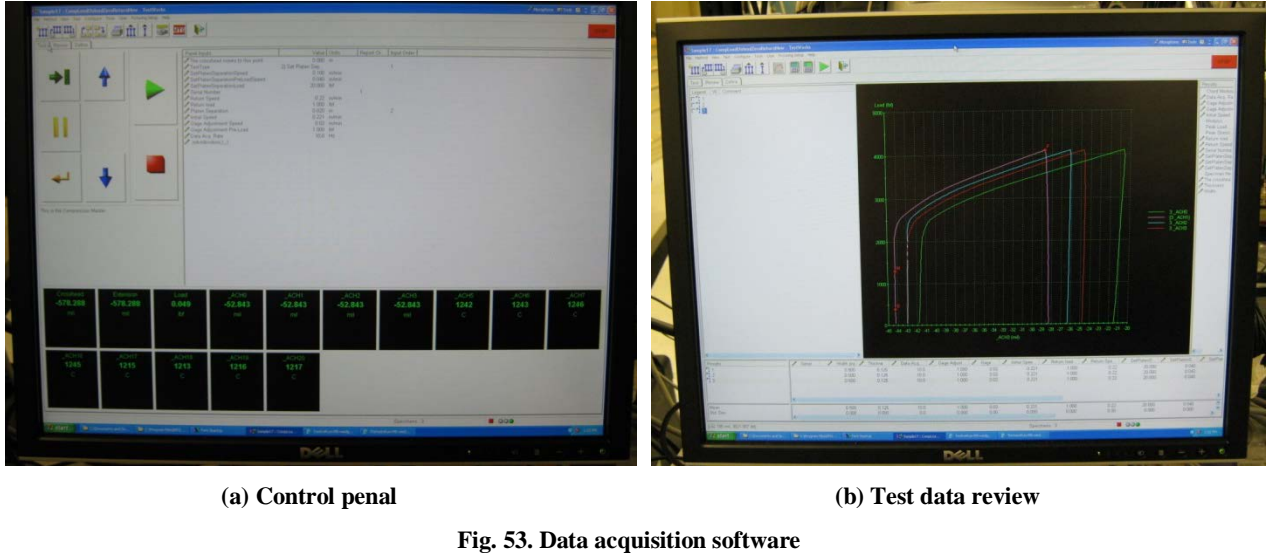
Fig. 53. Data acquisition software

Fig. 53 is a screen shot of the software being used to acquire the data of the applied load, the extension of the plug, and the radial expansion of the tested ring. During the test, the control panel window of the software in Fig. 53a shows the changing number of the measurement data, including one channel for the load cell signal, one channel for the loading frame crosshead position, one channel for the extension based on the crosshead position, and four channels for each proximity transducer. The raw testing data, shown Fig. 53b, is applied load from load cell vs. radial expansion recorded by proximity transducers.

When testing the ring specimen with the four-wedge expanded plug test method (Fig. 54b), the applied total load from the load cell consists of the loads of the entire set, including the aluminum plug, the steel wedges, and the testing ring. The steel wedges are rigid and free to move, and they are intended to transfer the load without deformation. Therefore, the load on the wedges is low enough to be disregarded. However, a significant amount of load is needed to deform the aluminum plug. To determine the load on the testing ring to convert hoop stress, the load on plug needs to be deducted from the total load from load cell. Thus the compressive test shown in Fig. 54a is conducted on the plug alone under the same conditions as the testing ring set to determine the load on the plug. The geometry of the single tested plug should be exactly same as the plug inside the ring specimen set. However, it is not necessary to test a single plug each time the ring specimen is tested. The standard procedure is to test four to five plugs alone and then to use the testing data to curve-fit a plug load. This curve-fitted plug load can be used for deduction from the total load in the ring specimen set.
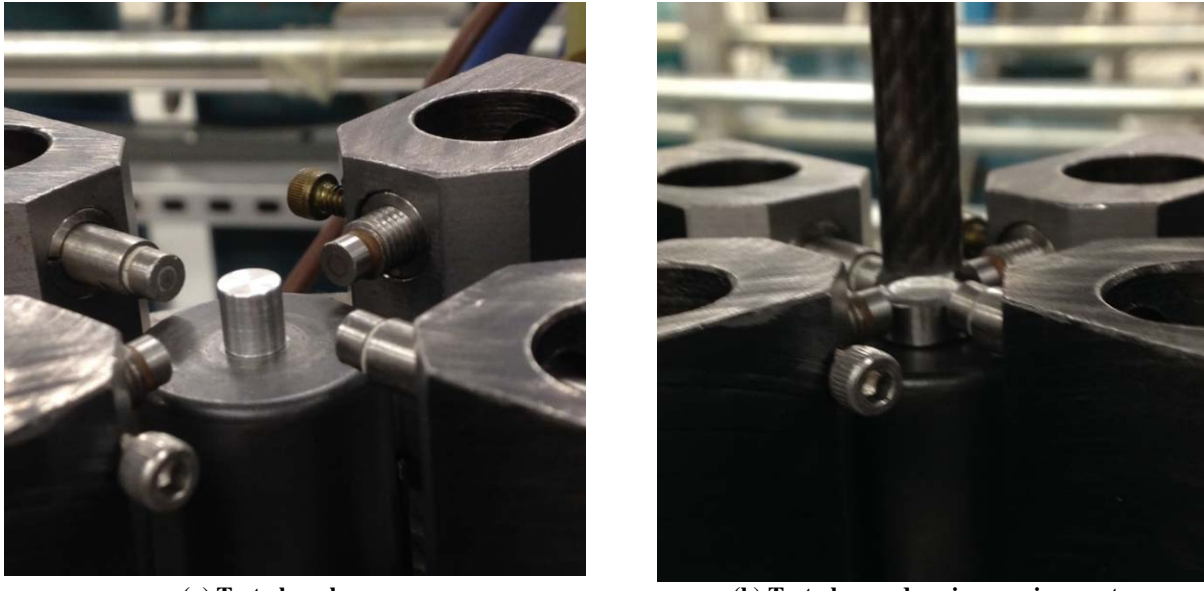
(a) Test plug alone	**(b) Test plug wedge-ring specimen set**

Fig. 54. Testing conducted for determining the ring specimen hoop stress.

5.1.2   First generation of specimen fabrication and pilot testing

The first generation plugs were machined from the purchased multipurpose 6061 aluminum with a diameter of 0.236 in, as shown in Fig. 55. The length of the plug ranged from 0.25 in. to 0.268 in. In order to align the plug or testing plug wedge-ring specimen set in the center of the MTS loading piston, the plug was machined in a small area, which is referred to as the alignment area. The alignment area of the plug was inserted into the associated alignment hole in the bottom support piston during the compression test (Fig. 56). The alignment area started with dimension D = 0.186 in. The compression test on the plug (Fig. 55a) revealed that the deformed plug was squeezed in the bottom support piston hole and was thus difficult to remove due to the large alignment area and the very narrow shoulder. Therefore, the plug alignment area was decreased to half of its original dimension, as shown in Fig. 55b and c.

(a) Plug with 0.25 in. long alignment area (D = 0.186 in.)	**(b) Plug with 0.25 in. long alignment area (D = 0.093 in.)**	**(c) Plug with 0.268 in. long alignment area (D = 0.093 in.)**
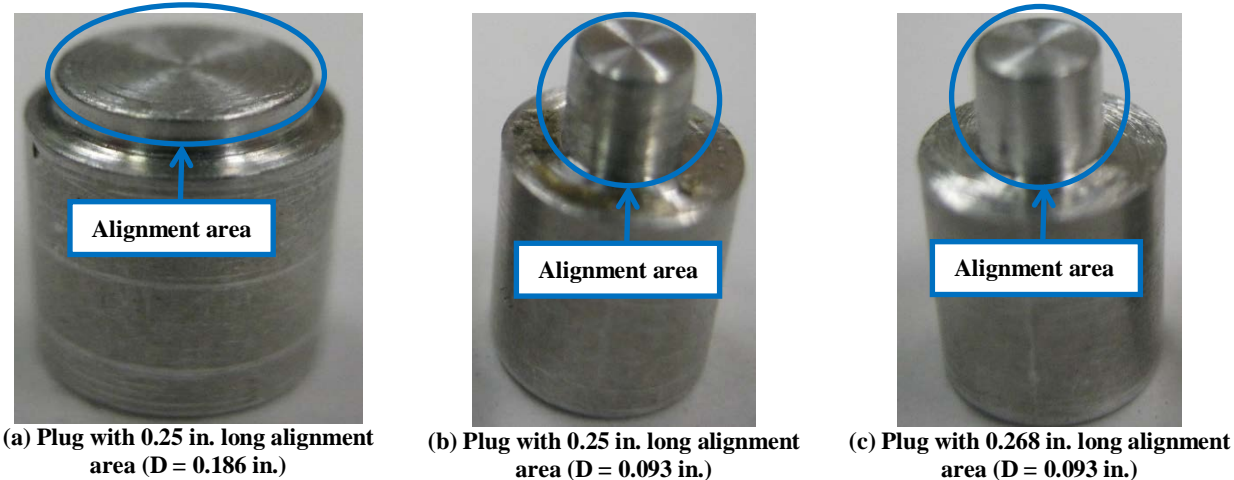
Fig. 55. First generation plug designs.

55

Fig. 57 shows the first generation plugs after the compression test. As in the FEA simulation, the compression test was conducted using displacement control scheme, and the MTS electromagnetic load frame was specified as moving down 0.08 in. after touching the top of the plug. With a narrow shoulder and a large alignment area, the bottom part of plug was squeezed into the alignment hole shown in Fig. 57a. With the alignment area reduced in size, the shoulder surface contacting with bottom piston was larger. However, the shoulder surface area on the bottom of the plug was only 60% of the top surface area of the plug contacting with top piston. Therefore, the resultant compressive and shear stress during the test on the bottom shoulder surface was larger than that on the top surface of the plug. The larger compressive and shear stress stretched the material out on the bottom surface of the plug, which resulted in the apparent bell shape shown in Fig. 57b and c.
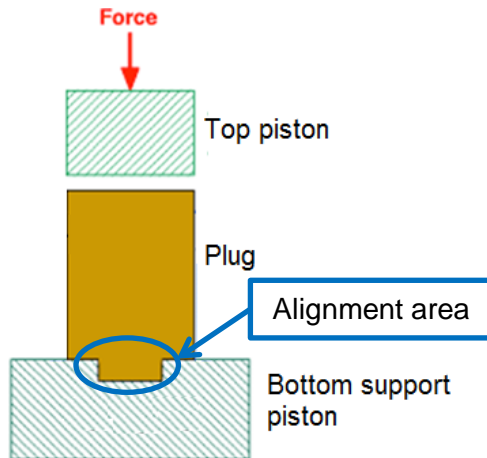
Fig. 56. Schematic of compression plug test.

| (a) Tested plug with 0.25 in. long alignment area (D = 0.186 in.) | (b) Tested plug with 0.25 in. long alignment area (D = 0.093 in.) | (c) Tested plug with 0.268 in. long alignment area (D = 0.093 in.) |
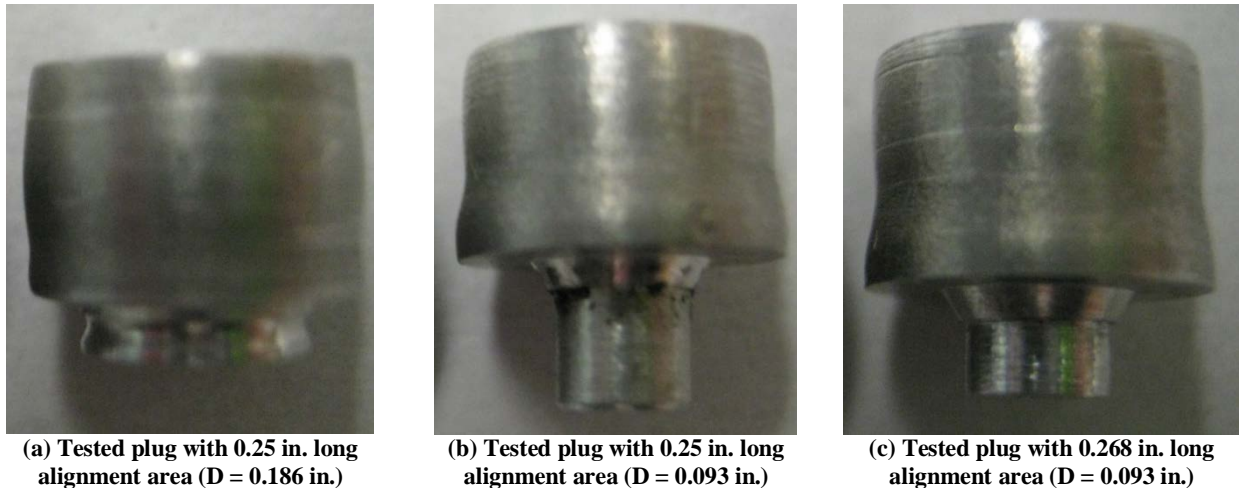
Fig. 57. Deformed first generation plugs after compression tests.

An untested first generation ring specimen with an aluminum plug and four wedge inserts is shown in the images in Fig. 58. The wedges are 0.17 in. long, the ID is 0.238 in., and the OD corresponds to the ring's ID. Hence the thickness of the wedges is 0.044 in. The plug length is 0.25 in., and the OD of the plug is 0.236 in. The ring length is 0.17 in., the OD is 0.374 in., and the thickness is 0.022 in. Fig. 58 reveals that there were big gaps between wedge inserts, plug, and wedges or the wedge and ring specimen. The plug was cut from an aluminum rod with diameter of 0.236 in., so it was smaller than the ID of the wedges. Due to the machine cutting procedure, a wedge insert was over cut in the

56

circumferential direction, leaving a big gap between the wedges when inserted into the ring testing specimen. Therefore, the plug, wedges and ring were not tight-fitted. Lubricant was applied between the plug and wedge inserts of the four first generation ring testing specimens.

Fig. 58. An untested first generation ring specimen with aluminum plug and four wedge inserts.

Fig. 59 shows the first four tested ring specimens. In tests 1 and 2, the plug was 0.25 in. long, and the alignment area OD was 0.186 in. In test 3, the plug was 0.25 in. long, and the alignment area was reduced by half. In test 4, the plug was 0.268 in. long, and the alignment area was the same as that of test 3.
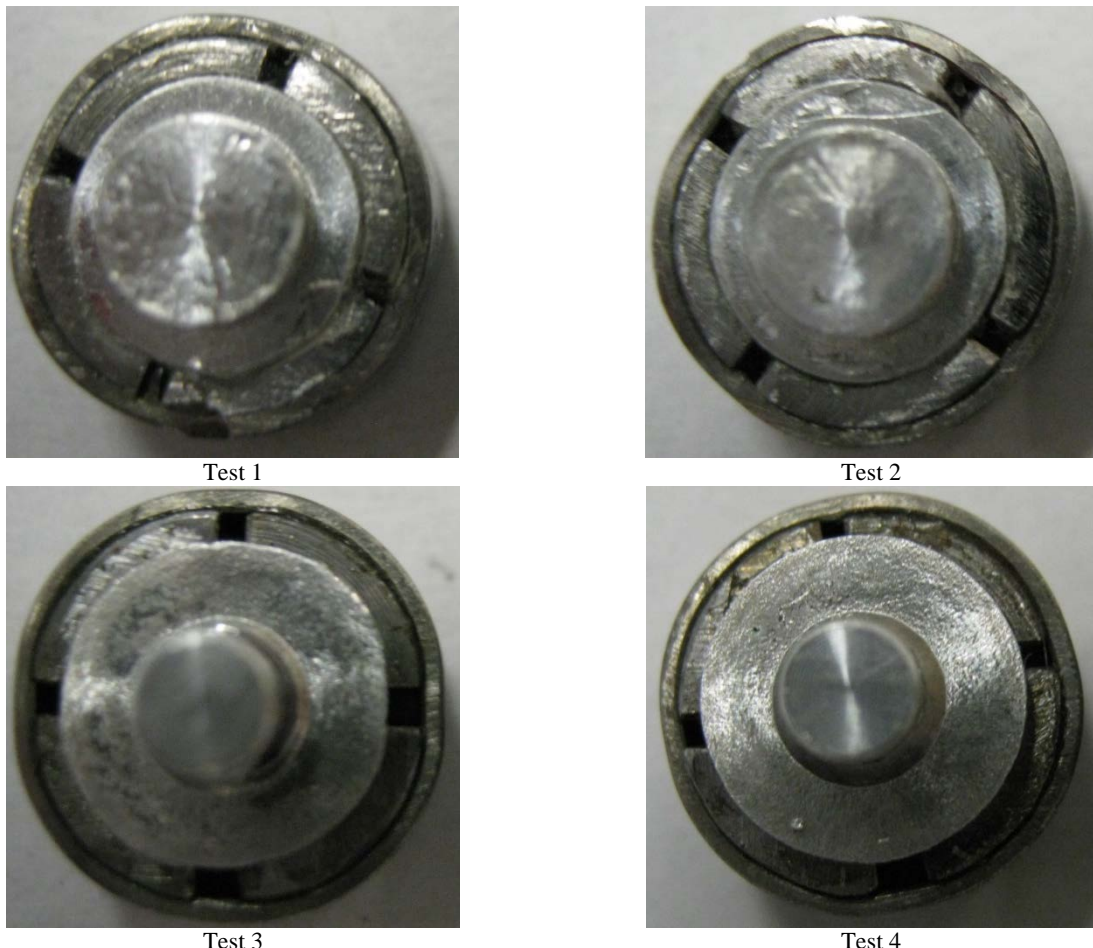
Test 1

Test 2

Test 3

Test 4

Test 3   Test 4
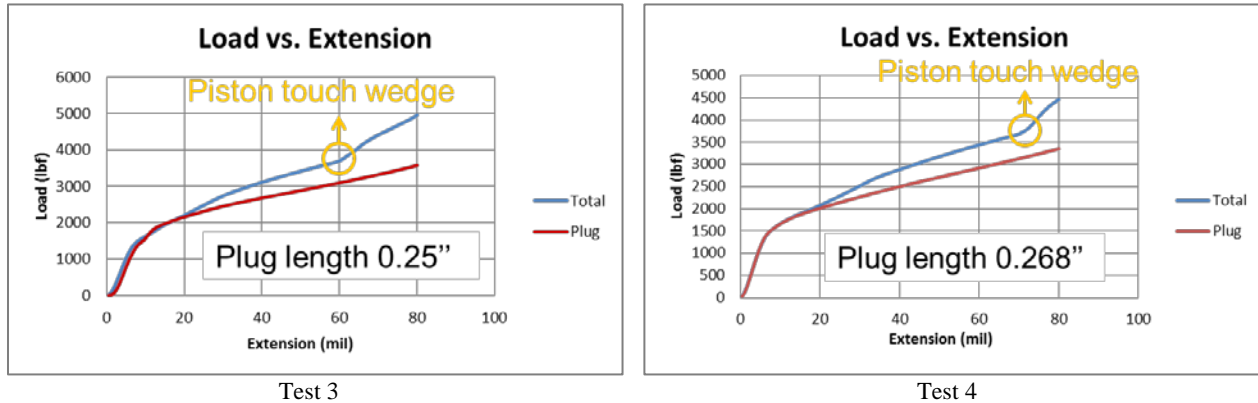
Fig. 60. Test data load vs. extension for the first generation ring specimen.

Test data for the first generation ring specimen in Fig. 60 shows that there was a sudden surge in the load near the end of the compression test, which indicates that the top piston touched the steel wedge inserts. There are several reasons for this undesirable occurrence.

- The plug length was too short.
- The bell shape of the plug resulting from the uneven shear stress on the bottom shoulder surface and on the top surface of the plug pushed the wedges up to touch the piston. The bell shape of the plug led to the bell shape of the ring specimen, as shown in Fig. 61. The bottom side of ring was expanded more than the top side.
- The plug-wedges-ring specimen set was intended to stay at the center between the top piston and the bottom support piston as designed duel piston concept. However, the plug, wedges and ring specimen were not tightly fitted, so they slipped off the center position during the test. Even when the plug length was extended to 0.268 in., the piston contacted wedges. Improvements were made to overcome the shortcoming of the test specimen design and fabrication, leading to the second generation design modification and specimen fabrication.

Test 3:Plug length 0.25 in.   Test 4:Plug length 0.268 in.
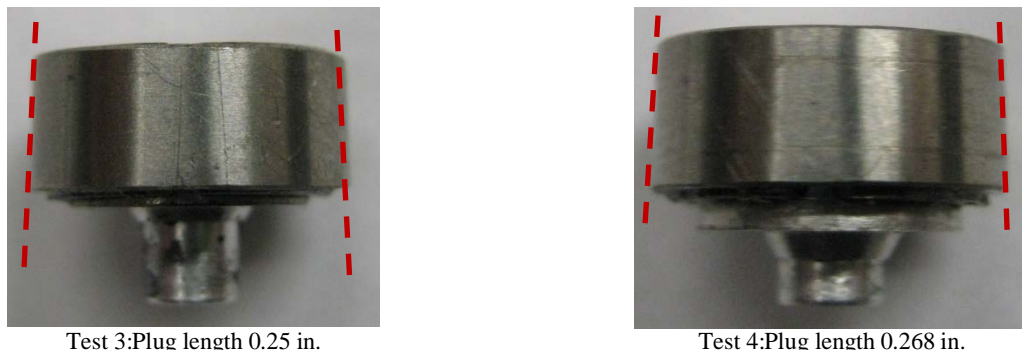
Fig. 61. Side view of tested first generation ring specimens.

58

5.1.3 Second generation of specimen fabrication and pilot testing

Fig. 62 shows the second generation plug design. The plugs were machined from purchased multipurpose 6061 aluminum with a diameter of 0.315 in. The OD of the plugs was machined to 0.238 in. to fit the ID of wedge inserts. The length of the plugs was 0.28 in., which is ~10% longer than the first generation plugs. The alignment area was further reduced to D = 0.05 in. to ensure a larger contact surface on the bottoms of the plugs. The bottom contact surface was ~80% of the top contact surface.
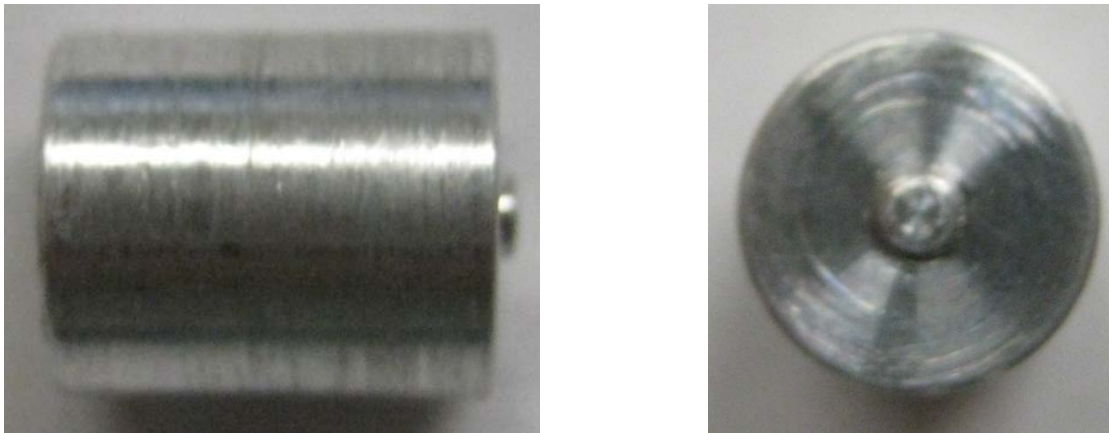
Fig. 62. Second generation plug design.

The hole on the bottom support piston was machined to fit the alignment area of the second generation plugs, as shown in Fig. 63. The hole was slightly larger than the diameter of the alignment area to aid in placement.

**Fig. 63. The hole on the bottom support piston machined
to fit the alignment area of the second generation plug.**

Fig. 64. A tested second generation plug.

The compression test on the second generation plugs shows that the plug deformed to a regular drum shape (Fig. 64) instead of the bell shape in Fig. 57. The resultant shear stress on the bottom contact surface was closer to that of the top surface due to the enlarged bottom contact surface that resulted from making the alignment area smaller.

Fig. 65. An untested second generation ring specimen with aluminum plug and four wedge inserts.

Fig. 65 shows one of the untested second generation ring specimens with an aluminum plug and four wedge inserts. The dimensions of the ring and wedges were exactly the same as those of the first generation ring specimen set. The dimensions of plug were changed, with a length of 0.28 in. and an OD of 0.238 in., as well as a new alignment area. The wedge insert machining was improved, and the gaps between wedge inserts were smaller than those of the first generation. The fit of the plug, wedges, and ring specimen were improved. There was no lubricant between the plug and wedges. However, there were still some gaps in the testing ring specimen set that would affect the test data, especially the radial strain. Because the deformed aluminum plug would fill up the gaps first and then would push onto the wedges to the expand ring specimen, the same amount of load did not work on the ring. The radial strain was underestimated according to the load.

| Test 5 | Test 6 | Test 7 | Test 8 |

| Test 9 | Test 10 | Test 11 | Test 11: side view |
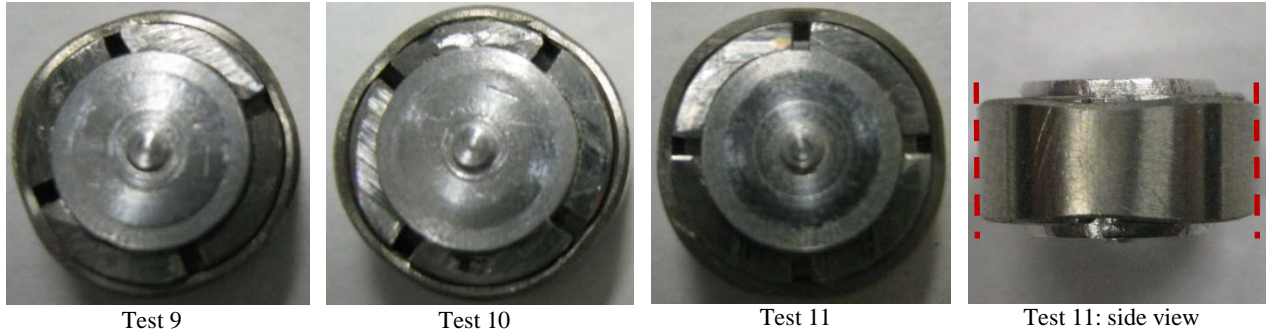
Fig. 66. Tested second generation ring specimens with aluminum plug and four wedge inserts.

Seven ring specimens were tested for the second generation fabrication, as shown in Fig. 66. The testing results were promising. The plug expanded the ring circumferentially more evenly than the first generation. The side view of the tested ring specimen shows that the ring expansion in the axial direction was uniform. There was no bell shape, and the piston did not contact the wedge during the test. The test data shown in Fig. 67 verify that there was no sudden load surge, so the plug length of 0.28 in. is appropriate for the test design.
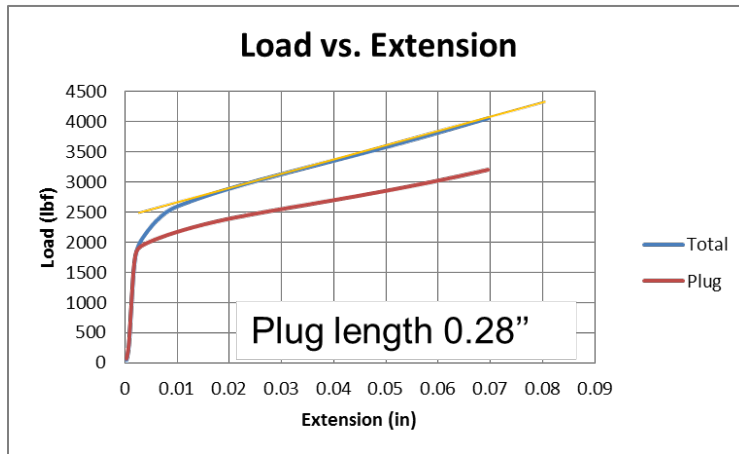
Fig. 67. Test data load vs. extension for the second generation ring specimen.

However, the dimension of the alignment area was too small, which caused machining difficulty and machining fault. When the alignment area was made larger than the fitting hole in the bottom piston due to a machining error, the alignment area had to be manually repaired in order to fit. This caused difficulties with testing. Furthermore, in a hot-cell environment, it would be not possible to make the repair. Therefore, the alignment area was further modified in the third generation design and fabrication.

5.1.4   Third generation of specimen fabrication and pilot testing

Fig. 68 shows the third generation plug design. The length of the plug was maintained at 0.28 in. The diameter of the alignment area was increased to 0.074 in. with a shrinking neck to allow for easier machining without reducing the contact surface area on the bottom of the plug. This design also made it easier to remove the deformed plug from the fitting hole after testing. The dimension of the fitting hole on the bottom support piston was adjusted accordingly.

61
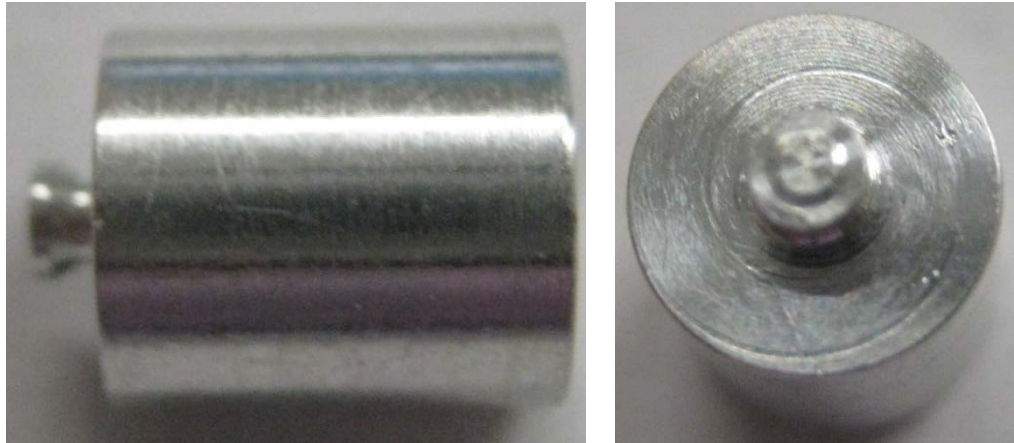
Fig. 68. Third generation plug design.

The tested third generation plug appeared to be similar to the second generation plug, but the conditions on the top and bottom surfaces of the plug were not even due to the alignment area. An area was bulging from the lower part of the plug, as shown in **Error! Reference source not found.**. This could cause the ring expansion to be uneven in the axial direction.

Fig. 70 shows an untested second generation ring specimen with the aluminum plug and four wedge inserts. The plug's OD of 0.238 in. is the same as that of the second generation plug, which was fitted with the wedge's ID. Thus, in the third generation ring specimen set, the plug, wedges and ring were tightly fitted. The gaps between the wedges were small but still visible.

Fig. 69. A tested third generation plug.

Fig. 70. An untested third generation ring specimen with aluminum plug and four wedge inserts.

Four ring specimen sets were fabricated and tested for the third generation design, as shown in Fig. 71. The test results were similar to those of second generation ring specimen sets. However, the side view of tested ring specimens shows apparent uneven ring expansion in the axial direction, even though it is not significant. Because of the alignment area on the bottom of the plug, the resultant larger shear on the bottom surface of the plug caused greater ring expansion on the bottom side.

Test 12

Test 13

Test 14

Test 15

Fig. 71. Tested third generation ring specimens with aluminum plug and four wedge inserts.

5.1.5   Fourth generation of specimen fabrication and pilot testing

To make the plug design even on the top and bottom surfaces, the alignment area was eliminated. The fourth generation plug was designed with flat top and bottom surfaces, as shown in Fig. 72. The plug's OD was maintained at 0.238 in. Four fourth generation plugs were tested for generating the plug load. Among them, three were 0.28 in. long, as in the previous design, and one was 0.29 in. long for the length study. To align the components, the hole on the bottom support piston was machined to be slightly larger than the plug's OD to allow the piston to fit with the plug's bottom surface, as seen in Fig. 73. The depth of the hole was 0.015 in.

Fig. 72. Fourth generation plug design.

**Fig. 73. Hole on bottom of support piston machined
to fit the plug's bottom flat surface for alignment.**

Fig. 74 shows a tested fourth generation plug with a flat bottom surface. The test results revealed that the hole for alignment on the bottom of the piston introduced constraint on the bottom of the plug, so the plug deformed during the compression test. That caused uneven conditions on the top and bottom surfaces of the plug, even though the plugs were designed to be the same on the top and bottom surfaces. As shown in Fig. 74, the top surface of the plug was free to stretch without any constraint; however, the bottom of the plug was confined in the hole. Therefore, the tested plug had an upside down bell shape, with bulging at the middle section.

Fig. 74. A tested fourth generation plug.

Comparison of the test data for the four plug test (Fig. 75) indicates that the load of the longer plug (0.29 in.) shifted, which might have been caused by buckling. Therefore, the 0.28 in. length was determined to be a favorable parameter for the plug design.
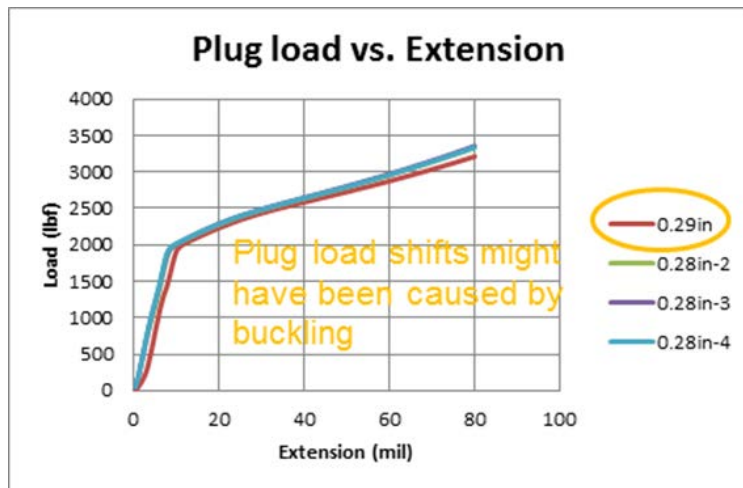
Fig. 75. Test data load vs. extension for the fourth generation plug.

Fig. 76 shows an untested fourth generation ring specimen with the aluminum plug and four wedge inserts. The plug, wedges, and ring were tightly fitted. The plug was flat on the top and bottom surfaces. There was no alignment area on the plug. As when testing the plug alone, the hole on the bottom piston was used for alignment with testing ring specimen sets. There were five ring specimen sets tested for the fourth generation design and fabrication as shown in Fig. 77 and Fig. 78. Fig. 77 shows the tested fourth generation ring specimen set 17. The side view of the expansion plug tested specimen shows that the ring expanded unevenly in the axial direction. Due to a constraint on the bottom of the plug caused by the alignment hole, the bottom of the ring expanded less than the top part of the ring with the free surface of the plug. As a result, the ring was shaped like a partial cone. The wedge inserts opened up larger gaps on the top than the bottom of the ring specimen, as shown in Fig. 77.

65

Fig. 76. An untested fourth generation ring specimen with aluminum plug and four wedge inserts.

| Side view | Top view | Bottom view |

Fig. 77. Tested fourth generation ring specimens with aluminum plug and four wedge inserts: Test 17.

| Test 16 | Test 18 |

| Test 19 | Test 20 |

Fig. 78. Tested fourth generation ring specimens with aluminum plug and four wedge inserts: Tests 16–20.

Test 16 was not completed because the pressure of the hydraulic pump was set too low, so the pump loosened the grip on the bottom support piston. After the pressure of the hydraulic pump was reset, expansion plug tests 17–20 were carried out successfully. The plug length was 0.28 in. in the ring specimen sets except for Test 18 ring specimen set, which used a plug 0.29 in. long. Tests 18–20 show nonuniform ring expansion similar to that in Test 17. The obvious reason is that the hole in the bottom piston used for alignment introduced constraint on the bottom of the plug, causing uneven conditions on the tops and bottoms of the plugs. These issues were the basis for changes in the fifth generation design to resolve the shortcoming of the alignment method.

5.1.6   Fifth generation of specimen fabrication and pilot testing

For the fifth generation of test specimen fabrication, all the plugs were machined at a length of 0.28 in. and an OD of 0.238 in. Top and bottom surfaces of the plugs were flat, as shown in Fig. 79. From the fourth to the fifth generation, the plug design was the same, except that the length of the plugs was not varied. The final design used a length of 0.28 in.
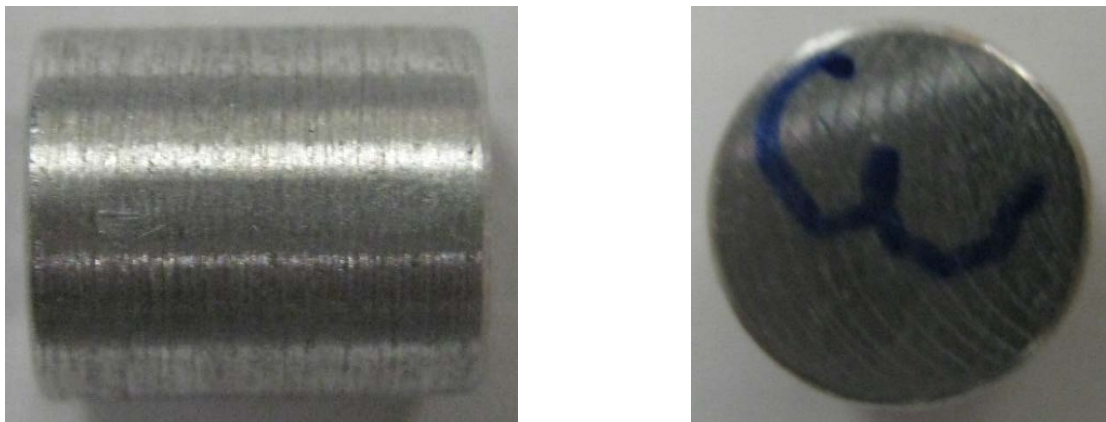
Fig. 79. Fifth generation plug.

The most important enhancement in the fifth generation pilot testing was to improve the alignment method. To eliminate the constraint from the shallow-center hole on the bottom piston, the elastic rubber was introduced in the alignment design. As shown in Fig. 80, a hole was machined on top of the bottom piston at a depth of 0.03 in. and a diameter of 0.6 in. Elastic rubber (blue) was molded inside the hole, and the inner hole was 0.25 in. in diameter to align the plug in the center of the piston. During the compression test, the bottom surface of the plug could stretch due to the elasticity of the rubber, so the constraint was minimized. After the tested specimen was removed, the elastic rubber recovered to its original position and can be used again for the next compression test.

**Fig. 80. Hole on the bottom support piston with elastic rubber
to fit the plug bottom's flat surface for alignment.**

The tested plugs show a reasonable response to the compression tests. As shown in Fig. 81, there was no trace of confinement on the bottom of the plug. The top and bottom surfaces of the plug appeared to stretch out in a similar way. Bulging occurred at the middle of the plug. Four plugs were tested to generate the plug load, and the tests were repeatable. This alignment method was used for pilot testing on the plugs and the ring specimen sets.

**Fig. 81. A tested fifth generation plug by using the hole
on bottom piston with elastic rubber for alignment.**

For fabrication of the fifth generation ring specimen set, electrical discharge machining (EDM) was used to machine the wedge inserts. As shown in Fig. 82, the fitting between the plug, wedges, and ring specimen was improve significantly, especially the gaps between the wedge inserts. There was no lubricant between the plug, wedges, and ring. The tightly fitted plug, wedges, and ring in the testing specimen can significantly improve the ring radial expansion corresponding to the compression load.

Fig. 82. An untested fifth generation ring specimen with an aluminum plug and of wedge inserts.

Four ring specimen sets were fabricated and tested in the fifth generation pilot testing, as shown in Fig. 83. The ring specimens deformed uniformly in the circumferential direction, as seen from the top view. The side view shows that the ring specimens expanded uniformly in the axial direction. Pilot testing was successful, and the test data processing shown below was based on the test data from these fifth generation pilot tests.

Test 21: top view

Test 21: side view

Test 22: top view

Test 22: side view

Test 23: top view

Test 23: side view

Test 24: top view

Test 24: side view

Fig. 83. Tested fifth generation ring specimens with aluminum plug and four wedge inserts.

5.2 TEST DATA PROCESSING ON FIFTH GENERATION PILOT TESTING

With the success of the fifth generation pilot testing, the expansion plug wedge method for the ring specimen design was finalized. The dimensions of the ring and wedges were the same in all five generations: M5 rings had an OD of 0.374 in., a thickness of 0.022 in., and a length of 0.17 in. Stainless steel wedge inserts had the same length as that of the ring, and the OD was machined to fit the ring ID. The ID of the wedges was designed to fit the OD of the aluminum plug at 0.238 in. and a length of 0.28 in.

Since no lubricant was applied to the contact surfaces between the plug and wedges or between the wedges and the ring, the resultant shear stress due to friction on the contact surfaces must be considered, especially under the high compression load. There were also some shear stresses on the top and bottom surfaces of the plug contacting the pistons, which also did not include lubricant. The initial evaluation indicated that the shear stresses on the top and bottom surfaces of the plug were slight due to the smooth contact surfaces and low friction coefficient at the interface. The χ factor discussed in Sect. 4 was generated under the condition of fully lubricated interfaces and thus did not take the friction-induced shear stress on the contact surfaces into consideration. Due to considerations for hot cell operations, the option to apply lubricant at interfaces was ruled out. Therefore, a new test data processing procedure must be developed to deduct shear stress and the associated energy from the total applied load and the total external energy. The net load or net energy on the ring specimen can then be accurately estimated and combined with radial expansion measurements to generate the hoop stress-strain curve.

5.2.1 Curve-fit plug load

As mentioned in Sect. 5.1.1, in order to deduct the load on the plug from the total load on the ring specimen set, the compression test must be conducted on the plug alone under the same condition as the testing the ring specimen set to determine the plug load. The four plugs were tested in the fifth generation pilot testing, and the test data were used to curve-fit a plug load, as shown in Fig. 84. This curve-fitted plug load can be used for deduction from the total load on the ring specimen set.

Load vs. extension curves from the four plug testing data were on top of each other in Fig. 84, which indicates that the plug testing is very repeatable. During the compression test, the aluminum plug went through the elastic deformation to the plastic deformation. The slopes changed significantly for elastic and plastic domains, so curve fitting was conducted separately for elastic and plastic domains. Fig. 85 shows the curve fitting parameters for the plug load. E represents the elastic part of the curve fitting parameters, and P represents the plastic part of the curve fitting parameters. There were six order polynomial equations of fitted curves for both elastic and plastic parts. The fitted curve matched with testing data very well, so it was an acceptable representation of a plug load.
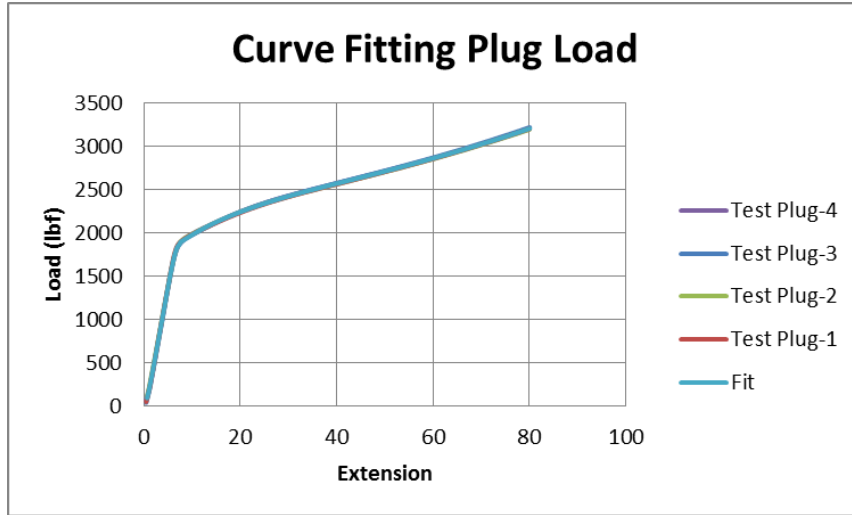
Fig. 84. Curve-fit a plug load from four plug testing.

E1	-3.09E-01	P1	4.75E-07
E2	5.42E+00	P2	-1.55E-04
E3	-3.77E+01	P3	2.05E-02
E4	1.29E+02	P4	-1.30E+00
E5	8.93E+01	P5	5.31E+01
E6	-5.44E+00	P6	1.56E+03

Fig. 85. Curve-fitting parameters for the plug load
(E = elastic; P = plastic).

5.2.2 Deduct load frame system deformation from the measured extension

The MTS electromagnetic loading frame in Fig. 52 was used to apply compression load and record loading measurement with the extension of the loading frame. If no deformation occurred in the loading frame system during the compression test, the extension of the loading frame was equal to the compression extension of the plug. However, the MTS electromagnetic loading frame is not rigid enough to discount its compliance. Thus, load frame system compliance was measured in separate tests with the top piston compressing directly onto the bottom piston. System compliance was generated from three repeatable tests, as shown in Fig. 86. Then the generated system compliance was entered into the test data spreadsheet to deduct the load frame system deformation from the extension given in Fig. 87. The adjusted extension of the loading frame now was equal to the plug compression extension, which can be used for analyzing test data.
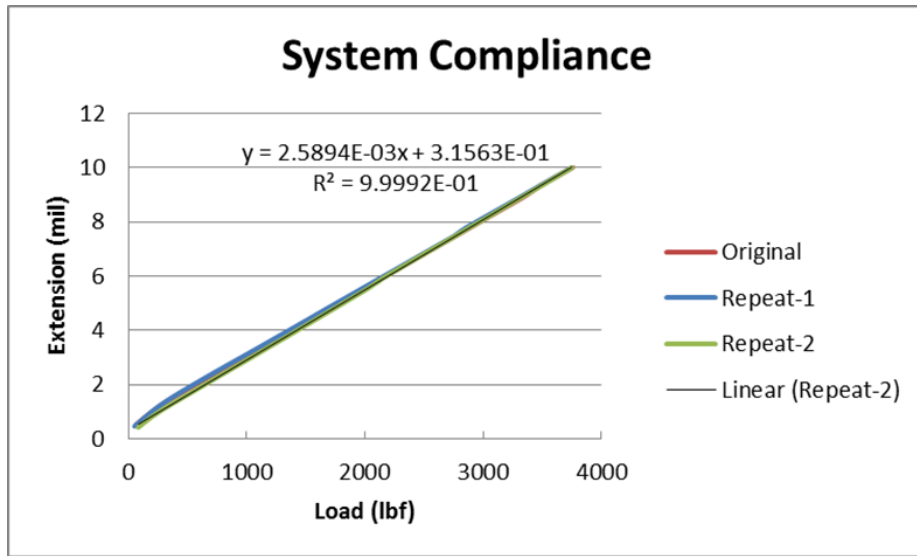
Fig. 86. Load frame system compliance test data.

Fig. 87. Deduction of load frame system deformation from the extension.

5.2.3   Calculate radial dilatation Δr and hoop strain

Fig. 52b shows that the radial expansion of the ring specimen was measured by four proximity transducers. Radial dilatation Δr averaged from four proximity transducer data, as shown in Fig. 88 in one of the test data spreadsheets.

Q	R _ACH0 (mil)	S	T _ACH1 (mil)	U	V _ACH2 (mil)	W	X _ACH3 (mil)	Y	Z Radial dilatation (in)
	-48.546	0	-51.01	0	-47.867	0	-44.386	0	0
	-48.503	0.043	-51.026	-0.016	-47.898	-0.031	-44.332	0.054	1.25E-05
	-48.573	-0.027	-51.073	-0.063	-47.916	-0.049	-44.347	0.039	-2.5E-05
	-48.508	0.038	-51.032	-0.022	-47.879	-0.012	-44.333	0.053	1.425E-05
	-48.548	-0.002	-51.063	-0.053	-47.892	-0.025	-44.34	0.046	-8.5E-06
	-48.529	0.017	-51.058	-0.048	-47.896	-0.029	-44.344	0.042	-4.5E-06
	-48.497	0.049	-51.054	-0.044	-47.869	-0.002	-44.332	0.054	1.425E-05
	-48.55	-0.004	-51.1	-0.09	-47.885	-0.018	-44.357	0.029	-2.075E-05
	-48.493	0.053	-51.071	-0.061	-47.853	0.014	-44.346	0.04	1.15E-05
	-48.509	0.037	-51.079	-0.069	-47.85	0.017	-44.352	0.034	4.75E-06
	-48.528	0.018	-51.115	-0.105	-47.845	0.022	-44.376	0.01	-1.375E-05
	-48.463	0.083	-51.058	-0.048	-47.815	0.052	-44.366	0.02	2.675E-05
	-48.522	0.024	-51.116	-0.106	-47.825	0.042	-44.382	0.004	-9E-06
	-48.48	0.066	-51.082	-0.072	-47.794	0.073	-44.39	-0.004	1.575E-05
	-48.488	0.058	-51.098	-0.088	-47.777	0.09	-44.396	-0.01	1.25E-05
	-48.503	0.043	-51.112	-0.102	-47.772	0.095	-44.42	-0.034	5E-07
	-48.452	0.094	-51.084	-0.074	-47.723	0.144	-44.42	-0.034	3.25E-05
	-48.512	0.034	-51.1	-0.09	-47.706	0.161	-44.438	-0.052	1.325E-05
	-48.486	0.06	-51.084	-0.074	-47.657	0.21	-44.439	-0.053	3.575E-05
	-48.477	0.069	-51.069	-0.059	-47.609	0.258	-44.424	-0.038	5.75E-05
	-48.52	0.026	-51.074	-0.064	-47.591	0.276	-44.42	-0.034	5.1E-05

Fig. 88. Radial dilatation calculated from four proximity transducer data.

The hoop strain can be calculated from radial dilatation Δr from Eq. (5)

$$Strain = \frac{\Delta r}{r_{ring}} \tag{5}$$

where, r_{ring} is the ring's outer radius.

5.2.4 Energy approach to convert hoop stress

Because of the shear stress on the contact surfaces, an energy approach was developed to convert hoop stress, as follows,

$$External\ Work = Internal\ Strain\ Energy \tag{6}$$

$$Work_{total} = Strain\ Energy_{plug} + Strain\ Energy_{ring} + Strain\ Energy_{wedge} + Energy\ dissipation_{system} \tag{7}$$

$$W_{total} = W_{plug} + SE_{ring} + SE_{wedge} + \Delta E, (SE_{wedge} < 0.3\%\ SE_{internal}) \tag{8}$$

$$SE_{ring} = W_{total} - W_{plug} - \Delta E \tag{9}$$

$$SE_{ring} = P_{ring}2\pi r l \Delta r \tag{10}$$

$$P_{ring} = \frac{SE_{ring}}{2\pi r l \Delta r} \tag{11}$$

$$\sigma_\theta = \frac{P_{ring}r}{t} = \frac{SE_{ring}r}{2\pi r l \Delta r t} = \frac{(W_{total} - W_{plug} - \Delta E)}{2\pi \Delta r t l} \tag{12}$$

where
W_{total} = work of total load on plug-wedge-ring specimen,
W_{plug} = work of plug load on plug alone,
SE_{ring} = strain energy of ring,

74

ΔE = energy dissipation due to friction, etc.,
P_{ring} = nominal internal pressure on the ring,
Δr = ring total radial dilatation,
t = ring specimen thickness,
l = ring specimen length, and

The energy conservation was expressed in Eq. (6) for the expansion plug ring test. The external work was the work done by the total load in the plug-wedge-ring specimen during the compression test. Internal strain energy consists of the strain energy of the plug, the ring, and the wedge inserts. Internal energy also included the energy dissipation, which was mostly due to friction. Therefore, the energy balance could be stated in detail as in Eq. (7).

Due to the low friction on the plug and piston contact surfaces, the strain energy of the plug was equivalent to the work applied to the plug when testing the plug alone. Because the conditions were the same when testing the plug alone and when testing the plug-wedge-ring specimen set, the strain energy of the plug could be replaced by the work on the plug alone. The energy balance equation was rewritten as Eq. (8). The rigid wedge inserts are designed to transmit the load uniformly onto the ring specimen. The wedges were made of high strength steel and designed to be separated during the expansion process, so they consume very limited strain energy. FEA results further verify that the strain energy of the wedges is less than y 0.3% of internal strain energy. Therefore, the strain energy of wedges' terms in Eq. (8) were not considered further in the hoop stress conversion.

The equation was further simplified as Eq. (9) to work out the strain energy on the ring, which is used to convert the hoop stress on the ring. The strain energy on the ring occurred when the ring specimen deformed under the compression load transferred through the wedges from the plug. In Eq. (9), the strain energy on the ring was calculated from the work of the total load deducted by the work on the plug alone and the system's energy dissipation due to friction. The strain energy of the ring was also equal to the work of the nominal internal pressure P_{ring} on the ring in the radial direction, as shown in Eq. (10). The nominal internal pressure P_{ring} could be further expressed by the strain energy of the ring in Eq. (11). According to the thin-walled pressurized cylinder theory—which was the basis of the expanded plug method—the hoop stress created by the internal pressure could be estimated using Eq. (12). In Eq. (12), nominal internal pressure was replaced by the expression from the strain energy on the ring in Eq. (11), and the strain energy on the ring was then replaced by the work equivalent given in Eq. (9).

During the compression test, total load on the plug-wedge-ring specimen and the plug's load on the plug test alone were recorded with the extension of the load frame. The work of the total load on the plug-wedge-ring specimen and the work of the plug load on the plug alone can be calculated from the load (force) and its extension (displacement). By employing Eq. (12) and estimating the friction energy, the test measurements of the load and the extension from the MTS electromagnetic load frame can be converted into the hoop stress σ_θ through the energy approach.

5.2.4.1   Energy approach to convert stress-strain curve of FEA data

The developed energy approach to convert hoop stress was applied in the FEA simulation data. The strain energy of the ring was converted into the ring hoop stress. The hoop strain was calculated from the ring's radial dilatation. The converted hoop stress-strain matched the tensile test data very well in the elastic and plastic regions. In 0.2% of the offset region, the yield stress agreed with the tensile test data. It proved that the energy approach was theoretically successful for converting hoop stress.
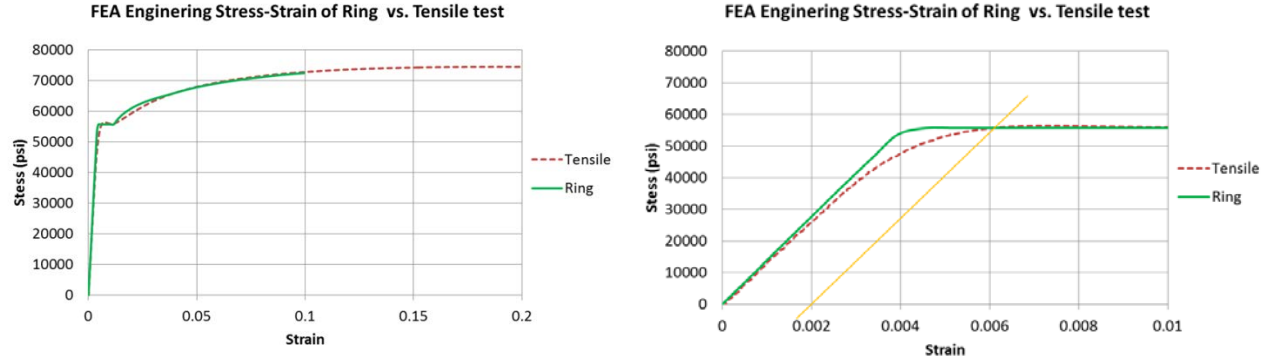
Fig. 89. FEA hoop stress–strain curves vs. tensile test data for expanded plug test design with four wedge inserts.

5.2.4.2 Calculation of the work of the total load and the work of the curve-fitted plug load

As mentioned before, the test measurements from the load frame were load and extension. In order to use the energy approach to convert the hoop stress, the work of the total load and the work of the plug load needed to be calculated from the load and extension. Fig. 90 shows the load vs. extension data for the fifth generation ring specimen test. The plug load was the curve-fitted data from four plug testing as discussed in Sect. 5.2.1. The extension was adjusted with consideration of the load frame system compliance as discussed in Sect. 5.2.2. The work was calculated from the blue shaded area (Fig. 90) enveloped by the total load and the plug load.
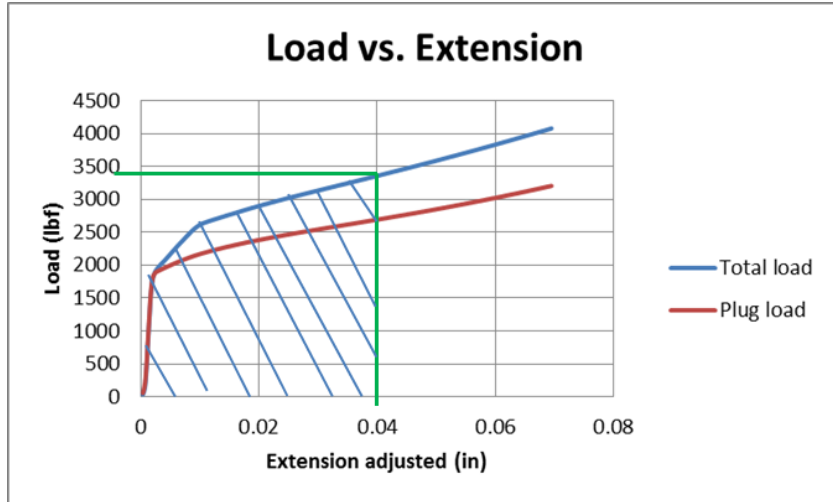
Fig. 90. Test data load vs. extension for the fifth generation ring specimen.

In the test data spreadsheet, the work was calculated for each time step following Eq. (13),

$$Work = \Sigma Load * \Delta Extension \tag{13}$$

The shaded area in Fig. 90 was discretized by extension increment into a small area. The work was calculated on the discrete area and then totaled, as shown in Fig. 91, with integration at each time frame. The calculated work of the total load and the work of the plug load at each extension increment were shown in Fig. 92

76

Fig. 91. Test data spreadsheet showing the calculation of work.
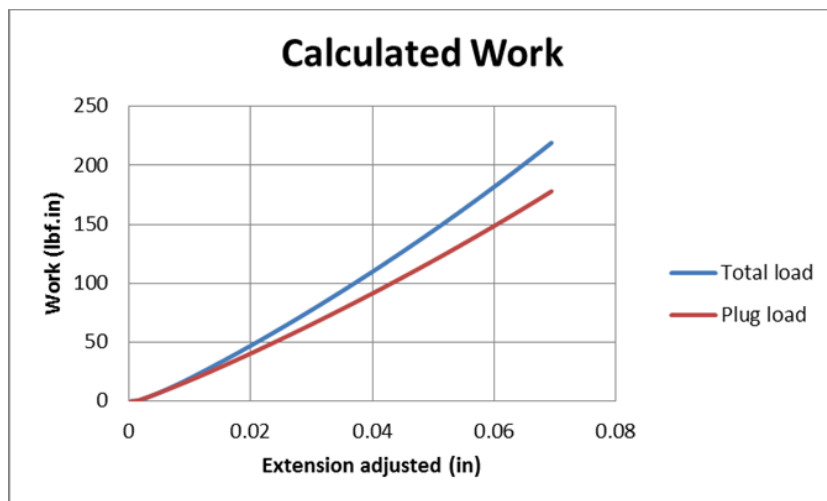
**Fig. 92. Calculated work of the total load and the
work of the plug load vs. the extension.**

5.2.4.3   Calculate ring strain energy without consider friction energy

In Eq. (9), the work of the total load and the work of the plug load were calculated from the measured total load and the curve-fitted plug load with its extension for ring test specimen#23, as discussed in Sect. 5.2.4.2. However, energy dissipation due to friction was unknown in the testing. The first step to calculate the friction energy was temporarily ignored. The strain energy of the ring was simply replaced by the work of the total load deducted by the work of the plug load, as shown in Eq. (14). The hoop stress was converted with Eq. (15). The strain was calculated from radial dilatation Δr measured by four proximity transducers as discussed in Sect. 5.2.3.

$$SE_{ring} = W_{total} - W_{plug} - \Delta E$$

calculated   calculated   unknown

By ignoring friction energy, then

77

$$SE_{ring} = W_{total} - W_{plug} \tag{14}$$

$$\sigma_\theta = \frac{P_{ring}r}{t} = \frac{SE_{ring}r}{2\pi rl\Delta rt} = \frac{SE_{ring}}{2\pi\Delta rtl} \xrightarrow{\ 1\ } \sigma_\theta = \frac{W_{total} - W_{plug}}{2\pi\Delta rtl} \tag{15}$$
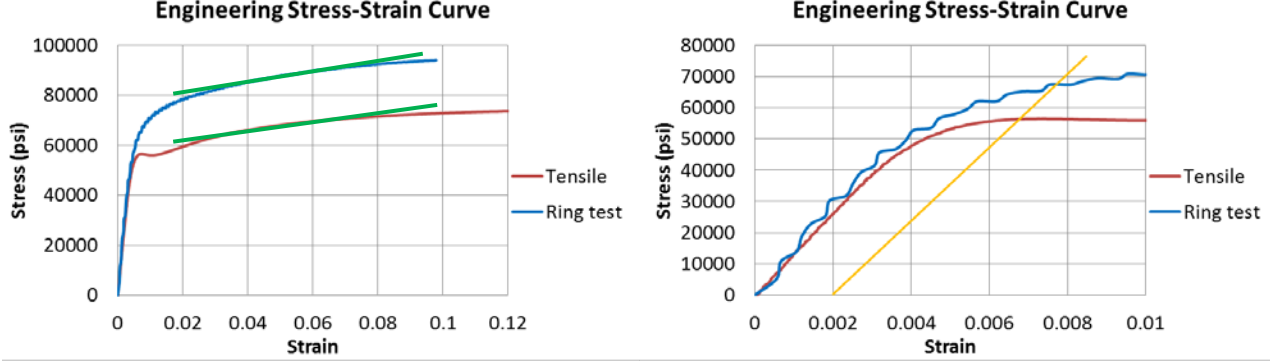
Fig. 93. Ring test#23 engineering hoop stress-strain curve without considering friction energy ΔE.

The converted hoop stress-strain curve was shown in Fig. 93 and compared with the tensile stress-strain curve. In the elastic region, ring test data agreed well with tensile data, which indicates that the friction energy during the ring elastic deformation was small enough to be disregarded. In the plastic strain hardening region, the hoop stress-strain curve of the ring test appeared to be parallel to the tensile stress-strain curve. The strain hardening trend was similar between the ring test data and tensile data. The ring test result has a higher stress level than that of the tensile test due to disregarding the friction energy dissipation. As shown in Fig. 93, using a constant factor could bring down ring test data to match that of tensile test data trend in the material hardening region.

5.2.4.4   Estimate ΔE by FEA

Energy dissipation in the ring test was caused by shear stress from friction at the interfaces of the plug and wedges, the wedges and the ring, and the piston and the plug. The frictions at those contact surfaces are unknown. During the ring test, energy dissipation could not be measured, as indicated in Eq. (9), where the friction energy ΔE is unknown. To deduct friction energy from the work of the total load of the ring test data to match that of the tensile test data, FEA simulation was used to estimate ΔE.
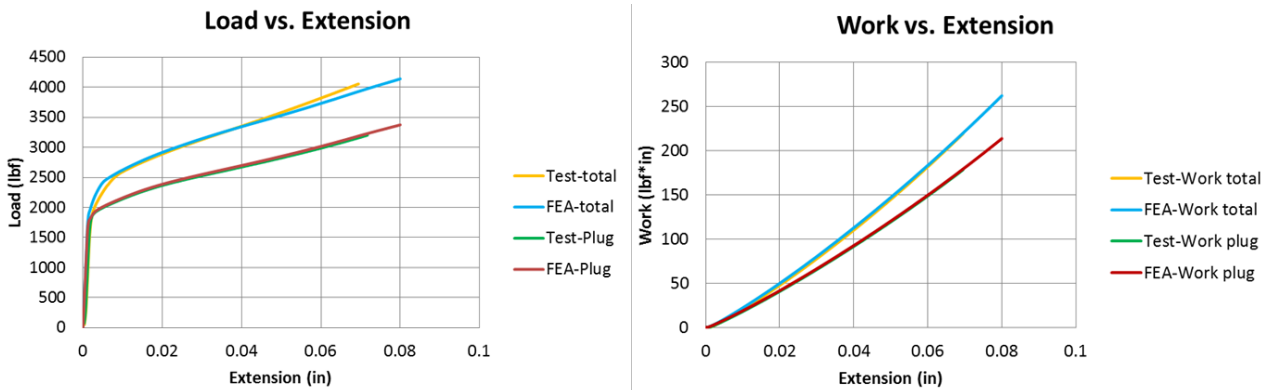
Fig. 94. FEA simulations to get the best match between test and FEA data.

A detailed plug-wedge-ring system was modeled in ABAQUS with realistic geometry, and the compression tests were simulated in FEA. The friction coefficients on the contact surfaces were estimated in the simulations. A series of simulations was performed to obtain the best match between test and FEA

78

data with calibrated friction coefficients. As shown in Fig. 94, with a friction coefficient of 0.04 on contact surfaces between the piston and the plug and a friction coefficient of 0.45 on contact surfaces among the plug and wedges, as well as the wedges and ring, the FEA total load agreed with the test load, and the FEA plug load was on top of test plug load. Calculated works matched with each other between test and FEA data. Fig. 95 shows final deformation of the ring specimen set in this simulation case compared to the tested ring specimen. Ring deformations appeared to be identical to each other, so friction energy in fifth generation ring tests could be estimated based on the friction coefficients in this simulation case.
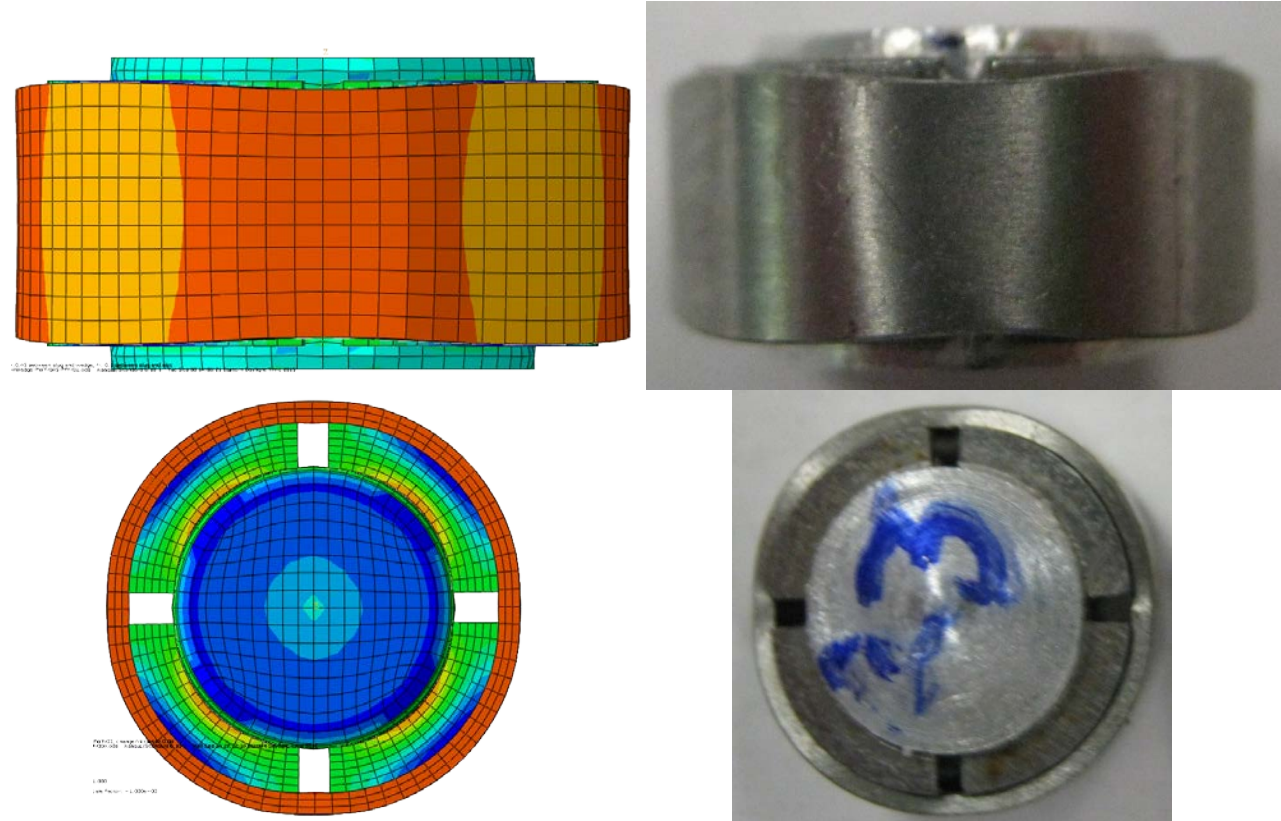
Fig. 95. Final deformation of ring specimen set in FEA simulation compared to tested ring specimen.

In FEA, friction energy ΔE can be obtained with the calibrated friction coefficients. In order to apply FEA friction energy in processing test data, FEA friction energy vs. extension curve was fitted with a six order polynomial. The test friction energy ΔE was estimated using the six order polynomial equation at each extension increment as shown in Fig. 96.
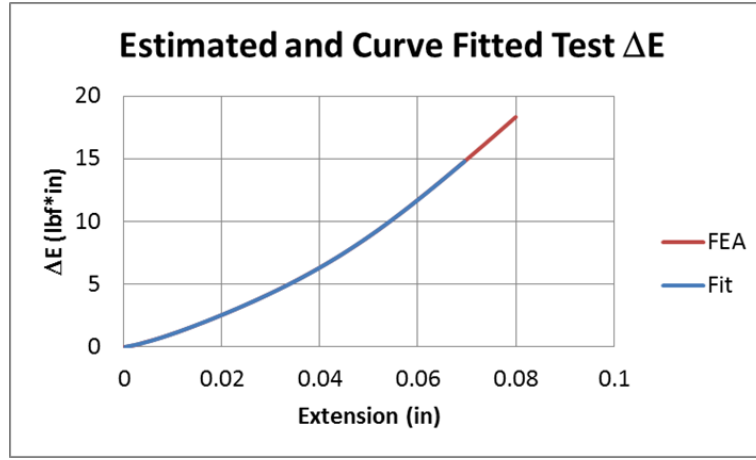
Fig. 96. Estimated friction energy ΔE from FEA.

5.2.4.5   Generate and apply α factor for strain hardening profile adjustment

With the success of the friction energy estimation, the strain energy of the ring could be more accurately calculated using Eq. (9). Equation (9) can be rewritten as Eq. (16), with generated α factor in Eq. (17). α factor was defined as a ratio of friction energy ΔE to the work of the total load deducted by the work of the plug load. α factor vs. strain curve was generated as shown in Fig. 97. α factor was further investigated. It was determined that α factor was nearly constant for the strain in the strain hardening region. For the fifth generation pilot testing, α factor was averaged as constant 0.23 in Fig. 97.

$$SE_{ring} = W_{total} - W_{plug} - \Delta E$$

$$\text{calculated} \quad \text{calculated} \quad \text{estimated}$$

$$SE_{ring} = (W_{total} - W_{plug}) * (1 - \alpha) \tag{16}$$

$$\alpha = \Delta E / (W_{total} - W_{plug}) \tag{17}$$
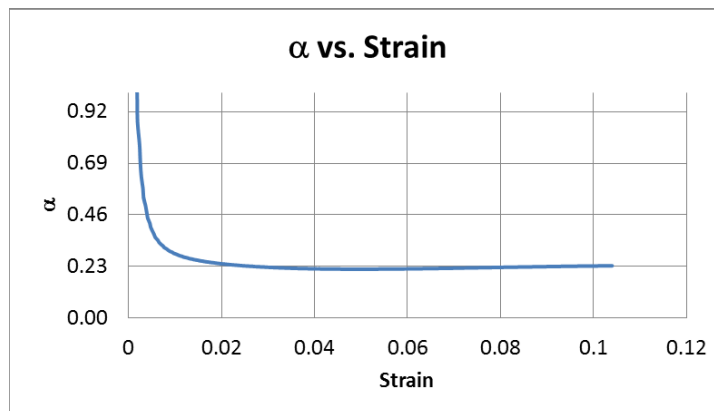
Fig. 97. Generated α factor vs. strain.

$$\sigma_\theta = \frac{P_{ring}r}{t} = \frac{SE_{ring}r}{2\pi r l \Delta r t} = \frac{SE_{ring}}{2\pi \Delta r t l} \xrightarrow{\mathbf{1}} \sigma_\theta = \frac{W_{total} - W_{plug}}{2\pi \Delta r t l} \xrightarrow{\mathbf{2}} \boxed{\sigma_\theta = \frac{(W_{total} - W_{plug}) * (1 - \alpha)}{2\pi \Delta r t l}} \tag{18}$$

80

By applying α factor, Eq. (17) was further corrected into Eq. (18), which was used to estimate the hoop stress through the proposed energy approach. Eq. (18) was made equivalent to Eq. (12) by replacing friction energy ΔE with α factor. Applying an α factor of 0.23 in Eq. (18), the converted hoop stress vs. the calculated radial strain was shown in Fig. 98. As discussed above, ring test data matched well with tensile test data in the elastic region. α factor was only used to adjust the strain hardening profile of the ring test data. Compared to the converted hoop stress in Fig. 93, α factor brought down the converted hoop stress level in the strain hardening region so the ring test hoop stress-strain curve matched perfectly with the tensile test stress-strain curve.
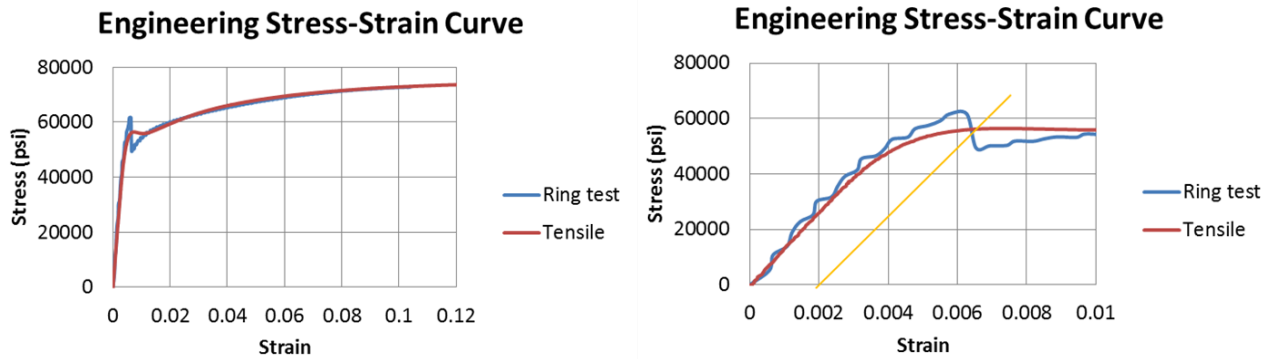
Fig. 98. Ring test #23 engineering hoop stress-strain curve with α factor for friction energy.

Because of different treatments in the elastic and strain hardening regions, a transition area occurred in the processed hoop stress-strain curve.

5.2.5   Smooth transition area

Numerical power-law function was generated to smooth the transition area, as shown in Fig. 99. The transition area in the hoop stress-strain curve between the elastic and strain hardening region would be gapped with generated power function data. Fig. 100 shows a smoothed transition area by the power function for the fifth generation pilot test data on ring specimens 22–24. The significant jump between the elastic region and the strain hardening region was eliminated. The hoop stress-strain curves had a better match with the tensile test data at the transition area, which helped to improve estimation of the yield stress.

81
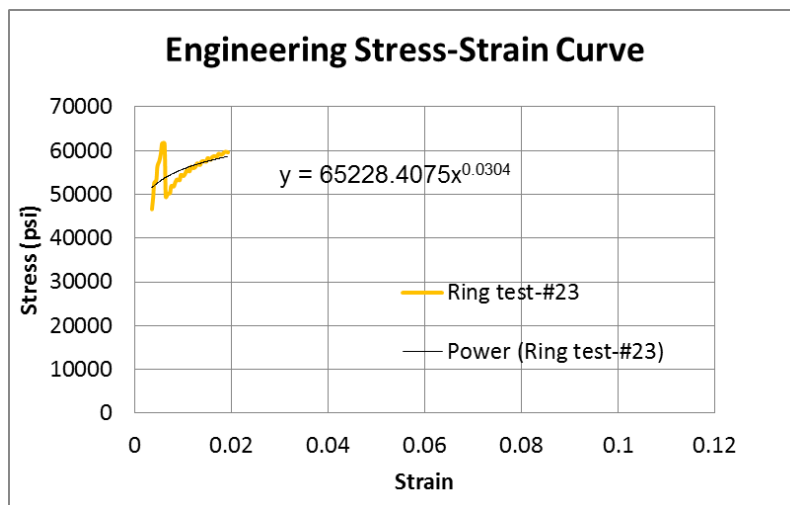
Consistency was observed from the fifth generation pilot testing. However, test specimen 21 behaves differently compared to others at the transition region from the measured load vs. the extension data, as shown in Fig. 101. Further investigation was needed to determine the cause. The converted hoop stress-strain curve could not match with tensile test data, especially at the transition area.
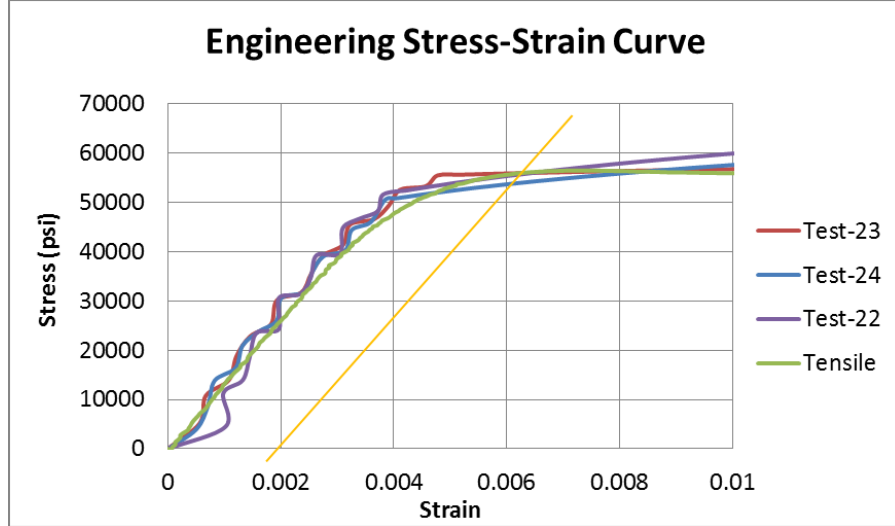
**Fig. 100. Smoothed transition area for fifth generation
pilot test data on ring specimens 22–24.**
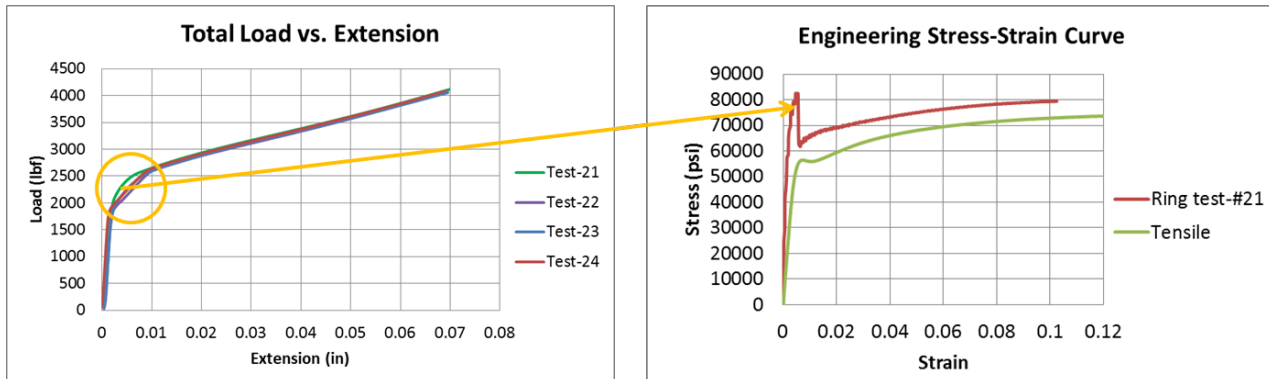
Fig. 101. Test specimen 21 variation at the transition region.

5.2.6   Converted hoop stress-strain curve of test data

Fig. 102-104 show the converted hoop stress-strain curves from ring test specimens 22–24 by the proposed energy approach. α factor of 0.23 was used to process all test data. In general, the ring test converted material hoop stress-strain curve agreed well with tensile test data. Ring specimen 23 test data had the best match. In the elastic region, all test data match well. In the strain hardening region, ring specimen 22 had the largest difference between the ring test data and tensile test data; the difference was less than 10%.

In summary, with the proposed test method and the optimized test specimen design demonstrated in the pilot testing, the proposed expanded plug wedge testing protocol validates that the measured piston

compressive load, plug extension, and ring radial expansion can be effectively and accurately converted into the hoop stress-strain curve for clad tubing material characterization.
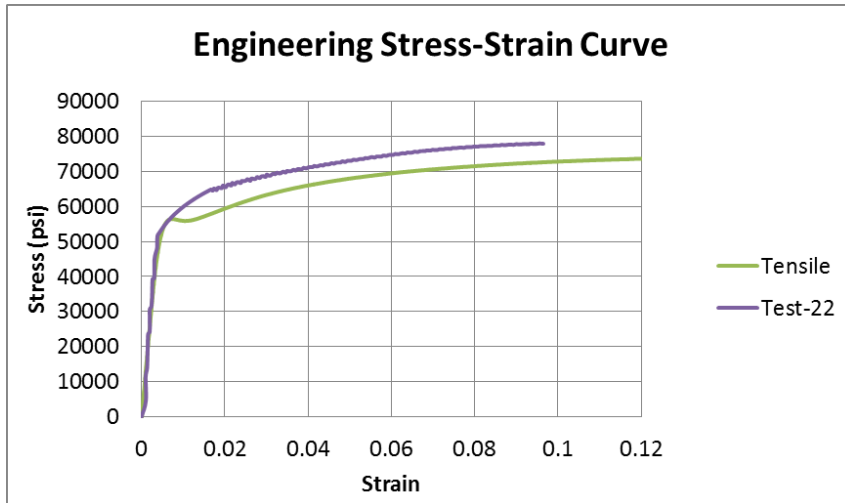
Fig. 102. Converted hoop stress-strain curve of ring test specimen 22.
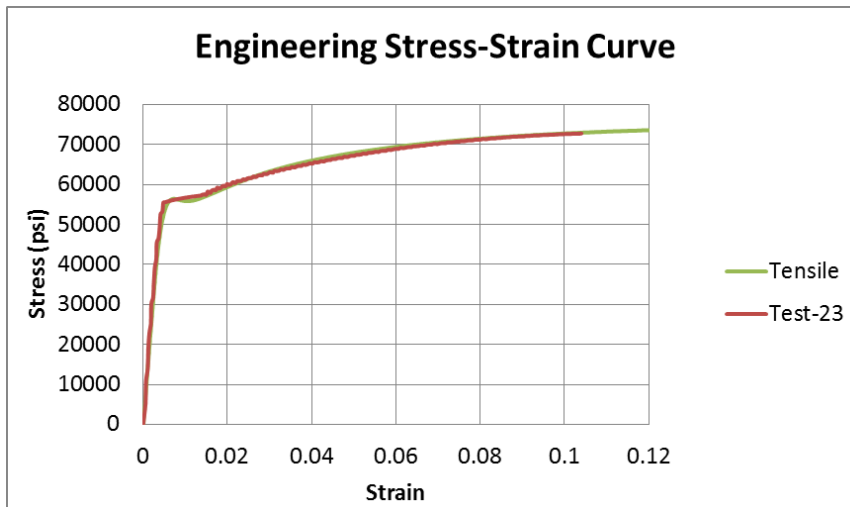
Fig. 103. Converted hoop stress-strain curve of ring test specimen 23.
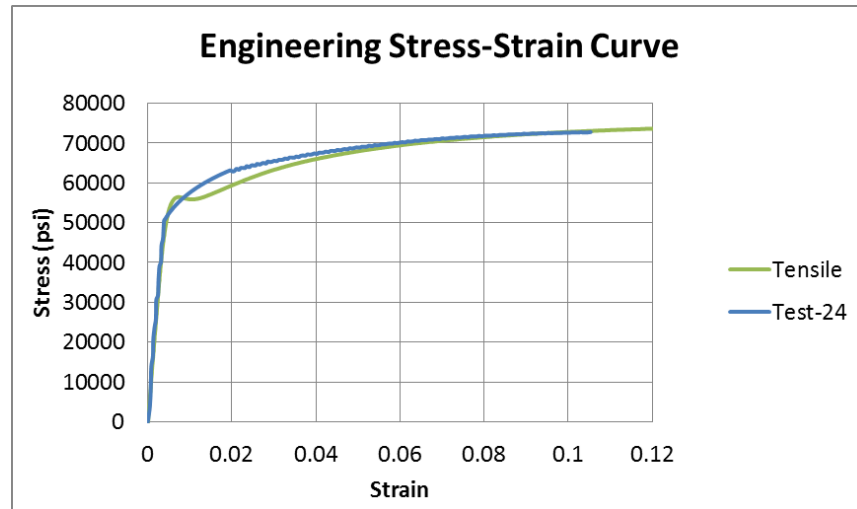
Fig. 104. Converted hoop stress-strain curve of ring test specimen 24.

6.   CONCLUSION

Finite element models were established to simulate the current ORNL expanded plug method for mechanical property testing. A uniaxial compressive test and volumetric compressive test were performed. Test data were used in ABAQUS to calibrate coefficients of the hyperelastic material model of a polyurethane plug at room temperature. These data were used as parameters in the FEM model. The expansion plug test system with the unirradiated M5 clad and the polyurethane plug was evaluated using the established FEM model at room temperature.

Early FEA results showed highly nonuniform stress and strain distribution in the unirradiated M5 clad at room temperature. Significant compressive stresses were observed in the resultant axial stress, which were induced by clad bending due to the clad bulging effect. The barreling effect results in a very large localized shear stress in the clad wall. This effect often led to the material's shear failure at 45° angle along the clad wall. Compressive stress in cladding further induced lateral expansion of the clad wall. In this case, the circumference strain estimated from the expansion plug test overestimates the strain deformation component of the defined hoop stress due to the additional lateral expansion induced by the compressive stress. Therefore, the compressive axial stress and shear stress in the previous used plug-clad system cannot be ignored and must be corrected to obtain accurate results of expansion plug testing.

The defined hoop stress obtained from the previously used simplified scale factor approach significantly underestimates the true combined stress fields experienced by an expansion plug tested clad system, as indicated by this FEM analysis. The combined effects of the overestimated circumference strain and the associated underestimated stress will result in nonconservative predictions both in strength and ductility of the tested clad, as well as the associated mechanical properties. FEA proves that stress fields in a clad material induced by the expansion plug test can be quite complicated, and they do not resemble pressurized cylinder clad stress-strain behaviors.

A ring expansion clad test at an elevated temperature of 350°C was also evaluated in FEA. FEM simulations with unirradiated Zircaloy-4 and irradiated Zircaloy-4 clad and a copper plug were conducted. Similar deficiencies of the previously used ring test using the expanded plug method existed in the FEA results at elevated temperature.

Systematic studies were conducted to overcome the deficiencies associated with the previously used expansion plug test. The goal was to create a completely uniform expansion of the specimen in the immediate area along the clad wall where test gages were positioned.

First, a modified expansion plug testing protocol was developed based on the results of the earlier FEA study. The first proposed design modification of the expanded plug test was to use aluminum as the expansion plug material. Second, a series of size effect studies for the axial length of clad and expansion plug were performed. The sizing tests determined the optimized length that will result in a more uniform stress and strain distribution within the gage section. Third, lubrication in the plug/liner specimen wall interface was considered to reduce interfacial shear stress and the consequences of axial compressive stress. FEM simulation results of these three modifications showed a definite improvement in the stress and strain distribution at the gage section, as well as the significant reduction in the axial stress induced by the barreling effect.

In addition to the first proposed modification, an expanded plug test with rigid wedges inserted between the clad and the plug has been developed. FEM simulation indicates that this approach results in more uniform stress and strain distribution at the gage section than with the first proposed design modification.

FEM results also show significantly lower clad axial compressive stresses than that of the previous ORNL expansion plug method. A general procedure has been developed to determine the hoop stress σ_θ with χ factor in FEA. The generated stress-strain curve agrees well with tensile test data in both the elastic and plastic regions. The modified expansion plug testing protocol has been developed and validated in FEM simulation.

Based on FEA design, the ring specimen was fabricated for test validation. The design for the wedge inserts was modified to reduce the number of wedges from eight to four. This resulted in a more feasible specimen fabrication and an easier sample assembly. Five generations of ring-wedge-plug pilot specimens have been designed, fabricated, and tested. More than 50 pilot tests have been performed on 24 ring specimens and plugs. The fifth generation pilot testing successfully obtained uniform ring radial dilatation. The fifth generation ring specimen sets were considered to be the most optimized design and fabrication; the M5 rings had an OD of 0.374 in. and a thickness of 0.022 in. The length of the ring was 0.17 in. The stainless steel wedges were the same length as the ring, and the OD was machined to fit the ring ID. The ID of the wedges was machined to fit the OD of the aluminum plug, which was 0.238 in. The length of the plug was studied in detail, and the final design chosen was 0.28 in. A center alignment hole machined on top of the bottom piston with molded elastic rubber was used to align the plug in the center of the piston for the fifth generation pilot testing.

Since there was no lubricant applied on the contact surfaces between the plug and wedges and between the wedges and the ring in the final design, the resultant shear stress on the contact surfaces cannot be disregarded, especially under the high compression load. The χ factor in Sect. 4 was generated without lubricant application. The option to apply lubricant at interfaces was ruled out due to hot cell limitations. Thus, the test data processing procedure must provide for deducting the interface shear stress or the associated friction energy from the total compression load or total energy.

The test data processing procedure based on the energy approach was developed to convert the test load-displacement measurements into hoop stress-strain curves for fifth generation pilot testing. Friction energy due to shear stress was estimated in FEA. Instead of using χ factor, α factor was applied to deduct friction energy. The power function was generated to smooth the transition area. The proposed ring test converted material hoop stress-strain curve, and the results agreed well with tensile test data.

In conclusion, with the proposed test method and the optimized test specimen design demonstrated in the pilot testing, the proposed expanded plug wedge testing protocol validates that the measured piston compressive load, plug extension, and ring radial expansion can be effectively and accurately converted into the hoop stress-strain curve for clad tubing material characterization.

7.   FUTURE WORK

Further detailed study is needed on this subject. The proposed tasks for developing the modified expansion plug test are listed below.

Task 1: Perform pilot testing on a Zr-4 clad specimen to further validate the test method and procedure.

Task 2: Develop a pilot testing protocol for the wedge-plug approach and the wedge driver concept.

Task 3: Develop a pilot testing protocol to accommodate the high temperature condition.

Task 4: Prepare an expansion plug wedge test in the hot cell environment.

Task 5: Initiate standardization of the proposed modified expansion plug testing protocol.

(1) Initiate a dialogue with Argonne National Laboratory (ANL), Pacific Northwest National Laboratory (PNNL), and other national labs to form a to perform round robin testing of the proposed new approach and to compare the approach to other conventional approaches for fuel clad mechanical properties evaluation.

(2) Communicate with entities in the nuclear industry, such as fuel clad vendors and the nuclear utilities, regarding the proposed new approach for clad tensile properties evaluation.

8. REFERENCES

1. Wikipedia, "Cylinder stress."
   http://en.wikipedia.org/wiki/Cylinder_stresses.

2. Codecogs, "Thin Walled Cylinders Under Pressure."
   http://www.codecogs.com/library/ engineering/ materials/cylinders_and_spheres/thin-walled-cylinders-and-spheres.php.

3. Efunda, "Thin-walled Pressure Vessels."
   http://www.efunda.com/formulae/solid_mechanics/mat_mechanics/ pressure_vessel.cfm.
   Engineering Fundamentals. 19 June 2008.

4. William Ray Hendrich et al., "Expanded Plug Method for Developing Circumferential Mechanical Properties of Tubular Materials," United States Patent, Patent No. US 7140259 B2, Nov. 28, 2006.

5. W. J. McAfee, W. R. Hendrich, T. E. McGreevy, C. A. Baldwin, and N. H. Packan, "Postirradiation Ductility Demonstration Tests of Weapons-Derived Fuel Cladding," Flaw Evaluation, Service Experience, and Materials for Hydrogen Service, PVP-Vol. 475, July 2004, pp. 213–220.

6. Karl-Fredrik Nilsson et al., "The segmented expanding cone-mandrel test revisited as material characterization and component test for fuel claddings," *Nuclear Engineering and Design*, 241, 445–458 (2011).

7. Sun-ki Kim et al., "Hoop strength and ductility evaluation of irradiated fuel cladding," *Nuclear Engineering and Design* 239, 254–260 (2009).

8. Zhenyuan Hang and Xufeng Mi, "Behaviors of polyurethane filled double skin steel tubular members," *Applied Mechanics and Materials* 94-96, 196–200 (2011).

9. Efunda, "Material Properties,"
   http://www.efunda.com/materials/polymers/properties/polymer_datasheet.cfm, accessed December 10, 2015.

10. AK Steel, "430 Stainless Steel Product Data Sheet,"
    http://www.aksteel.com/pdf/markets_products/stainless/ferritic/430_Data_Sheet.pdf, accessed December 10, 2015.

11. Ridely Thrash et al., *Southwire Company Overhead Conductor Manual,* Second Edition, Southwire Company, Carrolton, Georgia, 2007.

12. Kurt Miller, "Testing Elastomers for Hyperelastic Material Models in Finite Element Analysis,"
    http://www.axelproducts.com/downloads/TestingForHyperelastic.pdf, accessed December 10, 2015.

13. *Abaqus Analysis User's Manual* (6.10), http://abaqusdoc.ucalgary.ca/books/usb/default.htm, accessed December 10, 2015.

14. Roger A. Jaramillo, W. R. Hendrich, and N. H. Packan, *Tensile Hoop Behavior of Irradiated Zircaloy-4 Nuclear Fuel Cladding,* ORNL/TM-2006/163, Oak Ridge National Laboratory, December 2006.

15. "Review of Fuel Failures in Water Cooled Reactors," IAEA Nuclear Energy Series No. NF-T-2.1.

16. Michael C. Billone, "The Mechanical Properties Expertise Group Update on Round Robin Test Results," Argonne National Laboratory Report, February 2002.

17. Jy-An John Wang et al., *Progress Letter Report on U-Frame Test Setup and Bending Fatigue Test for Vibration Integrity Study (Out-of-Cell Fatigue Testing Development – Task 2.2),* ORNL/TM-2011/531, January 2012.

18. John Gilbert Kaufman, *Properties of Aluminum Alloys: Tensile, Creep, and Fatigue Data at High and Low Temperatures,* The Aluminum Association, Inc. and ASM International®, Washington, DC and Material Park, Ohio, September 2002.

19. Roger L. Brockenbrough and B. G. Johnston, "USS Steel Design Manual, Jan. 1981," *Structural Alloys Handbook* **3,** 5 (1994).

20. http://www.roymech.co.uk/Useful_Tables/Tribology/co_of_frict.htm.